Rheological study of a new semi-rigid giant polysaccharide for the mechanical reinforcement of hydrogels

Tom Saint-Martin

THESE DE DOCTORAT DE L'UNIVERSITE PIERRE ET MARIE CURIE

Spécialité: Physique et Chimie des Matériaux

(Ecole Doctorale 397: Physique et Chimie des Matériaux)

Rheological study of a new semi-rigid giant polysaccharide for the mechanical reinforcement of hydrogels

-

Étude rhéologique d'un nouveau polysaccharide semi-rigide géant pour le renforcement mécanique d'hydrogels

Par Tom SAINT-MARTIN

Présentée et soutenue publiquement le 19 septembre 2017

Devant un jury composé de :

M. Bruno JEAN (CERMAV - CNRS)	Rapporteur
M. Christophe CHASSENIEUX (IMMM - Univ. du Maine)	Rapporteur
M. Luc PICTON (PBS - Univ. de Rouen)	Examinateur
M. Tristan BAUMBERGER (INSP – Univ. Paris Diderot)	Examinateur
Mme. Laurence TALINI (SIMM - Univ. Pierre et Marie Curie)	Directrice de thèse
M. Tetsuharu NARITA (SIMM – CNRS)	Co-directeur de thèse
Mme. Guylaine DUCOURET (SIMM – CNRS)	Encadrante de thèse - Invitée

Contents

Remerciements

Au terme de ces trois années, je voudrais prendre le temps de remercier les personnes qui ont été acteurs de cette thèse à mes côtés.

Je remercie Tetsuharu et Guylaine pour m'avoir permis de travailler dans les meilleures conditions possibles grâce à votre investissement et votre confiance. Tetsu, tu m'as également permis d'aller soutenir mon travail dans différentes conférences nationales et internationales qui furent des expériences incroyables et qui n'auraient, sans toi, pas été. En bref, ce fut un réel plaisir de travailler avec vous et je n'aurai pas pu imaginer meilleur encadrement pour ma thèse.

Je remercie les rapporteurs et membres de mon jury pour avoir soulevé d'intéressantes discussions autour de mon travail que vous avez pris le temps de lire, d'écouter puis d'évaluer.

Je remercie mes co-bureaux, Charles et Armand, qui avez partagés mon bureau durant trois années. Travailler à vos côtés a été un plaisir et nos discussions les meilleurs breaks imaginables. En bref, de collègues, vous êtes aussi devenu des amis et dorénavant vous ne garderez plus que ce statut.

Je remercie les membres de mon groupe de recherche au sein du laboratoire SIMM, Costantino, Étienne, Dominique, Alba et Matteo pour vos commentaires très utiles durant nos réunions d'équipes bimensuelles et pour votre bienveillance.

Je remercie tous les membres du laboratoire SIMM qui m'ont accueilli et donner la chance de travailler dans de fabuleuses conditions techniques et une ambiance de travail professionnelle et joviale, en témoigne les fameuses « bières du lundi », les incroyables « week-ends labo » et l'ensemble des activités extérieures faites ensemble.

Je remercie le Pr. Kaneko et le Dr. Okajima pour m'avoir permis de travailler sur le sacran en nous offrant des échantillons de ce nouveau polysaccharide et m'avez invité au premier symposium international sur le sacran organisé au Kyshu Institute of Technology en 2015.

Je remercie Marc Schmutz pour avoir réalisé les imageries de gels de sacran par cryo-fracture et cryo-SEM et avoir pris du temps pour essayer de comprendre les rendus.

Je remercie le Groupe Français de Rhéologie pour m'avoir offert un bourse m'ayant permis de présenter au congrès international de rhéologie s'étant tenu à Kyoto en 2016.

Enfin, je remercie mes amis, ma famille et Sonia pour m'avoir soutenu durant toutes ces années et m'avoir rendu la vie si simple.

Introduction

Filament-forming proteins play important roles in cell mechanics and motility, and it is known that these filaments commonly show strain-hardening under large strain[1]. The rigidity-induced strain-hardening can be promising in the context of mechanical reinforcement of hydrogels, still, it is a challenge to synthesize a model system. The relation between viscoelastic properties and network architecture of gels made of rigid chains is not well experimentally studied.

In this work, as a model polymer capable to form a rigid network, we used a novel cyanobacterial polysaccharide "sacran". This negatively charged giant polysaccharide (M_w > 16 million g/mol, contour length > 10 μm), extracted from extracellular matrix of a Japanese alga, is capable to form liquid crystalline nematic phase (above 0.25 wt%) under shear, indicating the presence of rod-like rigid regimes[2]. The intrinsic persistence length is estimated to be 60 nm, thus at a micrometric scale sacran behaves as flexible chain. However, once sacran chains are crosslinked and a gel is formed, the mesh size can be comparable to the persistence length, thus at this length scale (several tens of nm), the sacran chain is expected to be rigid.

In this work, physical and chemical gels of sacran are prepared and rheologically studied. Sacran is a polyelectrolyte containing 22 mol% of carboxyl functions and 11 mol% of sulfate functions. Physical hydrogels can then be formed with specific divalent or trivalent cations[3]. In order to characterize the rheological properties of the physical gels of sacran, alkaline earth metal divalent cations, $CaCl_2$, $SrCl_2$ and $BaCl_2$ are used as physical crosslinkers. Sacran networks crosslinked by reversible ionic interactions can then be prepared. The sacran chains covalently crosslinked by using the hydroxyl groups abundantly present on the polyelectrolyte chains. The amount of the hydroxyl functions on sacran chains is estimated as 250 mol% of the monosaccharide residue[4]. Following an oxa-michael addition, these hydroxyl functions, negatively charged in basic conditions, react with divinyl sulfone (DVS) to covalently crosslink sacran chains.

The sacran gels prepared by these two different gelation methods are separately studied by rheology in order to understand the particularity of these sacran networks due to their rigidity. To probe the rheological linear regime of these sacran gels in a wide time scale and to probe the different length scales, the conventional "macrorheology" is complemented with non-conventional passive "microrheology" by single dynamic light scattering (DLS) and diffusing-wave spectroscopy (DWS). From macrorheology rheology are obtained the viscoelastic modulus at low frequencies (10^{-3} to 10 rad/s) which describe the rheology at the scale of the mesh size of the network. From microrheology are obtained the viscoelastic modulus at high frequencies (10 to 10^5 rad/s) which describe the rheology of singles polymer chains which constitute the network. The non-linear regime of sacran gels is tested by oscillatory strain sweeps in order to study their strain hardening behavior.

This thesis is composed of 6 chapters. In Chapter 1 is focused on the state of the art. Different strategies of mechanical reinforcements of hydrogels, strain hardening behavior of biological systems, and properties of sacran are briefly introduced. In Chapter 2, the materials and methods used in this work are described,

especially the different rheological techniques including passive rheology by dynamic light scattering and strain rate frequency superposition are introduced. The Chapter 3 is dedicated to rheological properties of sacran aqueous solutions. The applicability of the DLS/DWS microrheology is shown. The persistence length of the sacran is measured as a function of the concentration and its concentration dependence is discussed. In Chapter 4 linear rheological properties of the sacran physical gels are studied. Different rheological signatures of rigid network are shown to evidence the rigidity of the chains between crosslinking points. In Chapter 5 is devoted to nonlinear rheological properties of the sacran physical gels. In order to interpret strain hardening behaviors, for the divalent cations studied, the ionic crosslinking effect and the salt effect are discussed. Finally in Chapter 6 linear and nonlinear rheological properties of the sacran chemical gels are studied. A pronounced strain hardening behavior is observed and analyzed by using a nonlinear elasticity model which describe the strain hardening behavior with two structural parameters of the chain rigidity[5].

Symbols

a and b	rescaled factors of SRFS
b_K	Kuhn segment length
b	bond length
	distance between charges on the polyelectrolyte chain
C_f	ionic concentration of the solution
E_a	activation energy
G_e	elastic plateau moduli
G'	elastic moduli
G''	viscous moduli
G^*	complex moduli
$g_1(t)$	field autocorrelation function
$g_2(t)$	intensity autocorrelation function
K^{-1}	Debye-Hückel length
l_B	Bjerrum length
l_e	distance between two entanglements points
l_p	experimental persistence length
$l_{p,e}$	electrostatic persistence length
R_g	radius of gyration
$\langle \Delta r^2(t) \rangle$	mean square displacement
t_{gel}	time of stabilization of the elastic modulus
$l_{p,o}$	intrinsic persistence length
l^*	mean transport length
Q	strain-hardening ratio
β	elongation ratio
γ	strain amplitude
γ_c	critical strain amplitude
γ_{max}	strain at which the modulus starts to breakdown
$\dot{\gamma}$	strain rate
ε	drag coefficient
η_S	solvent viscosity
κ	chain bending constant
ν	scaling exponent or Flory exponent
ξ	mesh size
ρ	volumic density of polymer
$1/\tau_c$	kinetic constant
ω	frequency
ω_c	longest limit of the bending mode

1. Bibliography

1.1. Introduction of hydrogel

According to the definition of polymer gels in Dictionary of Polymers[6], "a polymer gel consists of a three dimensional crosslinked network and swells in a solvent to a certain finite extent, but does not dissolve even in a good solvent". This definition is limited to chemically crosslinked gels and excludes physical gels made by secondary molecular forces such as ionic, hydrogen bonds and hydrophobic interactions.

Hydrogels are materials useful in many applications as cosmetic, food or medical industries. Hydrogels are defined as networks composed of polymer chains that are hydrophilic. Hydrogels are highly absorbent, they can contain over 90 % of water. They can be composed by natural or synthetic polymeric networks. They also have a degree of flexibility similar to natural tissue due to their amounts of water. The swelling properties are due to the high thermodynamically affinity that this class of materials has for the solvent itself.

Nevertheless, applications of hydrogels was limited by the low mechanical behaviors of these materials which are very brittle. The mechanical reinforcement of hydrogels is then a challenge in order to further diversify the applications of hydrogels. In the past 15 years, hydrogels with a high versatility and a high tunability of their properties have been developed. Indeed, many new gel-form materials, with a plethora of aims were developed and tested in different fields of engineering (e.g. environmental, electronics, biomedical), biotechnology and other disciplines[7,8].

Since the pioneering work of Wichterle and Lim in 1960 on crosslinked HEMA hydrogels[9], and because of their hydrophilic character and potential to be biocompatible, hydrogels have been of great interest to biomaterial scientists for many years[9–12]. For example, natural hydrogel materials are being investigated for tissue engineering; these materials include agarose, methylcellulose, hyaluronan, and other naturally derived polymers.

One way to classify hydrogels is on the basis of the type of crosslinking interactions. Two general classes, chemical gels and physical gels are commonly used.

Hydrogels are called "chemical" or "permanent" gels when the polymer chains are covalently crosslinked. The activation energy of the covalent bonding is high and the network does not flow. When polymer chains are crosslinked by non-covalent interactions, such as electrostatic interactions, hydrogen bonding, hydrophobic interactions, etc, the obtained gel is called physical gel. All of these interactions are reversible, and can be dissociated by changes in conditions such as ionic strength, pH, temperature, application of stress, or addition of specific solutes with stronger affinity with the polymer. The activation energy is much lower than that of covalent bonding and the lifetime of the physical crosslinks can take various values. When the physical crosslinks are sufficiently long-lived and dissociation does not occur at the observation time scales, the physical gels behave similarly to the chemical gels. While when the physical crosslinks are short-

lived compared to the observation time scales, the network structure is transient and flows. Rheological response is similar to that of entangled polymer solutions with a terminal flow.

In general, both chemical and physical hydrogels are not homogeneous, since crosslinking points are not homogeneously distributed, polymer concentrations can have spatially heterogeneous. Hydrogels contains also 'defects' which do not contribute to the elasticity of the network, such as dangling chains and chain loops.

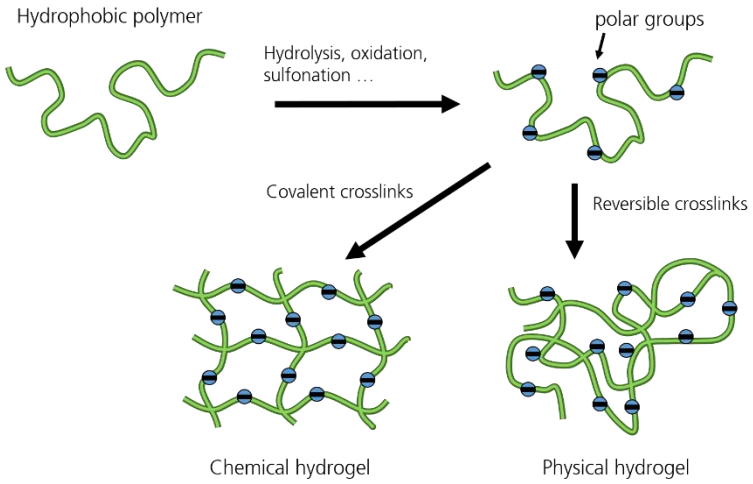

Figure 1 Schematic of methods for formation of hydrogels by chemical or physical bonding[8].

1.2. Mechanical reinforcement of hydrogels

Most of synthetic hydrogels are brittle. Their poor mechanical properties limits their applications. There are two principal reasons why the usual hydrogels are mechanically weak.

Heterogeneous network structure

The network structure of the crosslinked chains is heterogeneous. Crosslinking is in general heterogeneously distributed and the crosslinking density and the polymer concentration can vary depending on the position. Then the network is deformed, the stress can concentrate on certain weak regions and the network irreversibly breaks.

Lack of dissipative mechanism

Under large deformation, a crack can appear at a network defect and the stress can locally concentrate on the crack tip and the fracture can rapidly propagate. Usual hydrogels are very elastic but not sufficiently viscous as the solvent, water, has very low viscosity, no particular dissipative mechanism which can prevent the stress concentration exists.

Recent advancements in polymer el sciences have allowed gel scientists to design new network structures which overcome the weak points written above and mechanically tough hydrogels have been synthesized. Here we cite several examples.

1.2.1. Homogeneous gels

1.2.1.1. Slide ring gels[13,14]

One of the earliest examples of the tough hydrogels developed in the beginning of the twenty first century in Japan is a "slide ring" gel. Ito et al. have developed this novel "topological" hydrogels named topological[15]. A supramolecular architecture based on polyrotaxane, in which a number of cyclic molecules are threaded onto a linear polymer and are trapped by capping the chain with bulky end groups, is used to create movable crosslinks, as shown in Figure 2 (a). The basic concept of this reinforcement is the movable crosslinks which was theoretically Edwards et al. 25 years ago[16].

The cross-links, which consist of two cyclic molecules, can slide along the polymer chains and thereby behave as pulleys to equalize the internal stress in the hydrogel. In this sense the gel is homogeneous. The sliding motion of movable cross-links results in remarkable mechanical properties significantly different

from those of conventional polymeric materials with fixed crosslinks. Polyrotaxanes (PRs) made of α-cyclodextrins and poly(ethylene glycol) having bulky dinitrobenzene groups as end-caps, are synthesized and in solution the pairs of cyclodextrins are coupled to form sliding crosslinking points which form an interlocked figure-of-eight. Topological gels show extreme softness and strong shape recovery. Such a polymeric material with movable crosslinks was theoretically considered as a sliding gel by de Gennes in 1999[17].

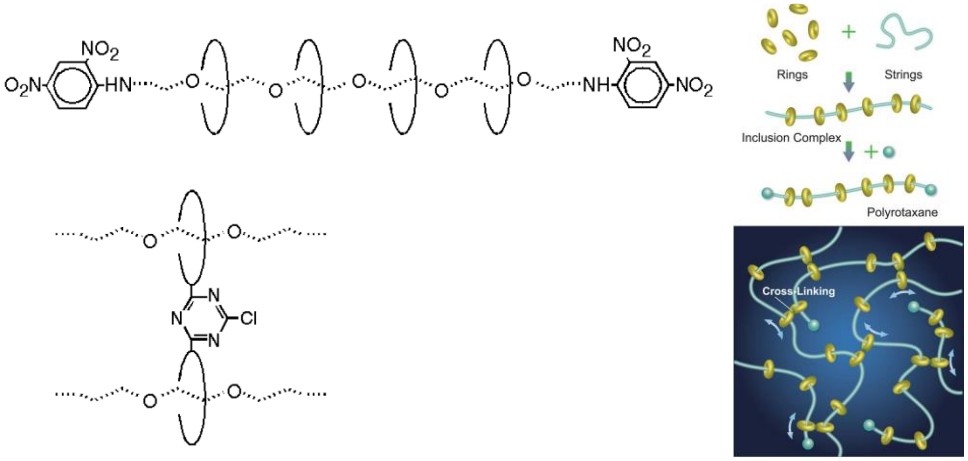

Figure 2 Schematic view of topological gels composed from PR strings and slide-rings[13].

The sliding motion of α-cyclodextrins on chains has been evidenced by dynamic light scattering by the appearance of a dynamic mode between the cooperative diffusion mode and the self-diffusion mode[18]. SANS experiments performed on hydrogels show classically an increase of the scattering intensity $I(q)$ when their crosslinking density increases. This increase is explained by the frozen inhomogeneities due to the crosslinking. This experiment was performed on slide-ring gels and lower scattering intensities than those expected have been obtained[19]. These low values are attributed to the reduction of spatial inhomogeneities in these gels which are due to the movement of the crosslinking points along chains which accommodates the macroscopic strain imposed to the network. These slide-ring hydrogels can absorb water up to 400 times their dry weight and 1600 times the weight of the PEG contained. These swelling are also totally reversible without any damage[15].

Loading-unloading tensile cycles performed on physical hydrogels classically show a J-shape and a large hysteresis in stress-strain curves due to the recombination of physical crosslinks during deformation. Conventional organic hydrogels covalently crosslinked follow an S shape but do not show hysteresis because no recombination is possible. For slide-ring gels, a J shaped curve is observed, but with no hysteresis[20]. Moreover, thanks to the pulleys properties, these gels can support strains of 2,000 %[15].

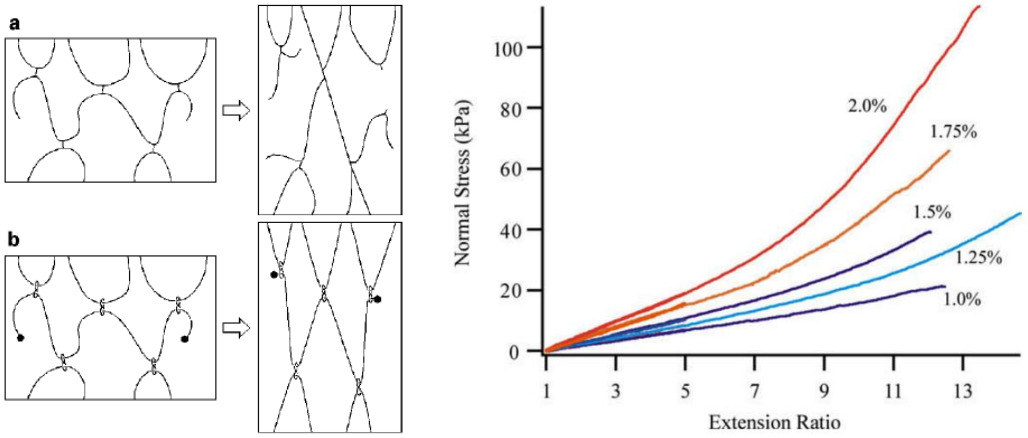

Figure 3 Left: Comparison of conceptual models between a chemical gel and the polyrotaxane gel on tensile deformation. (a) In the chemical gel elastically active chains are gradually broken because the heterogeneous distribution of crosslinks localizes the stress to a certain chains. (b) The polymer chains in the polyrotaxane gel can pass through figure-of-eight crosslinks to equalize the tensions cooperatively and avoid localization of the stress and many chains are uniformly stretched. Right: Typical J shaped stress strain curves of slide-ring gels with different concentration of crosslinkers[21].

Mechanical behavior of slide-ring gels have been studied as a function of the density of their crosslinking points and abnormal results have been obtained in regard of the conventional rubber elasticity.[22] When the density of crosslinking points increases in the studied slide-ring network, first a classical increase of its elasticity occurs, however, above a critical density, its elasticity starts to decrease. A theory of the alignment entropy of cyclic molecules in addition to the conformational entropy of polymer chains has been proposed.

1.2.1.2. Tetra-PEG gel[23]

Another strategy to reduce the inhomogeneities of hydrogels, which are one of the origins of reduced mechanical properties of hydrogels, was developed by Sakai & al. The formation of homogenous hydrogels is here produced by combining two well-defined symmetrical tetrahedron-like macromonomers of the same size. These two macromonomers have four end-linking groups which react with each other. The self-reaction is avoided in order to obtain a network composed by macromonomers alternatively connected, as schematically represented in Figure 4.

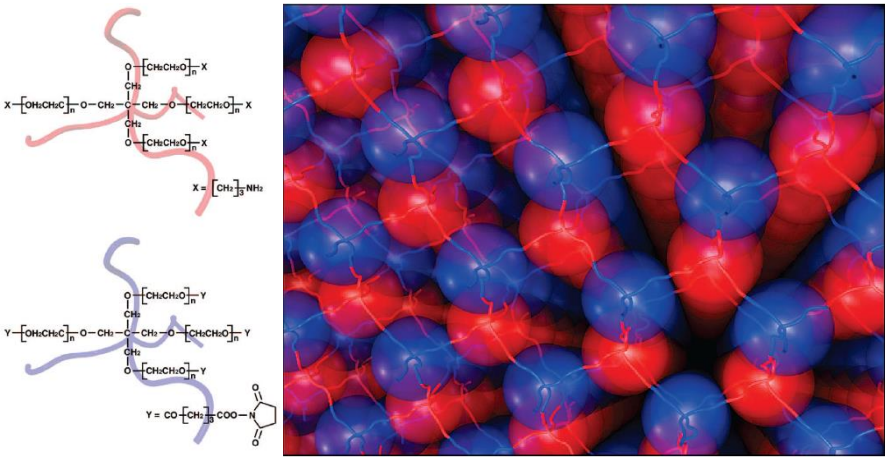

Figure 4 Left: molecular structures of TAPEG (up) and TNPEG (down). Right: Schematic illustration of the homogeneous network structure composed by these two macromonomers[23].

The two constitutive macromonomers are the tetra-NHS-glutarate-terminated PEG (notified TNPEG) and the tetraamine-terminated PEG (TAPEG). Monodisperse macromolecules are obtained from a controlled anionic polymerization with a restriction of mobility of the four arms by steric repulsion. Then a mixing of the aqueous solutions containing TNPEG and TAPEG lead the formation of the homogenous hydrogel composed of an alternation of elastic blobs without any entanglements[24,25].

These tetra-PEG hydrogels have been studied by SANS with variation of the length of their arms. Polymer gels usually exhibit an upturn in the low-q region of scattering intensity curves due to their inhomogeneities. On the contrary, tetra-PEG gels do not show any upturn confirming their homogeneity[26].

Tensile tests have been also performed in order to confirm the mechanical reinforcement of hydrogels by their homogenization. These tensile tests have been conducted for tetra-PEG gels composed of macromonomers at different molecular weights. From this study performed as a function of the macromonomers molecular weights, a threshold have been evidenced: below 10^3 g/mol, hydrogels are brittle and poorly stretchable and above this critical molecular weight they reach high deformability even compared to polyacrylamide hydrogels which the same network concentration, as presented in Figure 5.

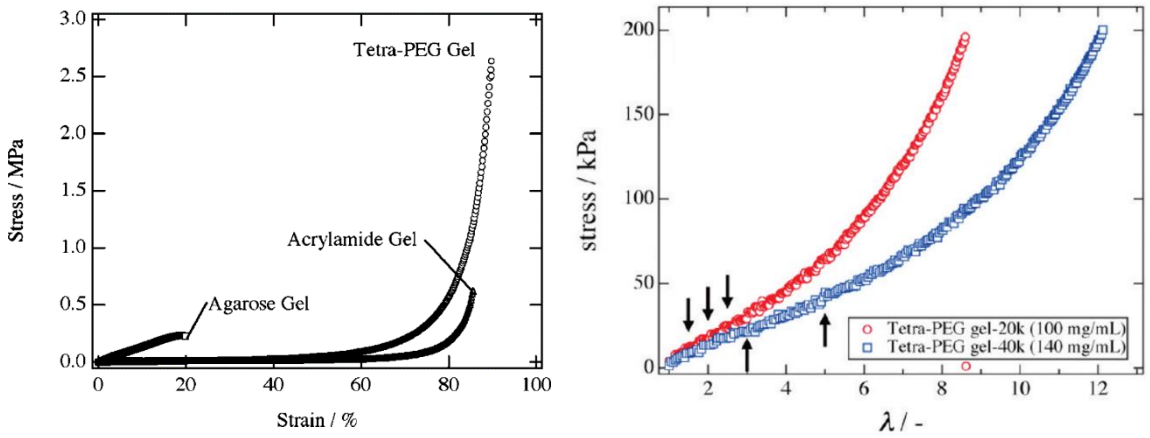

Figure 5 Left: Comparison of tensile tests performed on agarose gel, polyacrylamide gel and tetra-PEG gel for the same network concentration and the same experimental condition.[23] Right: Tensile curves of tetra-PEG gels with two different molecular weight of macromonomers (2 10^4 g/mol in red and 4 10^4 g/mol in blue[23,27].

From these tensile tests, Sakai & al. have evidenced the increase of deformability with the hydrogel homogeneity obtained from a new strategy. SANS measurements under deformation also demonstrate the absence of inhomogeneities and directly linked with mechanical behaviors observed from the deformation of these gels.[26] Finally, fracture tests have proven the absence of entanglement in these networks[28].

1.2.2. Dissipative gels

Different types of dissipative hydrogels have been reported in the last decade. Most of them are based on reversible physical crosslinks which can dissociate and reassociate to dissipate a large quantity of fracture energy.

1.2.2.1. Nanocomposite gels[29,30]

In order to increase the hydrogels dissipation, Haraguchi & al. have incorporated inorganic components into organic hydrogels and created a novel class of hydrogels named "nanocomposite hydrogels", or "(nano)hybrid hydrogels".

Nanocomposite hydrogels (NH) consisting of poly(N-isopropylacrylamide)(PNIPAm) networks reinforced by inorganic clays. PNIPAm gels are interesting due to their sensibility to external stimuli such as temperature, solvent, pH, light… These NH hydrogels are prepared by photo-initiated free-radical polymerization in the presence of exfoliated inorganic clay in an aqueous solution of NIPAm followed by the polymerization of these monomers using a redox initiation of potassium persulfate. Without addition of chemical crosslinker, these gels are defined as physical with neighboring clays connected by polymer chains. Clays act as multifunctional crosslinking agents for the PNIPAm, as represented in Figure 6. It is

important that polymer chains attached to clay sheets are flexible, taking random conformations in the space between clay sheets.

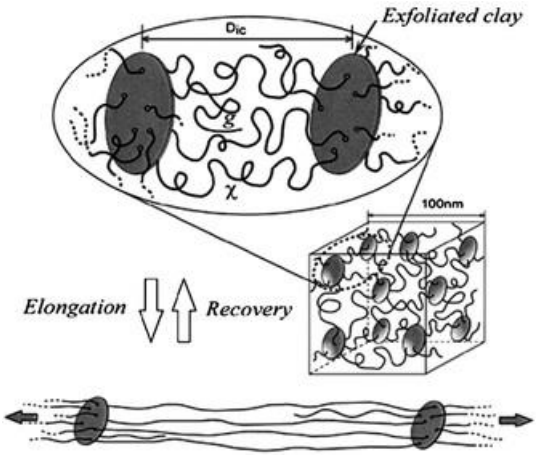

Figure 6 Structure of Haraguchi's nanocomposite hydrogels.

From these uncross-linked NH hydrogels, mechanical properties have been enhanced in terms of deformability (breaking around 1000 %) and linear modulus (several tens of kPa), as shown in Figure 7. The high deformability, compared to classic organic hydrogels, is explained by the low degree of effective physical crosslinking induced by clays. The results obtained by Haraguchi & al. are summarized in Figure 7.

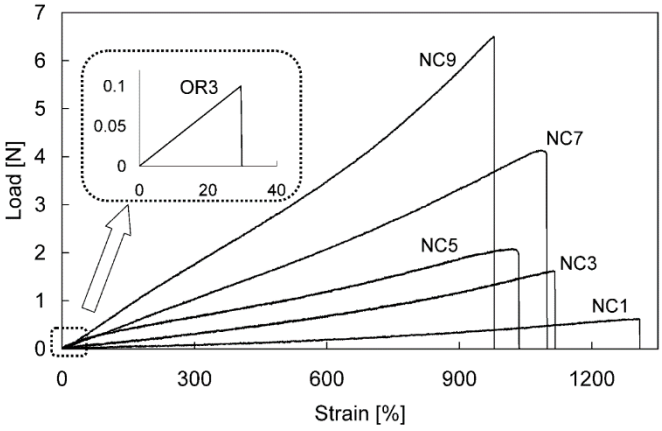

Figure 7 Stress-strain curves of nanocomposite PNIPAm/clays hydrogels composed with different clays contents (NC1 to NC9) compared with a corresponding organic hydrogel (OR3) [31].

Among them, nanocomposite gels (hereinafter abbreviated as NC gels) consisting of PNIPA and inorganic clay achieved the best mechanical properties together with excellent swelling, optical transparency, and stimuli sensitivities.

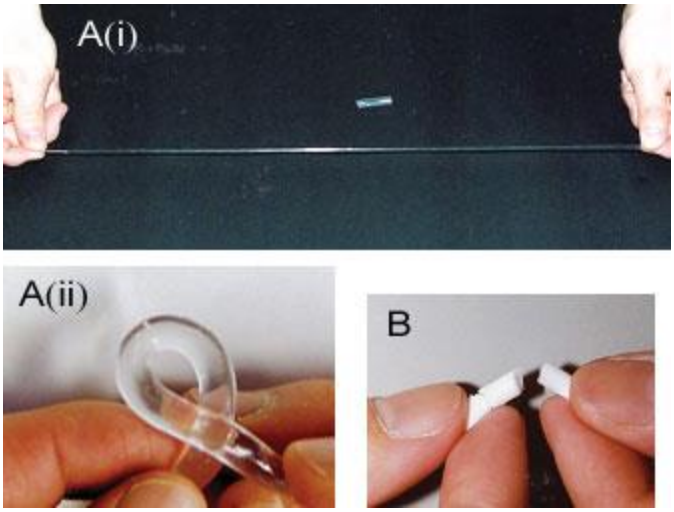

Figure 8 (a) Nanocomposites and (b) conventional gel with the same water/polymer ratio (10:1 (w/w/)). (i) elongation test (ii) torsion test[30].

NC gels exhibit striking mechanical toughness. As shown in Figure 8, they can be deformed to large extents without any sign of damage under stresses such as bending, compression, torsion or elongation. On the contrary, it is accepted that conventional hydrogels are readily fractured in any deformation modes.

The crosslinking density of nanocomposite gels and their inter-crosslinking distances can be controlled independently. Highly stable, structurally homogeneous, with extraordinary mechanical properties as a result of the polymer/clay network structure of the nanocomposite gels.

1.2.2.2. Double network gels[32,33]

The concept of double network (DN) hydrogels have been developed by Gong & al. and consists of two interpenetrating polymer networks swollen by water[32]. The first network is composed of a highly crosslinked rigid polymer network and the second is a loosely crosslinked flexible polymer network, as represented in Figure 9. The strategy of reinforcement is based on the irreversible breaking of the first network into microscopic clusters at large deformation, which can dissipate a large quantity of energy, by preventing the macroscopic failure thanks to the second network.

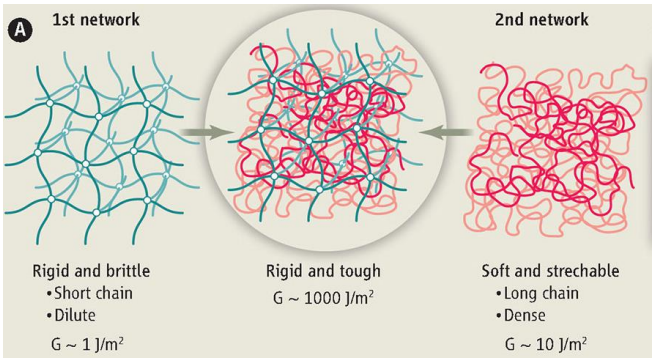

Figure 9 By combining different network materials, tough double-network materials can be created.

The first polyelectrolyte network is made of poly(2-acrylamido-2-methylporpanesulfonic acid) (PAMPS) and is interpenetrated with a neutral network composed by poly(acrylamide) (PAAm)[34]. The strategy is to find an optimum between the first rigid and brittle network and the second flexible and ductile network.

Double network hydrogels are classically synthesized from a two-step sequential free-radical polymerization. The synthesis of the highly crosslinked network of PAMPS is followed by its swelling by the second neutral monomer (AAm). The DN is synthesized by the polymerization of AAm monomers with a small density of crosslinker and the DN is then immersed in water and reaches its swelling equilibrium[32].

The molecular association have been evidenced by SANS and U-SANS and the structures of PAMPS and PAAm networks have been characterized as more homogeneous when synthesized in presence of the co-monomer than in pure water[35].

Mechanical properties observed from these DN are clearly enhanced compared with those obtained from individual components (stiffness, strength and toughness) due to a synergistic effect. A variation of the crosslinking density of the second network have showed that more it is loosely crosslinked more the gel exhibits high mechanical strength. When changing the crosslinking density of the second network from 0 to 1 mol% and by keeping constant the structure of the first network, elastic modulus around 300 kPa are obtained but highest fracture parameters are obtained from the un-crosslinked second network. DLS experiments are performed and a slow mode is observed for low crosslinking densities of the second network[36].

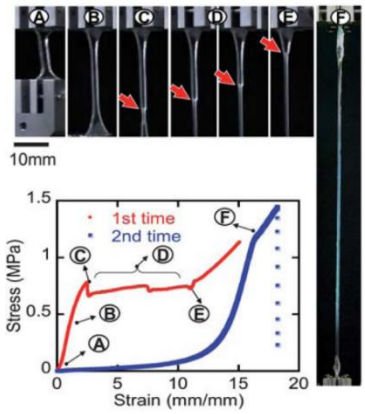

Figure 10 Uniaxial tensile test performed on a DN gel at constant rate 0.13 s^{-1}. Loading and unloading curves have been represented by following the evolution of the stress as function of the strain applied. The necking process evolution during the experiment is shown by imaging.

Uniaxial tensile tests have been performed on these DN gels and have shown a necking phenomenon. Narrowed zones appear along the sample and then grow up during elongation. This neck zone propagation is observed in stress-strain curves by a plateau region[37]. This phenomenon is attributed at the first network breaking into small clusters. These clusters play then the role of physical cross-linking points for the loosely crosslinked second network. This role is comparable with sliding cross-linker. This mechanism have been confirmed by SANS under deformation[35].

1.3. Bio-inspired reinforcement of hydrogels by rigid polymer

In the living organisms, the cells mechanics is always controlled by protein filaments. These filaments can form a network and the obtained gel shows interesting nonlinear rheological properties. This study have for goal to propose an experimental model at this behavior based on the rheological study of a semi-rigid polymer.

1.3.1. Strain hardening behavior of biological gels made of filaments

In living organisms, the cells mechanics is controlled by rigid protein filaments. A cytoskeleton is a network of filaments and tubules present in the cytoplasm, extending from the nucleus to the plasma membrane[38].

In Figure 11, different elements composing of the cytoskeleton are shown. The cytoskeleton of eukaryotic cells provides structure and organization, resistance and transmission of stresses, and drives shape change and movement. Like other eukaryotic cells, neurons have a cytoskeleton that consists of three main polymers: microtubules (green), intermediate filaments (purple) and actin filaments (red). These protein filaments can form various ordered structures in the presence of other proteins, including sheet-like structure, dendritic filaments, filaments with repelling arms, branched filaments, etc. examples are shown in Figure 11 (b)-(g).

The diameters of microtubules, intermediate filaments and actin filaments are within a factor of three of each other. But the relative flexibilities of these polymers differ markedly, as indicated by their persistence lengths: from least to most flexible, microtubules (5,000 μm) actin filaments (13.5 μm) and intermediate filaments (0.5 μm).

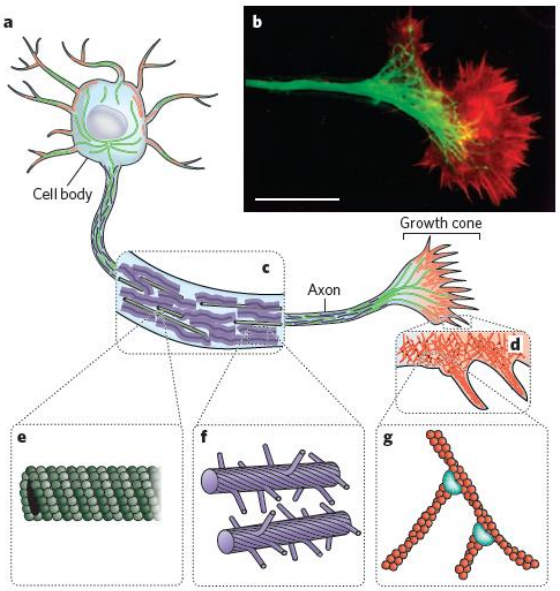

Figure 11 (a) Schematic illustrations of a neuron showing composition of cytoskeleton by filaments. (Image reproduced[39]) (b) A fluorescence micrograph of the neuronal growth cone, which migrates in response to chemical cues during the development of the nervous system. Scale bar: 20 μm. (c) The neuronal axon, a long membrane-bounded extension, in which neuro-filaments (a class of intermediate filament in neurons) form a structural matrix that embeds microtubules, which transport materials from the cell body to the axon terminals at the synapse. (d) The growth cone containing dendritic actin filament networks and parallel actin-filament filopodia. (e) Microtubules consisting of 13 proto-filaments of tubulin dimers arranged in a hollow tube. (f) neuro-filaments having flexible polymer arms that repel neighboring neuro-filaments and determine the radius of the axon. (g) Actin filaments arranged into networks.

These protein filaments commonly show a strain-hardening behavior: the viscoelastic moduli increases with increase in strain in nonlinear domains. In Figure 12, dynamic shear storage modulus measured at different strain amplitudes for a series of crosslinked biopolymer networks are shown. The ratio of the maximal modulus to that at the elastic plateau in the linear domain increases up to 10 or even higher.

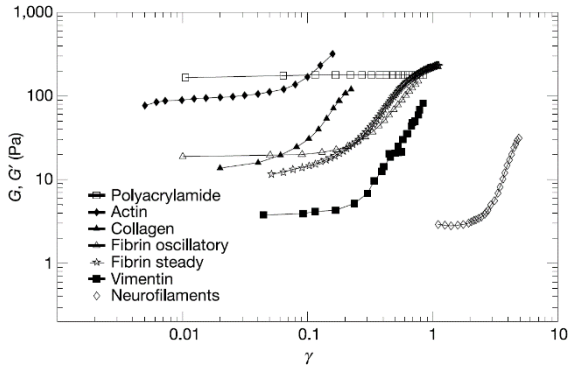

Figure 12 Dynamic shear storage moduli measured at different strain amplitudes for a series of crosslinked biopolymer networks[1].

1.3.2. Rigid polymer networks

Referring to the previous part, the strain hardening behavior could be linked with the rigidity of protein filaments. In this part, we discuss the particularity of semi-rigid (or semi-flexible) polymer chains organized in solutions or gels.

One of the properties that can characterize a polymer is the chain flexibility. Flexibility is evaluated by the two characteristic lengths of the polymer, the persistence length and the contour length. The persistence length is defined as the length over which correlations in the direction of the tangent are lost. The contour length is the end-to-end length of the chain. When the persistence length is much shorter than the contour length, the chain is considered as flexible. When the persistence length is much longer than the contour length, the chain is considered as rigid. Between the two cases, when the two lengths are comparable, the chain is semi-flexible (Figure 13).

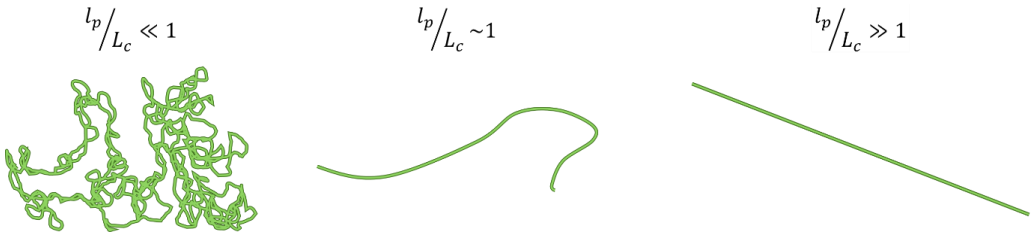

Figure 13 Schematic illustration of the three chain configurations: flexible, semi-rigid and rigid according to the relative sizes of the length of persistence and the contour length.[40]

Importantly, even for the flexible and semi-flexible chains, at the length scale shorter than the persistence length, the part of the chain can be rigid, and its mechanical properties are governed by the bending elasticity of the chain. At the length scale longer than the persistence length, the mechanics are statistically treated by the entropic elasticity of the chain. When a network is formed, the mesh size is the important characteristic length. The ratio of the mesh size to the persistence length will be an important measure of the elasticity of the rigid network (network having rigid chains between the crosslinks). In this work we work on hydrogels having a persistence length comparable to the mesh size. Different length scales in the network of semi-rigid chains are illustrated in Figure 14.

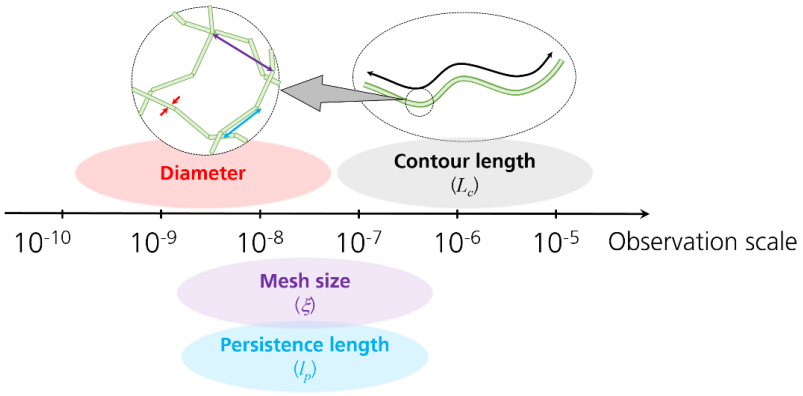

Figure 14 Diagram showing the orders of magnitude of characteristic lengths.

1.3.3. Strain hardening behavior

The main part of strain-hardening behaviors of rigid polymer networks are explained by nonlinear high tension along chains stretched beyond the Gaussian range[41–43]. Subjected to deformation, such cross-linked biopolymer networks stiffen at increasing strain, enhancing the energy needed for further deformation[44]. Theoretical studies of this strain-stiffening response consider networks consisting of numbers of filaments that, as the sample is deformed, distort in an affine manner.[1,45] However, numerical studies of discrete networks in two dimensions do show non affine behavior at low and intermediate densities[46,47].

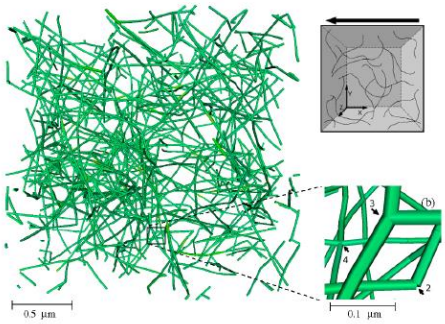

Figure 15 3D discrete network model of crosslinked filaments. (a) View of a network with filaments of initial length 1.3 μm, actin concentration 1.56 mg/ml, and average cross-link distance l_c = 0.254 μm (59.6 cross-links/μm³, 1.95 cross-links/filament). The filament radius is magnified for plotting reasons. (b) Zoom-in of a part of the network in (a), displaying cross-links that connect 2, 3, and 4 elements. (c) Schematic representation of the network in (a), with the arrow indicating the direction of the applied shear displacement in the x-y plane[48].

Figure 16 shows the network of Figure 15 at three stages of strain. The torsional energy is ignored, since it is negligibly small (the total torsional energy is 2 % of the total energy at Γ = 0.1, 0.3 and 0.5%. The color of each element corresponds to the value of the normalized energy difference $(E_{ax} - E_{bn})/\bar{E}$ (< 0 red; ~ 0 green; > 0 blue), where E_{ax} and E_{bn} are the axial stretching energy and bending energy, respectively, and $\bar{E}$ is the network's total energy at each strain level. At small strains, most elements in the network are in a state of bending. However, as the network is deformed, filaments reorient in the direction of strain by rotation and translation, resulting in percolations of stretched filaments connecting the top and bottom of the representative volume element. This is seen in Figure 16 (c) by the strings of blue elements. The reorientation of filaments can be viewed by zooming into the network, in Figure 16 (d) and (f). The highlighted red section reorients at intermediate strains (Γ < 0.3) and stretches at larger strains.

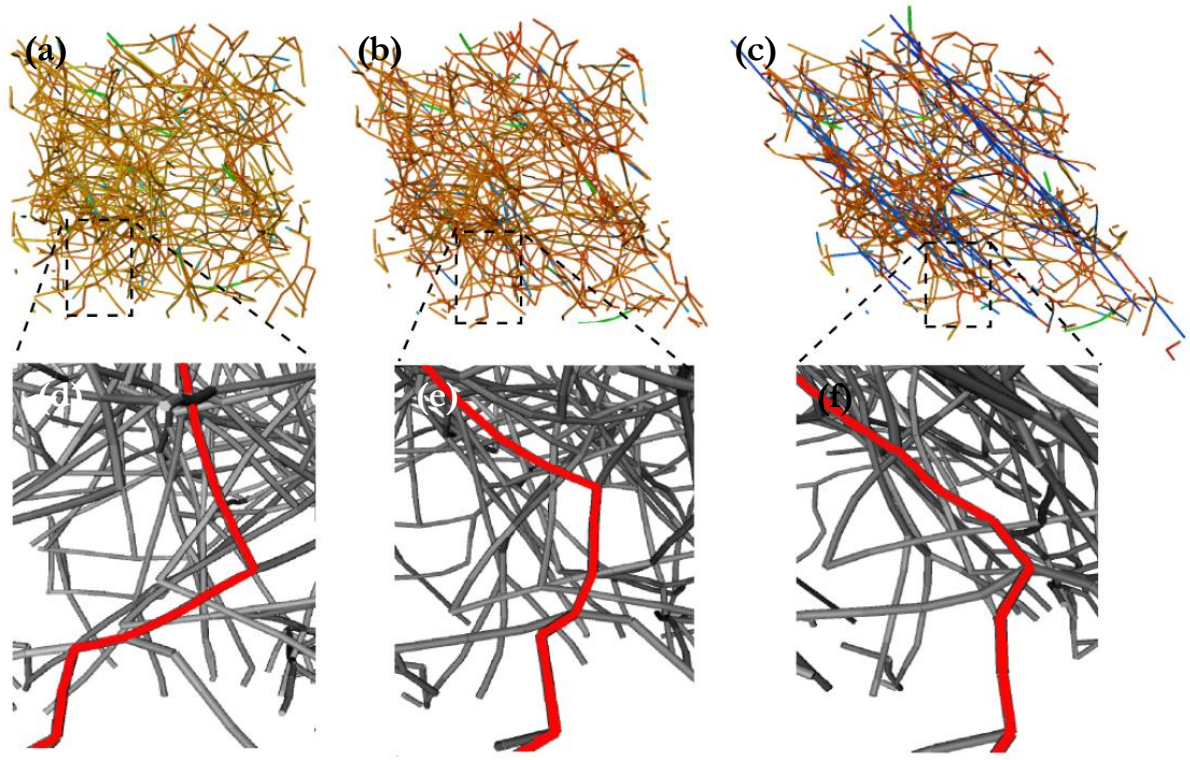

Figure 16 Network of Figure 15 under shear at different strain levels. (a) $\Gamma = 0.1$, (b) $\Gamma = 0.3$ and (c) $\Gamma = 0.5$. The color of each element corresponds to the value of the normalized energy difference $(E_{ax} - E_{bn}) / \bar{E}$ (< 0 red; ~ 0 green; > 0 blue), where E_{ax} and E_{bn} are the axial stretching energy and bending energy, respectively, and $\bar{E}$ is the network's total energy at each strain level. The lower-left region of the RVE is enlarged in (d),(e),(f) to highlight a network section (in red) that reorients and stretches under deformation[48].

Actin networks have been intensively studied in order to understand the correlation between the structure of the actin bundles and the strain-hardening behavior observed for these gels. Actin globular proteins are able to associate themselves in large and rigid filaments forming double helical structure, with contour length and persistence length around 10 μm. The strain-hardening behavior observed in actin gels is caused by nonlinear high tension along actin filaments. When the stress applied to an actin network increases, actin filaments align themselves along the stress axe. These aligned filaments form anisotropic structures.

Biological and polymeric networks show highly nonlinear stress-strain behavior manifested in materials that stiffen with increasing deformation. For such networks, their deformation can involve both filament's bending and stretching, where the latter can be either entropic or enthalpic nature[49]. An attempt to describe the different types of deformation for rigid and flexible chains has been made and a universal model has been proposed.

A unified chain deformation model that describes the force deformation curve in terms of the chain bending constant κ and the bond length b. Figure 17 shows a diagram of the different strain regimes as a function of the reduced force applied to the network ($\tilde{f}$) and the effective chain bending constant, κ. The reduced force applied to the network is written as[5]:

$$\tilde{f} = fb \,/\, (k_B T)\,, \qquad 1$$

where f is the applied forces to the network, b is the bond length and T is the absolute temperature. For flexible chains having a low bending constant, the linear deformation regime is found at $\tilde{f} < 1$. With an increase in the reduced force, the non-linear deformation regime appears, in which the chain behaves as flexible chain described by the freely-jointed chain (FJC) model (the FJC mode describes a polymeric chain with a constant bond length and no correlations between the directions of these different bond vectors). With an increase in the bending constant, the chain becomes more rigid and another non-linear deformation regime appears in which the chain behaves as rigid chain described by the wormlike chain (WLC) model (the WLC model is a special case of this freely rotating chain model which limits the bond angles at very small values ($\theta \ll 1$)). This result indicates that the bending elasticity is dominant for the rigid chains. The value of the reduced force corresponding to the transition between the linear deformation regime and the non-linear WLC deformation regime decreases with an increase of κ.

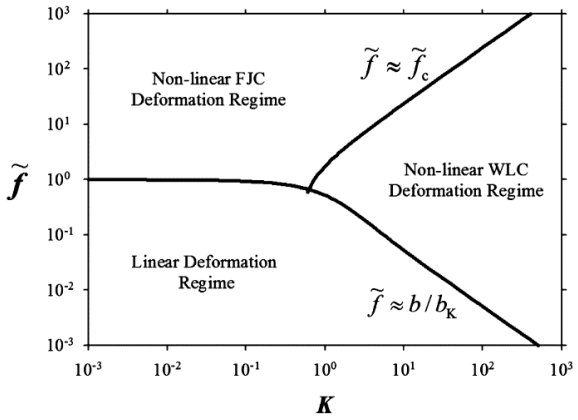

Figure 17 Diagram of different strain regimes. $\tilde{f}$ is a reduced force, $\tilde{f}_c$ the crossover force, b is the bond length, b_k is the Kuhn length and κ is the effective chain bending constant[5].

Figure 18 describes the different deformation regimes as function of the deformation parameter βI_1 and the effective chain bending constant (κ). The elongation ratio (β) is defined as the ratio of the mean-square distance between the crosslinks in the undeformed chain and the square of the end-to-end distance of the fully stretched chain. I_1 is the first strain invariant of the deformation matrix, written as:

$$I_1(\{\lambda_i\}) = {\lambda_x}^2 + {\lambda_y}^2 + {\lambda_z}^2\,. \qquad 2$$

For shear deformation, $I_1(\gamma) = \gamma^2 + 3$.

At low elongation ratio, the entropic stretching control the elastic response of the network and, at very high elongation ratio. For network made from non-extensible chains the value of the deformation parameter βI_1 cannot exceed 1. For real chains, deformation of the segment length and angle can be expected. This corresponds to the bond stretching regime in the diagram. Between these two regimes, depending on the chain flexibility, two others regimes appear. The nonlinear FJC network deformation describes the nonlinear

behaviors at medium elongation ratio of flexible networks. The nonlinear bending deformation describes the nonlinear behaviors rigid WLC chain.

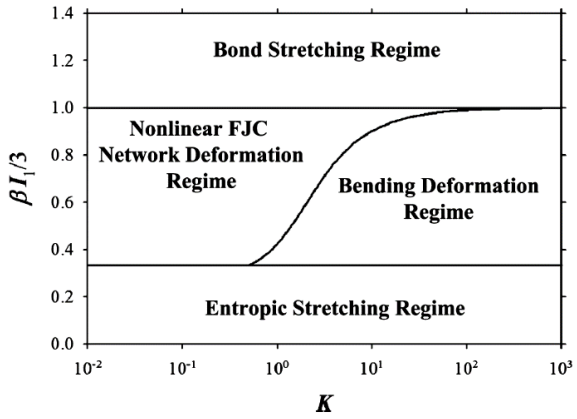

Figure 18 Diagram of different network deformation structure depending of $\boldsymbol{\beta I_1/3}$ (where $\boldsymbol{\beta}$ is the elongation ratio of the elastically active chain segment and $\boldsymbol{I_1}$ is first strain invariant of the deformation matrix) and $\boldsymbol{\kappa}$ the bending modulus[5].

With this model, the shear stress in the deformation can be written as[5]:

$$\sigma_{xy}(\gamma) = \frac{G\gamma}{3}\left(3 + \frac{2b_k}{b}\sqrt{\kappa^2 + \left(1 - \frac{\beta(\gamma^2+3)}{3}\right)^{-2}} - \frac{2b_k}{b}\sqrt{\kappa^2+1}\right), \quad 3$$

where γ is the shear strain, G is the network shear moduli, b_k is the Kuhn length, b is the bond length, β is the elongation ratio and κ is the effective chain bending constant.

1.4. Sacran, semi-rigid polysaccharide

A novel polysaccharide extracted from the extracellular matrix of a Japanese algae is used as model system of a rigid network hydrogel to study its rheological properties with the view of the bio-inspired mechanical reinforcement of hydrogels based on the rigidity of the chains. In this section, physical and chemical properties of this polysaccharide "sacran" are summarized. This polysaccharide was extracted for the first time in 2009 and its industrialization is ongoing.

1.4.1. Extraction

Sacran was extracted from the extra-cellular matrix from *Aphanothece Sacrum,* a fresh water cyanobacterium. Briefly, the bacteria samples were freeze-thawed and washed in pure water, followed by lyophilization. The samples were washed in ethanol, and then collected by filtration. The ethanol-washed samples were agitated in 0.1 mol/L NaOH aq. at 100 °C for 4 h to yield the transparent solution. The solution was dialyzed with water for more than 72 h, and was then filtrated. The filtrate was concentrated and the polysaccharide was precipitated as white fibers into isopropanol. The fibrous precipitates in isopropanol were collected and dried using a vacuum oven[2,50] (Figure 19).

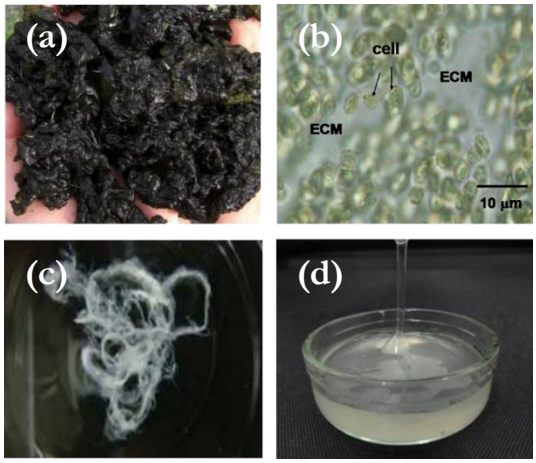

Figure 19 (a) Photograph of *A. Sacrum* in natural environment in the rivers of Kyushu, an area of Japan. (b) Photograph of *A. Sacrum* and microscopic imaging showing that extra-cellular matrix is present between cells. (c) Sacran fibers formed by the precipitation of an aqueous solution eluted in isopropanol. (d) Sacran solution at 0.5 wt%.

The extraction yield of sacran is around 70-80 wt% from dry *A. Sacrum* which means the main component of the extra-cellular matrix. TEM and AFM studies on sacran show that the contour length of chains are higher than 10 µm.

1.4.2. Composition

Sacran is a heteropolysaccharide composed of various monosaccharide residues. It contains as main monosaccharides: D-Glucose, D-Galactose, D-Mannose, D-Xylose, D-Rhamnose, D-Fucose, D-Galacturonic acid and D-Glucuronic acid, with composition ratio of 25.9 : 11.0 : 10.0 : 16.2 : 10.2 : 6.9 : 4.0 : 4.2 and contain some traces (around 1 mol%) of D-Arabinose, D-Galactosamine (cationic) et Muramic acid (amphoteric). Sacran is a polyelectrolyte negatively charged and contains 22 mol% of carboxyl functions ($-COO^-$) and 11 mol% of sulfonate functions ($-SO_3^-$). Structures of sacran (steric conformation of hydroxyl groups or other substitutes) are under investigation.

1.4.3. Liquid crystalline properties

In aqueous solutions, sacran can form nematic liquid crystalline phases even at lower concentrations than 0.5 wt%. as shown in Figure 20 (a), a 0.5 wt% solution of sacran in a glass dish illuminated by polarized white light shows Schlieren textures, a sign of nematic phases[2]. The presence of the nematic liquid crystals at low concentrations indicates that the sacran chain has high rigidity. It is hypothesized that the LC domains originate from the double helix structuration of sacran chains when the sacran concentration is above 0.5 wt%. Images by different microscopies suggest the presence of rigid bundles of sacran chain, eventually forming a loosely wound helices, Figure 20 (b-d).

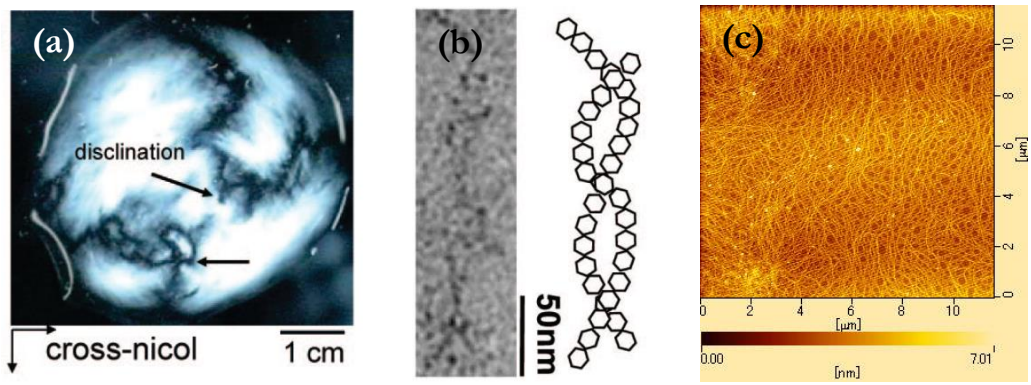

Figure 20 (a) Image of cross-polarized optical microscopy of a 0.5 wt% aqueous sacran solution and demonstration of a nematic phase; (b) Image of Atomic Force Microscopic (AFM) dried sacran chains from 10^{-4} wt% solution on mica substrate; (c) Image of Transmission Electron Microscopic (TEM) of dried sacran on a carbon-coated Cu grid and illustration of speculation on the helical shape of the sacran chains; (c) AFM images of dried sacran chains from 0.5 wt% solution[2].

1.4.4. Interactions with cations

Sacran is composed of multiple carboxyl and sulfate functions on sacran chains, and these negatively charged groups are used to ionically crosslink the chains by divalent or trivalent cations. A gelation study is performed by our Japanese collaborators by using various divalent and trivalent cations[3]. The beads formation test is performed: a droplet of sacran solution at 0.5 wt% is dropped in solutions of the cations

at various concentrations, and instantaneous formation of gel bead is observed as shown in Figure 21. The test shows that divalent cations of Mg^{2+}, Ca^{2+}, Mn^{2+}, Co^{2+}, Ni^{2+}, Cu^{2+} and Zn^{2+} do not form gel beads, Fe^{2+} induces precipitation of sacran chains and with Sr^{2+}, Ba^{2+} and Pb^{2+} gel beads are formed.

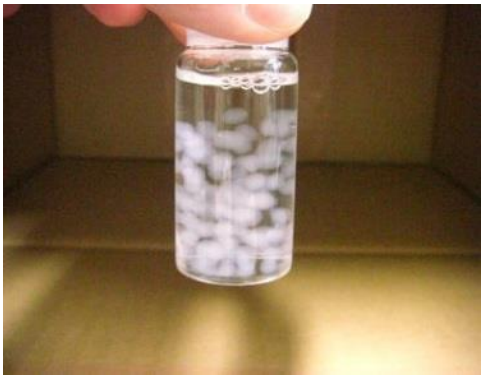

Figure 21 Image of gel beads formed by dropping polysaccharide solutions at a concentration of 0.5 wt% into alkaline and acid solutions of $YbCl_3$ [3].

If only the ionic interactions between negatives charges of sacran chains and divalent cations conduced to the gel bead formation, metal ions which have smaller ionic radius should be more effective crosslinkers. The results of beads formation for the four : Mg^{2+}, Ca^{2+}, Sr^{2+} and Ba^{2+} show that more the ionic radii of the cation is big, more the gelation of sacran is efficiency. The ionic radius of Mg^{2+}, Ca^{2+}, Sr^{2+} and Ba^{2+} are respectively 72, 100, 113 and 136 pm. The results show that the gelation is most effective when the size of the crosslinking cations is larger. A good correlation is observed between the intensity of the gelation and the radius of the crosslinking ion.

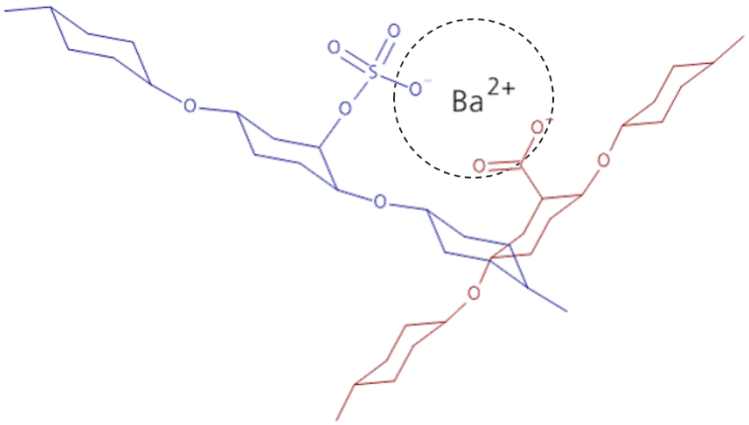

Figure 22 Schematic view of physical bonding (ionic) by interaction between a Ba^{2+} divalent cation and carboxyl or sulfonate functions of two sacran chains (blue and red), the ionic sizes observed in this pictures are not representatives.

Sacran is then able to be physically crosslinked by various divalent or trivalent cations which reacted with carboxyl and sulfate functional groups of sacran chains as shown in Figure 22. In order to define the

particular affinity of sacran chains with ions, a comparison with ions capable to crosslink alginate chains is showed in Figure 23. It is demonstrated that Lanthanides can crosslink sacran but not alginate.

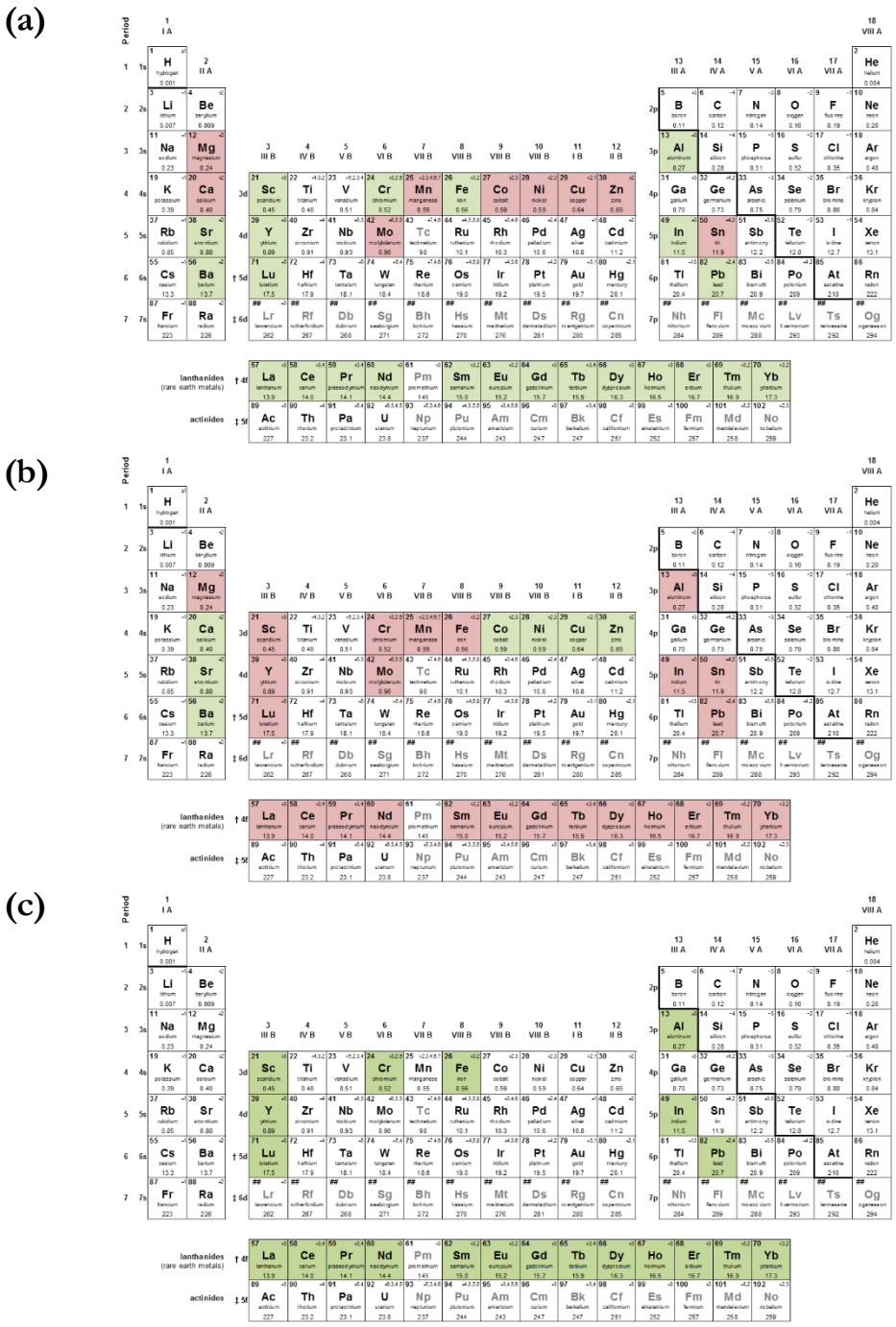

Figure 23 (a) table of ions able to form sacran gel (green) or not (red); (b) table of ions able to form alginate gel (green) or not (red); (c) table of ions able to jellified sacran chains but do not form alginate gels.

In order to compare the influence of ion species on gel elasticity, in this work of thesis we focus on Ca^{2+}, Sr^{2+} and Ba^{2+}. These three ions in alkaline earth metal family have been chosen in order to understand the gelation properties of Ca^{2+} by comparing the other ions. Sacran physical gels are prepared by simply mixing the solutions of sacran, and ion by adjusting their concentrations.

Divalent and trivalent cations are capable to form ionic interactions with sacran chains, but have also particular stabilization behaviors of proteins, named kosmotropy.

When the kosmotropic effect of an ion increases the attraction between the proteins increases with. The kosmotropy is linked with the charge density. When the charge density increase, the water around the ion is arranged. This effect is called salting-out and conduced to the precipitation of proteins. The kosmotropic effect is typically observed at salt concentrations between 0.01 and 1 mol/L.

The kosmotropic effect is classified by the Hofmeiser series which describes the ranking of the (salting-out and salting-in) ions to precipitate proteins. This series is based on the charges density of the ion.

1.4.5. Ionic gelation & water-water interactions

Ions introduced in polysaccharide chains to ionically crosslinked them are also able stabilized or destabilized water-water in the system. These interactions lead a stabilization of polysaccharide structure. This effect is classified by the Hofmeiser series[51].

Attempts to understand the Hofmeister Series at the molecular level has yielded numerous hypotheses, many of which refer to the way different salts modify the structural and dynamical properties of water. The most famous, and at the same time the most controversial, is the classification of cosolutes and ions as structure breakers (chaotropes) or structure-makers (kosmotropes), and their identification as salting-in and salting-out agents, respectively.

The terms "kosmotrope" (order-maker) and "chaotrope" (disorder-maker) originally denoted solutes that respectively stabilized or destabilized proteins or membranes. The kosmotropic behavior is linked with the property of increasing, or decreasing respectively, the structuring of water. Recently, the terms kosmotropes and chaotropes have been quantified in terms of hydrophobicity and hydrophilicity. Although useful, the terminology may sometimes be misleading as such properties may vary depending on the circumstances, method of determination or the solvation shell(s) investigated. For example a solute may not always act in the same way at different concentrations or in the presence of macromolecules or gels[52]. However, the extent of the hydrogen bonding quality is overriding. Kosmotropes shift the local equilibrium:

$$less\ dense\ water\ (\sim Expanded\ structure) \rightleftharpoons more\ dense\ water\ (\sim Collapsed\ structure),$$

to the left and chaotropes (which destroy the natural hydrogen bonded network of water) shift it to the right. Temperature and pressure both have effects on the kosmotropic/chaotropic status with the effects disappearing at high temperatures, particularly at high concentrations.

Ionic kosmotropes have influence on the directed and polarized arrangements of the surrounding water molecules. They have effects on the properties of water outside their immediate solvation shells[53,54]. Generally, kosmotropic effect of ions are described by the Hofmeister series. Large singly charged ions,

with low charge density, exhibit weaker interactions with water than water with itself and thus interfering little in the hydrogen bonding of the surrounding water. They are then defined as chaotropes. Whereas, small or multiply-charged ions, with high charge density, are kosmotropes. They exhibit stronger interactions with water molecules than water with itself and therefore capable of breaking water-water hydrogen bonds.

It is not unreasonable that a solute may strengthen some of the hydrogen bonds surrounding it, whilst at the same time breaking some other hydrogen bonds, so adding to the confusion in nomenclature.

The kosmotropic effect is classified by the Hofmeiser series which describes the ranking of the (salting-out and salting-in) ions to precipitate proteins. This series is based on the charges density of the ion. In Figure 24, the ions used in the study of sacran gelation are represented as spheres of different sizes which describe the evolution of their ionic radius.

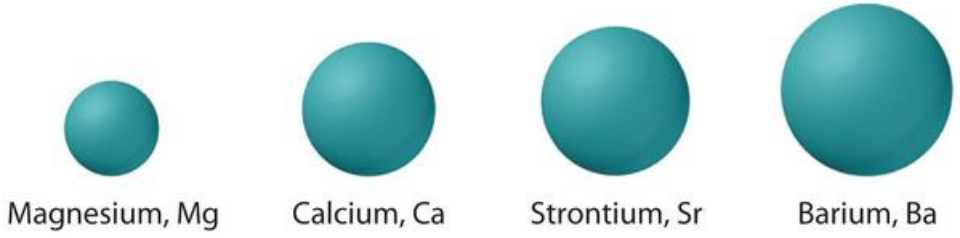

Figure 24 Schematic view of the ionic radii of cations from the earth alkali metals column: Mg^{2+}, Ca^{2+}, Sr^{2+}, Ba^{2+}; respectively equal to 86, 114, 132 and 149 pm.

This series basically describes the attraction between proteins as higher in presence of ions with higher charges density. Salting-out ions induce an increase of the viscosity and a decrease of the rotational decay of water. Salting-in ions induce the inverse behaviors. The strength of ion-water interactions affects the dynamics of water.

2. Material & Method

2.1. Sacran, semi-rigid polysaccharide

2.1.1. Aqueous solutions

After its extraction, sacran is stocked as its dry fibrous form, Figure 25 (a). These sacran fibers are dissolved in water at 90 °C for 48 hours in order to obtain a stock solution of 1 or 2 wt%. The sacran solution is very viscous and slightly colored, due to a very small amount of residual chlorophyll or other organisms, Figure 25 (b). It is very difficult to dissolve the sacran at a higher concentration than 2 wt% due to the high viscosity. The stock solution is then diluted with water at room temperature in order to obtain the sacran concentration wanted, typically between 0.1 and 0.5 wt%.

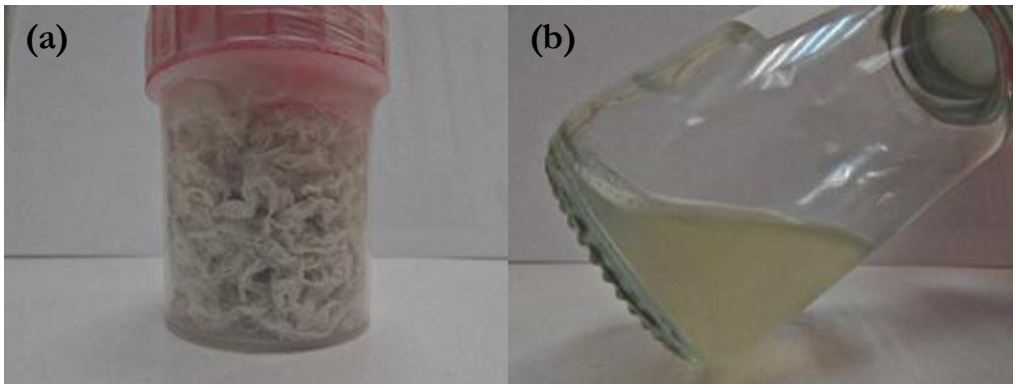

Figure 25 (a) dried sacran after extraction; (b) 1 wt% sacran solution.

The sacran aqueous solution are considered as shear thinning viscoelastic fluid. The elastic modulus is lower than the viscous one in the entire frequency range measured by standard rheology and which defined the rheological responses of the macroscopic material. The viscosity as a function of the shear rate for different sacran concentrations are shown in Figure 26. The viscosity is dependent of the chain concentration even for low concentrations of sacran. At 0.01 wt%, sacran solution have a viscosity around 0.1 Pa s and for 1 wt% the viscosity reaches 300 Pa.s. Sacran solutions become complex to manipulate above 0.5 wt%, for this reason the sacran concentration used for this study will be 0.5 wt% in order to obtain elastic gels possible to manipulate.

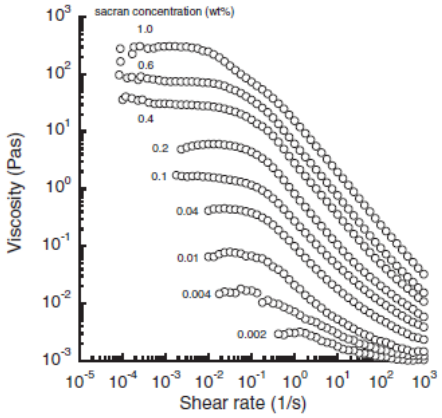

Figure 26 Evolution of the viscosity as function of the shear rate for sacran aqueous solutions concentrated by different amount of sacran[4].

Sacran solutions are then described as very viscous liquids with a viscosity very dependent of the chains concentration. Above 0.5 wt%, sacran solutions become complex to manipulate, but more concentrated materials could be obtained by drying. The persistence length is very dependent of the chains concentration.

2.2. Rheological setups

2.2.1. Macroscopic rheology

2.2.1.1. Macrorheology applied to hydrogels

Viscoelastic materials can be characterized by dynamic experiments when a sinusoidal oscillating stress or strain is applied to the material. For an ideal elastic solid the stress will be in phase with the strain whereas for an ideal liquid there will be a 90° phase difference between the stress and the strain. If the material is viscoelastic then the phase angle will be between 0 and 90° (Figure 27).

Frequently the rheological parameters G', G'' and δ are used where G' (the elastic modulus) is the ratio of the stress component in phase with the strain/strain and G'' (the viscous modulus) is the ratio of the stress component 90° out of phase with the strain/strain. The loss angle (δ) is given by:

$$tan\ \delta = G''/G'. \qquad 4$$

Analysis of the results of the above experiments is greatly facilitated if the viscoelastic behavior is linear. That is to say the ratio of stress to strain at any particular time or frequency is independent of the magnitude of the applied stress or strain.

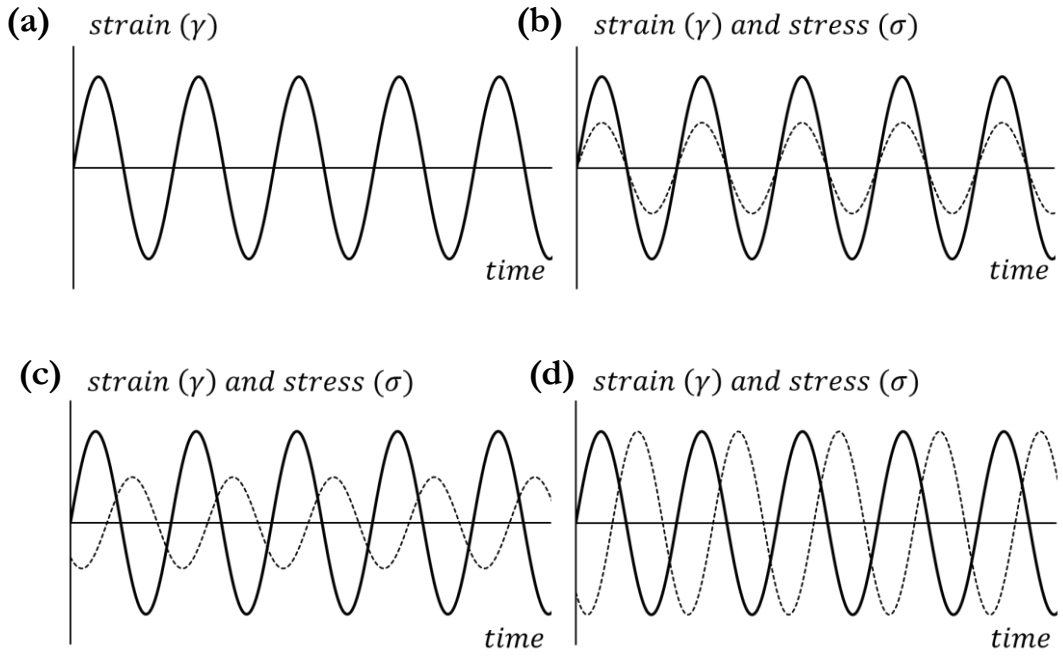

Figure 27 (a) Dynamic experiment showing response for (b) an elastic solid (stress and strain in phase), (c) a liquid (stress and strain 90° out of phase) and (d) a viscoelastic material (phase difference between 0 and 90 °)[55].

2.2.1.2. Conventional rheometer

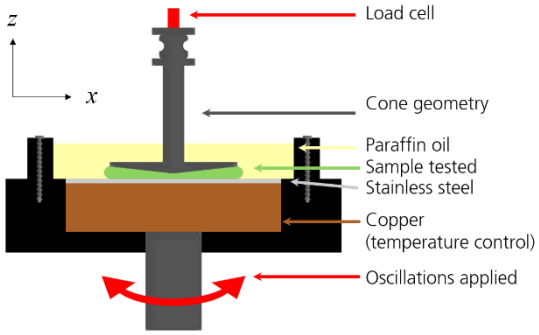

Figure 28 Schematic view of the strain controlled rheometer equipped with a cone/plate geometry. The geometry is trapped in an oil bath.

A strain-controlled ARES LS1 rheometer equipped with a rough cone and plate geometry (diameter: 25 mm, angle: 2°) composed of titanium and stainless steel, respectively. Each measurement was repeated twice to ensure reproducibility. The temperature was controlled at 25 °C by an Effet Peltier (Figure 28). After sacran physical gelation, samples are placed into the measurement geometry and the following three tests are consecutively performed.

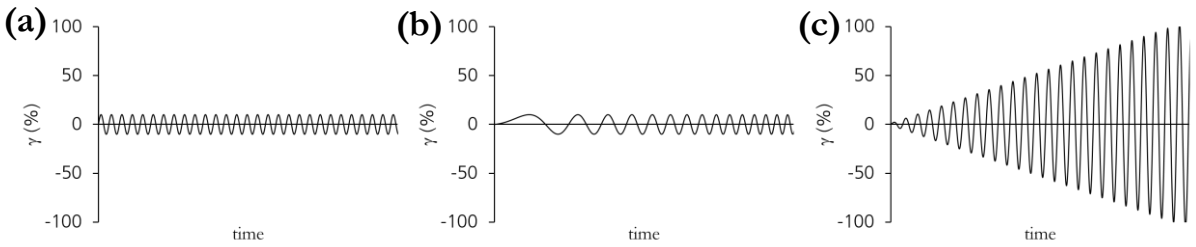

Figure 29 Schematic views of tests performed in this study from standard rheology at 25°C, (a) time sweep at constant frequency (6.28 rad/s) and strain (1 %); (b) frequency sweep at constant strain (1 %); (c) strain sweep at constant frequency (6.28 rad/s).

The same tests are performed in series for each sample tested by standard rheology in order to obtain a complete rheological study of each samples:

First, a dynamic time sweep is performed in order to measure the modulus evolution during time and follow the gelation kinetics (6.28 rad/s, 1 %), Figure 29 (a). A frequency sweep is then performed (between 0.1 and 100 rad/s) at fixed amplitude is performed in the linear domain (1 % of strain) in order to obtained rheological information in the linear domain of samples, Figure 29 (b). Finally, a destructive strain sweep (between 1 and 100 %) is performed to probe the non-linear domain of samples tested (this test is performed at 6.28 rad/s), Figure 29 (c).

The drying of hydrogels tested is blocked by using an oil bath which cover the sample tested by standard rheology. The oil is a paraffin extra fluid with a viscosity around 110 mPa.s at 20°C.

2.2.1.3. Strain Rate Frequency Superposition (SRFS)

Many soft solids, such as concentrated colloidal suspensions, foams, associating polymer solutions or hydrogels crosslinked by very weak interactions, show remarkably similar rheological responses. Their storage modulus G' is only weakly dependent on frequency and at most of the frequencies it is higher than the loss modulus G''. An example of the frequency dependence of the viscoelastic moduli of a suspension of hydrogel particles is shown in Figure 30 (a). A crossover between the elastic modulus and the viscous modulus can be observed at further lower frequency, corresponding to the transition from solid-like to liquid-like behavior. For many soft solids, the accessible frequency range by classical frequency sweep tests is not low enough to observe this structural relaxation.

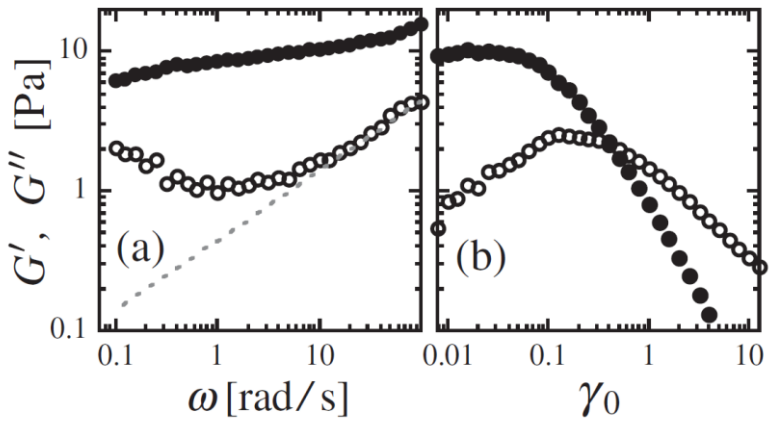

Figure 30 Oscillatory measurements of G' (solid circles) and G'' (open circles) as function of (a) the frequency (at constant strain, 2%); (b) the strain amplitude (at constant frequency, 1 rad/s) for a suspension of hydrogel particles.

In Figure 30 (b), a standard strain sweep test performed at constant ω varying the strain amplitude is observed. Above a critical yield strain, the storage modulus decreases as $G'(\gamma) \sim \gamma^{-\upsilon'}$. By contrast, the loss modulus increases in order to draw a well-defined peak before falling as $(\gamma) \sim \gamma^{-\upsilon''}$. These two power laws are typically defined by a ratio of $\upsilon'' \sim \upsilon'/2$ between the slope of the viscous modulus and the elastic one.

Other commonly used rheological test is the strain sweep at a constant frequency, probing the viscoelastic response at a fixed time scale. As shown in Figure 30 (b), with an increases in the strain amplitude, a crossover of G' and G'' can be observed. This result indicates that when the strain rate becomes important, it can drive the slow structural relaxation at the time scale of the strain rate, thus the probe frequency is not the only important time scale.

For oscillatory measurements, the natural scale of strain rate is $\dot{\gamma}_0 = \gamma_0 \omega$. Thus, if a structural relaxation process is present, its time scale $\tau(\dot{\gamma}_0)$ depends on the applied strain-rate amplitude as:

$$\frac{1}{\tau(\dot{\gamma}_0)} \sim \frac{1}{\tau_0} + K\dot{\gamma}_0{}^{\upsilon}. \qquad 5$$

However, in traditional strain or frequency sweeps, the amplitude of the strain rate varies for each data point. This makes it difficult to discern the effects of strain rate on the time scale $\tau(\dot{\gamma}_0)$ of a structural relaxation process. In order to solve this problem, frequency sweeps at constant strain rate amplitude ($\dot{\gamma}_0$) is proposed (Figure 31). This sweep is achieved by applying a strain amplitude inversely proportional to the oscillation frequency. As example, the results of the frequency sweep at constant strain rate are shown in Figure 32. At low frequencies, the response is liquid-like: G'' is larger than G'. At higher frequencies there is a pronounced peak in the loss modulus, followed by a shallow minimum and a final slow increase at the highest frequencies. The storage modulus rises continuously until it reaches a plateau where it shows only a very weak frequency dependence.

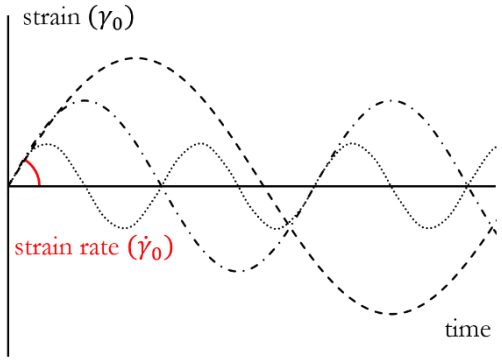

Figure 31 Schematic views of oscillatory frequency sweeps performed at constant $\dot{\gamma}_0$ for SRFS.

To highlight the striking similarities in the shape of the viscoelastic response, we shift the moduli in both magnitude and frequency, using $G^*_{scaling}(\omega) = G^*(\frac{\omega}{a(\dot{\gamma}_0)})/b(\dot{\gamma}_0)$, where a and b are the shift factors for the frequency and the magnitude, respectively.

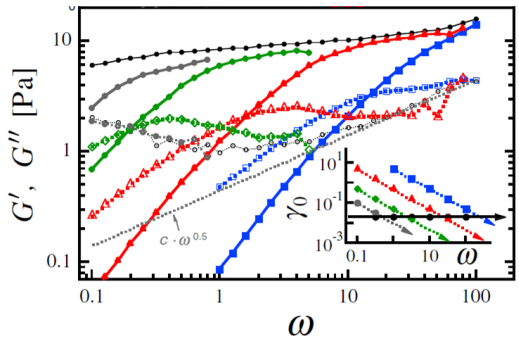

Figure 32 Frequency dependent of G' and G" for a suspension of hydrogel particles. Inset: schematic representation of SRFS series performed on the suspension of hydrogel particles $\dot{\gamma}_0 = \gamma_0\omega$. The strain rate is varied from 0.01 to 5 s^{-1}.

All the data can be superimposed onto a single master curve, as shown in Figure 33. The shift factors are plotted in the inset of the figure as a function of $\dot{\gamma}_0$. The value of $b(\dot{\gamma}_0)$ are almost constant less over the entire range of $\dot{\gamma}_0$ when $a(\dot{\gamma}_0)$ increases linearly with $\dot{\gamma}_0$. At low strain rates (less than 1 s^{-1}), the dependence between $a(\dot{\gamma}_0)$ and the strain rate asymptotically approaches unity, which suggests that the imposed strain rate is sufficiently low that it no longer impacts the viscoelastic behavior. At large strain rates (up to 1 s^{-1}), a power law dependence as $a(\dot{\gamma}_0) \sim \dot{\gamma_0}^{\upsilon}$, with $\upsilon \sim 1$, is observed. The observed scaling behavior is a direct consequence of a structural relaxation process, which leads to a decrease in $G'(\omega)$ and a concomitant peak in $G"(\omega)$ in linear viscoelastic measurements.

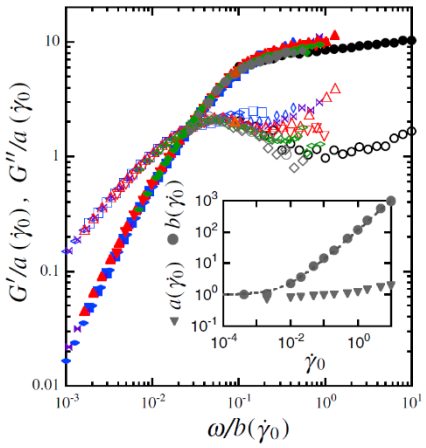

Figure 33 Master curve obtained from SRFS experiment, evolution of the elastic modulus (G') and viscous modulus (G") rescaled by factors a as function of the frequency rescaled by factors b, these factors depend of the strain rate applied to the gel. Inset: evolution of the SRFS scaling factors: a (modulus scaling factor) and b (frequency scaling factor) as function of strain rate applied to the tested sample.

The structural relaxation time decreases as $\dot{\gamma}_0$ increases, as expected from the equation 5. The relaxation peaks in the data shown in Figure 32 occur when $2\pi/\omega$ becomes comparable to $\tau(\dot{\gamma}_0)$.

The observed scaling suggests that G^* can be expressed as a function of frequency and strain amplitude:

$$G^*(\omega,\gamma_0) \sim {G_R}^*\left(\frac{\omega}{a(\gamma_0\omega)}\right) + {G_{HF}}^*(\omega) \quad , \qquad 6$$

where ${G_R}^*(\omega)$ describes the functional form of the linear viscoelastic behavior due to the structural relaxation process, and ${G_{HF}}^*(\omega)$ describes high frequency contributions that are independent of γ_0.

This method, called "strain rate frequency superposition", SRFS, is useful to probe a larger range of frequencies than a standard frequency sweep.[56] The SRFS is based on the same principle than the time temperature superposition (TTS), where frequency sweeps at different temperatures are shifted to obtain a master curve.

2.2.2. Passive micro-rheology

In the "passive" microrheology, the Brownian dynamics of probe particles are measured to determine rheological properties of the viscoelastic material in which the probe particles are dispersed. Contrary to "active" microrheology in which the rheological responses of probes particles under an external driving force are characterized, passive microrheology uses only the thermal energy k_BT of the probe particle, to evaluate the rheological response of the viscoelastic materials. Materials must be sufficiently soft to be probed by passive microrheology, so that the Brownian motion of the probe particles driven only by the thermal energy k_BT are measureable by the detection methods used. The relationship between the thermal energy density of a bead (radius R) with the elastic energy needed by the bead to deform a material with an elastic modulus G' and a length L is written as:

$$k_B T/R^3 = G'L^2/R^2. \quad (7)$$

Thus, the upper limit of elastic modulus measurable by passive microrheological techniques depends on both the size of probes and the spatial resolution of the detection technique to resolve small particle displacements of order L. The resolution of detecting typically ranges from 1 Å to 10 nm, allowing measurements with micron-sized particles in samples with an elastic modulus up to 500 Pa.

A viscoelastic material is modeled as an elastic network which is embedded in an incompressible Newtonian fluid. The elastic response of a viscoelastic material can be modeled by generalizing the standard Stokes-Einstein equation. This equation is generalized by the addition of a real component of the shear modulus to the complex shear modulus $G(\omega) = i\omega\eta$ corresponding to the purely viscous fluid. The dynamics of particle motions are characterized by the time dependent position correlation function of individual tracers. This correlation function is also known as the mean squared displacement (MSD).

Many soft materials are exhibiting both viscous and elastic behavior. Additionally, the responses typically depend on the time and length scales probed by the measurement. For such materials, the thermally driven motion of embedded spheres reflects both the viscous and elastic contributions, which are revealed in the mean square displacements (MSDs) of the tracers[57].

$$\langle \Delta r^2(\tau) \rangle \sim \tau^{\alpha}, \quad (8)$$

where α <1 and is called the diffusive exponent. The particles may exhibit sub diffusive motion (0< α <1) or become locally constrained (α = 0) at long times. This diffusive exponent is controlled by the viscoelastic properties of the sample tested. In case of a purely viscous medium around diffusing particles, α is equal to 1. For a pure elastic media, α is equal to 0. Finally, for a viscoelastic medium, α takes a value between 0 and 1. This diffusive exponent dependence on viscoelastic properties of the medium is represented in Figure 34.

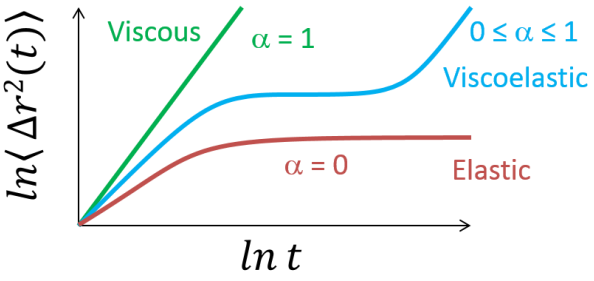

Figure 34 Schematic representation of the diffusive exponent dependence on viscoelastic properties of the medium.

A generalized Langevin equation is used to describe the forces on a small thermal particle of mass m and velocity $v(t)$ in a complex material:

$$m\dot{v}(t) = f_R(t) - \int_0^t \zeta(t-\tau)v(\tau)d\tau, \quad (9)$$

where $f_R(t)$ represents all the forces acting on the particle, including both the interparticle forces and stochastic Brownian forces. The integral represents the viscous damping of the fluid with a time dependent

memory function $\zeta(t)$ to account for the elasticity in the network. By taking the unilateral Laplace transform of the generalized Langevin equation and using the equipartition theorem, the viscoelastic memory function can be related to the velocity autocorrelation function[58]:

$$\langle v(s)\, v(0)\rangle = \frac{k_B T}{ms - \zeta(s)}, \quad 10$$

where s represents frequency in the Laplace domain. The inertial term is negligible except at very high (~ MHz) frequencies[59]. When the velocity autocorrelation is written in terms of the Laplace transform of MSD, the expression for the memory function in Laplace space becomes:

$$\tilde{\zeta}(s) = \frac{6k_B T}{ms - \zeta(s)}. \quad 11$$

To relate the microscopic memory function to the bulk viscoelasticity, the Stokes law is generalized to include a frequency dependent complex viscosity[57]. In the Laplace domain, this relates the complex shear modulus $\widetilde{G_s}(s)$ to the memory function $\tilde{\zeta}(s)$ as:

$$\tilde{G}(s) = \frac{s\,\tilde{\zeta}(s)}{6\pi R}. \quad 12$$

By combining these two equations, we obtain a relationship between the mean-square displacement of the tracers and the bulk modulus of the material:

$$\tilde{G}(s) = \frac{k_B T}{\pi R \langle \Delta \tilde{r}^2(s)\rangle}. \quad 13$$

This equation is a generalized, frequency-dependent form of the Stokes-Einstein relation for complex fluids. In the limit of a freely diffusing particle in a purely viscous solution,

$$\langle \Delta \tilde{r}^2(s)\rangle = \frac{6D}{s^2}, \quad 14$$

and the generalized Stokes-Einstein relation (GSER) recovers the frequency independent viscosity, $\eta_0 = \frac{k_B T}{6\pi R D}$, where D is the diffusion coefficient of the particle in the fluid. This result of the generalized Stokes-Einstein equation is remarkable: simply by observing the time-evolution of the MSD of thermal tracers, we obtain the linear, frequency dependent viscoelastic response of the sample surrounding them.

To compare with bulk rheology measurements, $\tilde{G}(s)$ is transformed into the Fourier domain to obtain the complex shear modulus $G^*(\omega) = G'(\omega) + iG''(\omega)$. $G'(\omega)$ and $G''(\omega)$ are not independent and obey to Kramers-Kronig relations. It is possible to determine both from the single, real function $\tilde{G}(s)$ by calculating the inverse unilateral Laplace transform and then taking the Fourier transform[60].

Equivalently, an alternative expression for the GSER in the Fourier domain is:

$$G^*(\omega) = \frac{k_B T}{\pi R\, i\omega\, \Im\left[\langle \Delta r^2(\tau)\rangle\right]}, \quad 15$$

where $\Im[\langle\Delta r^2(\tau)\rangle]$ is the Fourier transform of $\langle\Delta r^2(t)\rangle$, k_B is the Boltzmann constant, T is the temperature, R is the probe radius and ω is the frequency. For simplification, the Fourrier transform was replaced by gamma function following the method of Kuo et al[58]:

$$\Im[\langle\Delta r^2(\tau)\rangle] = \frac{1}{i\omega}\langle\Delta r^2(\tau)\rangle\,\Gamma[1+\alpha(\omega)], \quad 16$$

where $\alpha(\omega)$ is the local logarithmic derivative gave by $|\partial ln\langle\Delta r^2(\tau)\rangle|\partial ln\tau|_{\tau=1/\omega}$. Γ is the gamma function.

$G'(\omega)$ and $G''(\omega)$ can be expressed as:

$$G'(\omega) = G^*(\omega)cos\left[\frac{\pi\alpha(\omega)}{2}\right], \quad 17$$

and

$$G''(\omega) = G^*(\omega)sin\left[\frac{\pi\alpha(\omega)}{2}\right]. \quad 18$$

In order to take into account of the inertial effect, Indei et al. proposed the following expression[61]:

$$G^*(\omega) = \frac{k_BT}{\pi R\, i\omega\, \Im[\langle\Delta r^2(\tau)\rangle]} + \frac{m_{eff}\,\omega^2}{6\pi R} + \frac{R^2\omega^2}{2}\left[\sqrt{\rho^2 + \frac{2\rho}{3\pi R^3}\left(\frac{6\,k_BT}{(i\omega)^3\,\Im[\langle\Delta r^2(\tau)\rangle]} - m_{eff}\right)} - \rho\right]. \quad 19$$

where m_{eff} is the effective mass of a particle with the correction of the inertial effect of the fluid around it. m_{eff} is defined as $m_{eff} = m + M/2$ with $M = 4/3\ \pi R^3\rho$, where M is the mass of the medium per particle volume and ρ the water density.

2.2.2.1. Microrheology by dynamic light scattering (DLS)[62,63]

Experimentally one needs to know the mean square displacement of probe particles as a function of time in order to perform microrheology. There are different experimental methods reported. Dynamic light scattering techniques can be used to measure the mean square displacement of probe particles dispersed in viscoelastic media. The main advantage of the techniques is to measure rheological properties at high frequency. The frequency range covered by these techniques can typically be from 1 to 10^5 rad/s. With standard shear macrorheology covering typically from 10 to 10^{-3} rad/s, the microrheology can be complementary as shown in Figure 35.

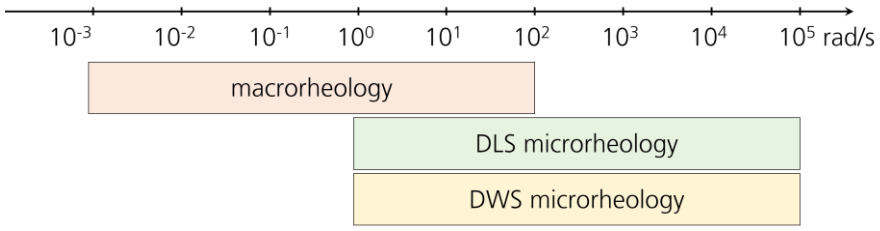

Figure 35 Frequency ranges probed by macrorheology, DLS microrheology and DWS microrheology.

There are two variations of the dynamic light scattering techniques used for passive microrheology, based on single scattering or multiple scattering. The classical dynamic light scattering (DLS) based on single scattering with a commercially available goniometer system ca be used for microrheology (Figure 36). When photons from a coherent light source (a laser is used) is scattered once from objects in Brownian motion, the scattered light intensity temporally fluctuates as a consequence of the object's motions. By analyzing the temporal fluctuations information on the dynamics of the object can be obtained.

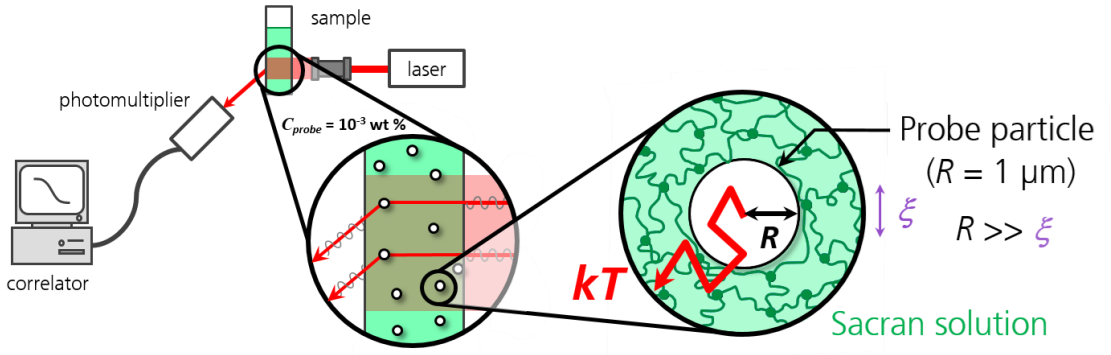

Figure 36 Schematic view of DLS setup and the diffusing hypothesis of DLS analysis. Particles concentration: 1.04 10^{-3} wt%.

In order to perform DLS experiment, a laser beam is focalized on the center of a sample placed on the rotational axe of a goniometer. The scattered light intensity detected by photo-multiplier at a given scattering angle θ is analyzed by a correlator to calculate the autocorrelation function of the intensity.

The wave vector $\vec{q}$ is defined as:

$$\vec{q} = \frac{4n\pi}{\lambda} sin\left(\frac{\theta}{2}\right), \quad 20$$

where λ is the wave length of the laser and n the refractive index of the solvent. The reciprocal of the vector $\vec{q}$ corresponds to the length scale of observation.

The intensity autocorrelation function $g_2(t,q)$ is given as:

$$g_2(t,q) = \frac{<I(t\prime,q)I(t,q)>}{<I(t,q)>^2}, \quad 21$$

where $<>$ defined the time average. The Siegert relationship is used to calculate the field autocorrelation function $g_1(t,q)$ which is written as:

$$g_2(t,q) = 1 + \beta|g_1(t,q)|^2, \quad 22$$

where β is the setup parameter varying between 0 and 1 depending on the incident light polarization and the size of the sensor window.

In the study of mono-disperse particles in diluted solution with a purely diffusive motion, the correlation function $g_1(t,q)$ decays as:

$$g_1(t,q) = \exp(-Dq^2t), \quad 23$$

where D is the diffusion coefficient of particles. DLS is usually used to determine the hydrodynamic radius R of an object (polymer or colloid) in solution/suspension if the viscosity of the solvent is known:

$$D = \frac{kT}{6\pi\eta R}. \qquad 24$$

If the hydrodynamic radius is known, the viscosity can be determined: this is a simple microrheological measurement. Probe particles of a known radius are introduced into the sample of a Newtonian solvent and the diffusion coefficient of the solvent thus the viscosity is measured. From $D = \langle \Delta r^2(t) \rangle / 6t$, one can write $g_1(t,q)$ as:

$$g_1(t,q) = exp\left[-q^2 \frac{<\Delta r^2(t)>}{6}\right]. \qquad 25$$

Assuming that this equation holds for non-Newtonian fluid, the value of MSD can be measured as a function time by DLS. Using this equation, the variations of $\langle \Delta r^2(t) \rangle$ are deduced from the correlation function $g_2(t,q)$ experimentally obtained.

2.2.2.2. Microrheology by diffusing-wave spectroscopy (DWS)

The diffusing wave spectroscopy (DWS) is a variation of dynamic light scattering using multiple scattering. Contrary to the single scattering DLS, photons have to be scattered multiple times by a high number of particles before its detection (Figure 37). Each scattering event by a particle modify its phase and this effect is accumulated throughout the light path crossing the sample, resulting in a high resolution of the displacement detection. The multiply scattered light intensity is analyzed in the same way as DLS to obtain the field autocorrelation function $g_1(t,q)$.

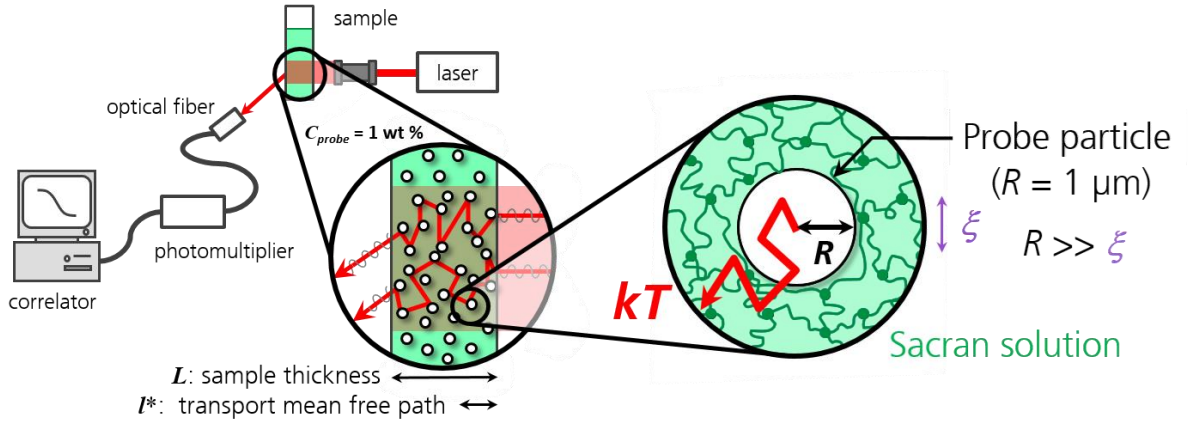

Figure 37 schematic view of DWS setup and the diffusing hypothesis of DWS analysis.

DWS is used for sample highly scattering through the insertion of large quantities of tracers (typically 0.1 – 1 wt% of probe particles). The sample is totally turbid.

The sensitivity of DWS is caused by the cumulative effect of diffusive events apply on each photon during their crossing of the sample. The detector record then a pattern of interference named "speckle noise". The tracers' dynamics information is in temporal fluctuations of light intensity on this speckle. In the same way, the scattering light signals can be correlated by a correlator, through $g_2(t)$, $g_1(t)$, is calculated.

The complete expression of the correlation function of electric field is:

$$g_1(t) = \int P(s)\, exp\left(-\frac{\vec{k_0}^2}{3} < \Delta r^2(t) > \frac{s}{l^*}\right) ds \,. \qquad 26$$

The incident light on the material has wave vector $\overrightarrow{k_0}$. Each photon performs random steps with a length of l^*. The total length of the following way by a proton in the sample is marked s. The statistic distribution of cross length is characterized by the distribution $P(s)$.

This equation means that each photon scattering steps in the diffusive medium contribute to the electric field decorrelation. At each step, $g_1(t)$ decrease as $exp(-{k_0}^2/3\,\langle\Delta r^2(t)\rangle)$. Now, along a way with a length s, a photon takes l^*/s steps and, at each step, this photon contribute to the decorrelation of the electric field, it is cumulative effect. The distribution of all this ways is regulated by $P(s)$. Finally, $g_1(t)$ is the integral on all lengths of all the possible configurations of the photon scattering.

To calculate $g_1(t)$, it is essential to know the measure geometry and $P(s)$. The distribution of ways lengths is different if the sample is observed by retro-diffusion or transmission. In transmission, $P(s)$ is narrow, the shorter way is imposed by the cellule size L. Only photons which have crossed this distance L can be detected. Statistically, these photons have known a step number equal to $(L/l^*)^2$ with an average distance between each step of l^*.

The correlation function of the electric field for different geometry have been calculated analytically.

For a transition geometry and with an extensive incident beam, the correlation of the electric field $g_1(\tau)$ is written as:

$$g_1(\tau) = \frac{\frac{L/l^*+4/3}{5/3} sinh\left(\sqrt{\chi}\right)+\frac{2}{3}\sqrt{\chi}cosh(\sqrt{\chi})}{\left(1+\frac{4}{9}\chi^2\right)sinh\left(\frac{L}{l^*}\sqrt{\chi}\right)+\frac{4}{3}\sqrt{\chi}cosh\left(\frac{L}{l^*}\sqrt{\chi}\right)} \,, \qquad 27$$

where $\chi = k_0\langle^2\Delta r^2(t)\rangle$.

The ratio L/l^*, this parameter is exclusively geometric and gave the maximal measure sensitivity. It is fixed by the experimental conditions. More the $L\ /l^*$ ratio is high more detectable displacement is low. Typically the value of L/l^* is 10 – 20.

3. Sacran solutions

3.1. Introduction

In order to understand the roles of the rigidity of the sacran chains in the mechanical properties of the physical and chemical gels, it is necessary to characterize the dynamic behaviors of the solutions at a single chain scale. Here we used two microrheological techniques which allow us to measure the high-frequency rheological properties which reflect the rigid chain dynamics. Different dynamic regimes in which complex modulus G^* shows scaling behaviors with frequency with various values of exponent were identified and explained by models.

3.2. Experimental section

3.2.1. Sacran extraction and solution preparation

In this work we used the polysaccharide samples prepared by our colleagues, Maiko Okajima and Tatsuo Kaneko in their laboratory. The polysaccharide was extracted from a fresh water cyanobacterium *Aphanothece sacrum* by the procedure described in the literature[50]. Briefly, the bacteria samples were freeze-thawed and washed in pure water, followed by lyophilization. The samples were washed in ethanol, and then collected by filtration. The ethanol-washed samples were agitated in 0.1 mol/L NaOH aq. at 100 °C for 4 h to yield the transparent solution. The solution was dialyzed with water for more than 72 h, and then filtrated. The filtrate was concentrated and the polysaccharide was precipitated as white fibers into isopropanol. The fibrous precipitates in isopropanol were collected and dried using a vacuum oven.

A stock solution of sacran was prepared by dissolving the dried sacran in pure water at 90 °C and was cooled at room temperature. From this mother solution, other solutions at various concentrations were prepared by dilution.

Polystyrene particles stabilized by surface OH groups used as probe for microrheology were purchased from Micromod (Rostock, Germany). OH groups were chosen as neutral hydrophilic functions to ensure the dispersion of the hydrophobic polystyrene particles in water. HCl and glucono-δ-lactone were purchased from Aldrich and used as received.

3.2.2. DWS microrheology

Sacran solutions containing polystyrene probe particles were prepared and transferred in measurement cells (plastic cuvettes for fluorescence spectroscopy having 4 mm optical pass and 10 mm width).

Diffusing-wave spectroscopy (DWS) was performed using a laboratory-made setup composed of a Spectra-Physics Cyan CDRH laser (λ = 488 nm, 50 mW). The laser beam was expanded to about 1 cm at the sample. The scattered light from the probe particles was collected by a multi-mode optical fiber placed in the transmission geometry, connected to a photomultiplier (ALV, Langen, Germany). The intensity autocorrelation function was calculated by a correlator (ALV, Langen, Germany). The raw data of $g_2(t)$ was converted into the field autocorrelation function $g_1(t)$ normalized by the value of $g_1(0)$ (determined by extrapolation) by using a software Excel. The relation between $g_1(t)$ and the mean-square displacement $\langle \Delta r^2(t) \rangle$ was rather complex, the values of $\langle \Delta r^2(t) \rangle$ were calculated by numerically resolving the eq(29) with a software Maple V. Finally the storage and loss moduli $G'(w)$ and $G''(w)$ were calculated by the method of Kuo et al.[58] on Excel.

3.2.3. DLS microrheology

Sacran solutions were filtered with a syringe filter (5 μm), then mixed with polystyrene probe particles. Then the solutions were transferred in measurement cells (glass test tubes having 10 mm outer diameter).

DLS microrheology measurements were performed by using a commercially available goniometer system (CGS-3, ALV, Germany) equipped with a Ne-He laser (λ = 633 nm, 14 mW) and an avalanche photon counter (Perkin Elmer, Vaudreuil, Canada) and a correlator (ALV 5003, Langen, Germany). The raw data of $g_2(t)$ was converted into normalized $g_1(t)$ in the same manner with the DWS microrheology on Excel. For DLS microrheology the relation between $g_1(t)$ and $\langle \Delta r^2(t) \rangle$ is mathematically simple (eq.25), the conversion can be easily performed on Excel. Finally G' and G'' are calculated in the same way as DWS (on Excel).

3.2.4. Macrorheology

Macroscopic rheological measurements of sacran solutions were performed with a strain-controlled TA Instruments ARES LS1 rheometer equipped with a rough cone and plate geometry (diameter: 50 mm, angle: 0.04 rad) composed of titanium and stainless steel, respectively. The mechanical history of the samples was the following: first, a strain sweep at fixed frequency (1 Hz) was performed to determine the linear viscoelastic regime. This measurement were stopped before reaching the end the linear regime. Then the elastic (G') and the loss (G'') moduli were measured in the linear viscoelastic regime in a pulsation range from 0.01 to 100 rad/s. Each measurement was repeated twice to ensure reproducibility. The temperature was controlled at 25 °C by an Effet Peltier.

3.2.5. Static light scattering

Static light scattering measurements were performed with the ALV CGS-3 goniometer system. For the scattering angles of 30 – 150 ° (corresponding to the q range of 146 – 39 nm^{-1}). Sacran solutions were filtered with a syringe filter (5 μm).

3.3. Results and discussion

3.3.1. Microrheology: impact of probe size and concentration

The microrheology by dynamic light scattering and diffusing-wave spectroscopy is a non-conventional rheological technique. From the mean square displacement of the probe particles dispersed in the viscoelastic medium, the complex modulus of the medium can be determined by using the generalized Stokes Einstein relation (GSER). Since the GSER is valid at the length scale shorter than the probe size, it is essential to choose appropriate probe size to obtain accurate viscoelastic moduli of the system. First of all, we performed microrheological measurements at different probe sizes and concentrations.

3.3.1.1. Diffusing wave spectroscopy (DWS)

Figure 38 shows the mean square displacement $\langle \Delta r^2(t) \rangle$ of probe particles of different radius R in the sacran solution at 0.25 wt% as a function of time. The values of $\langle \Delta r^2(t) \rangle$ for the three different probe particle sizes showed the same appearance, they were slightly shifted to the lower values with increase in the probe radius R, as expected from the generalized Stokes Einstein relation (GSER), showing $\langle \Delta r^2(t) \rangle \sim 1/R$. The signal-to-noise ratio decreases at very short time scales and at large displacement. The frequency range in which rheological data can be precisely obtained depends on the radius of the probe and the concentration. Both lower and upper limits increases with the probe size, mainly due to the decrease in the value of mean transport length l^*.

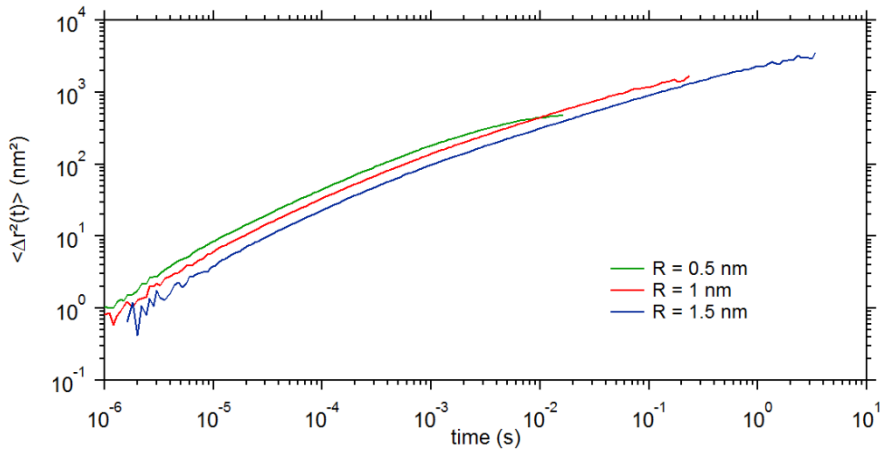

Figure 38 Mean square displacement $\langle \Delta r^2(t) \rangle$ of probe particles at different sizes as a function of time measured by DWS for a sacran solution at 0.25 wt% Particles radius: 0.5 μm (green curves), 1 μm (blue curves), and 1.5 μm (red curves). The probe concentration: 1 wt%.

In Figure 39, we plot as a function of time the product of $\langle \Delta r^2(t) \rangle$ and R, which is independent of R when the GSER is valid. As observed in this figure, the curves for 1 μm and 1.5 μm overlay each other, while that for 0.5 μm showed slightly lower value. This results indicates that there is no probe size dependence above 1 μm and the GSER can be applied, or that the various characteristic lengths of the system are shorter than the probe size. The reason why the particles with R = 1 μm shows slightly lower value of $\langle \Delta r^2(t) \rangle$ (but not higher) is unclear.

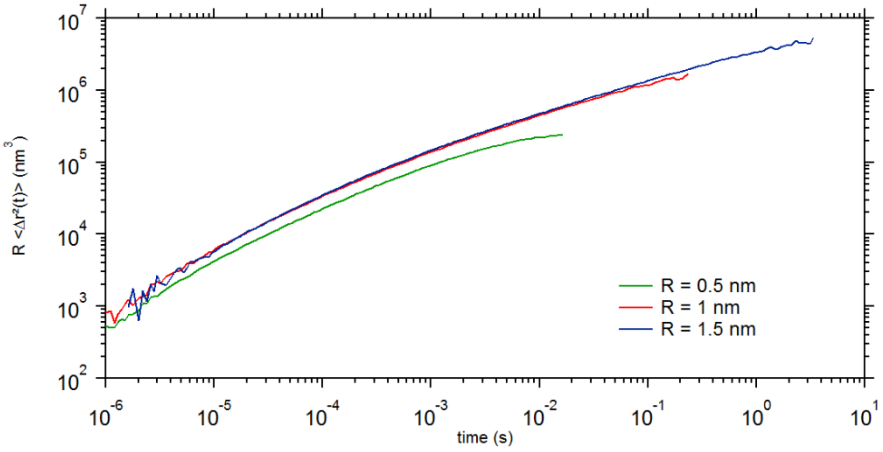

Figure 39 Mean square displacement $\langle \Delta r^2(t) \rangle$ normalized by the probe particles radius R as a function of time measured by DWS for a sacran solution at 0.25 wt% Particles radius: 0.5 μm (green curves), 1 μm (blue curves), and 1.5 μm (red curves). The probe concentration: 1 wt%.

In DWS measurements the value of $\langle \Delta r^2(t) \rangle$ depends also on the probe concentration since the value of l^* depends on the concentration. The probe concentration dependence was checked for the 1 μm particles in the same sacran solution as Figures 38 and 39. Figure 40 shows $\langle \Delta r^2(t) \rangle$ of the 1 μm probe particle at different concentrations as a function of time. The curves superpose each other, thus no probe concentration dependence is observed at these concentrations. With increase in the concentration, the range of $\langle \Delta r^2(t) \rangle$ with precision is shifted to lower values (the value of l^* increases with the concentration). It should also be noted that with an increase in the concentration the mean distance between the nearest particles decreases, and the inter-particle interactions might influence the particle displacement at high concentrations. For example, at 3 wt%, the inter-particle distance is estimated to be about $5R$. At this short distance the dynamics of the two neighboring particles might be correlated. In this work, we used 1 μm particles at 1 wt%, in order to guaranty a reasonable precision for both at short time scales ant at large displacement.

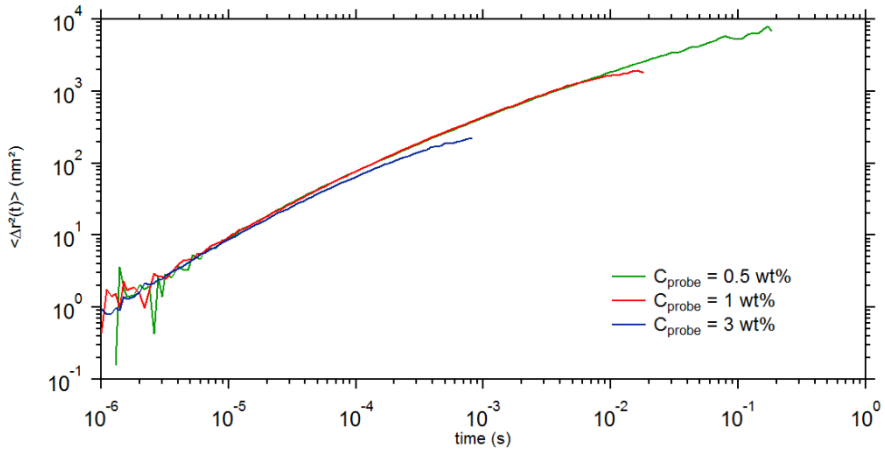

Figure 40 Mean square displacement $\langle \Delta r^2(t) \rangle$ of probe particles at different concentrations as a function of time measured by DWS for a sacran solution at 0.25 wt% Particles radius: 0.5 wt% (green curves), 1 wt% (red curves), and 3 wt% (blue curves). The probe radius: 1 μm.

3.3.1.2. Dynamic Light Scattering (DLS)

In general, for classical DLS measurements, the probe concentration do not influence the obtained autocorrelation function as far as the measurement is performed in the limit of single light scattering. This is because the characteristic measurement length scale $1/q$ is independent of the scattered concentration (intensity). This holds for DLS microrheology. However, the polymeric medium in the background also scatter certain amount of light, it can disturb the microrheological measurements in which only the scattering signals from the probe particles should be detected and correlated. Thus sufficient contrast between the scattering from the probe and that from the background polymer need to be guaranteed. This is the major difficulty of the DLS microrheology. Low contrast results in inaccurate moduli calculation.

For our DLS microrheology measurements, we used the probe particles of the same size as the DWS measurements, 1 μm in radius, at the concentration of 0.001 wt%. As shown in Figure 41, the scattering from the probe is about 10000 times as large as that from the sacran solution. The measurements were performed at 38°.

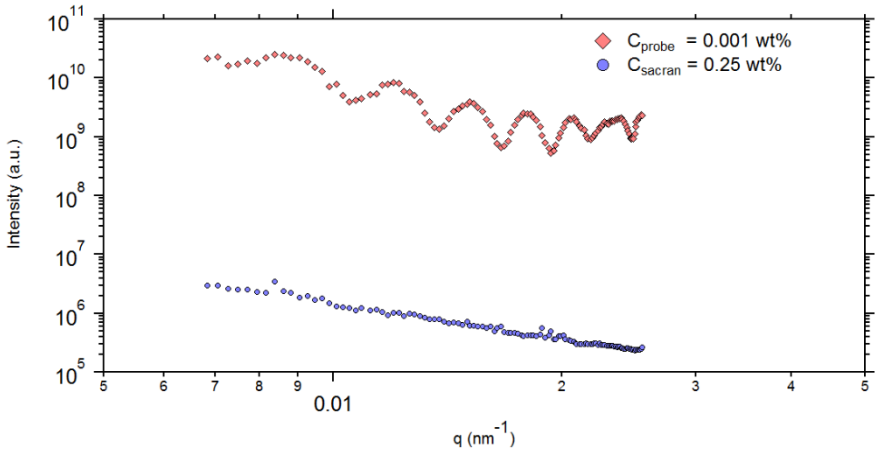

Figure 41 Scattered intensity by probes particles with a radius of 1 µm and concentrated at 0.001 wt% as a function of q in water and in 0.25 wt% sacran solution.

3.3.2. Comparison of the two techniques

Figure 42 and Figure 43 show the mean square displacement ($\langle \Delta r^2\ (t) \rangle$) of the probe particles as a function of time measured respectively by DLS and DWS microrheology in sacran solutions at different concentrations. The main difference between the two methods is the accessible range of $\langle \Delta r^2(t) \rangle$. With DLS microrheology at this experimental condition, $\langle \Delta r^2(t) \rangle$ is reasonably precisely measured between approximately 10^2 – 10^5 nm². For DWS microrheology, we have an accurate measurement window of 1 – 10^3 nm². Thanks to the multiple scattering events, small displacement of the particle is detected. In DLS microrheology is suitable for rather diluted systems to characterize large displacement at long time scales while DWS microrheology allows us to better characterize small displacement at short time scales thus suitable for soft hydrogels. At high polymer concentration scattering from the polymer may not be negligible, limiting application of DLS microrheology, while for DWS microrheology the probe/polymer contrast is usually guarantied practically at all the concentrations studied.

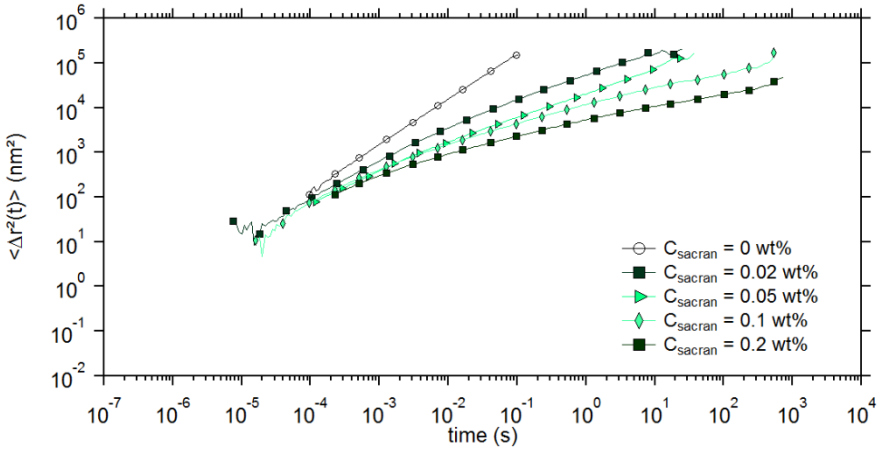

Figure 42 Mean square displacements of the microparticles in sacran solutions of different concentrations as a function of time measured by DLS.

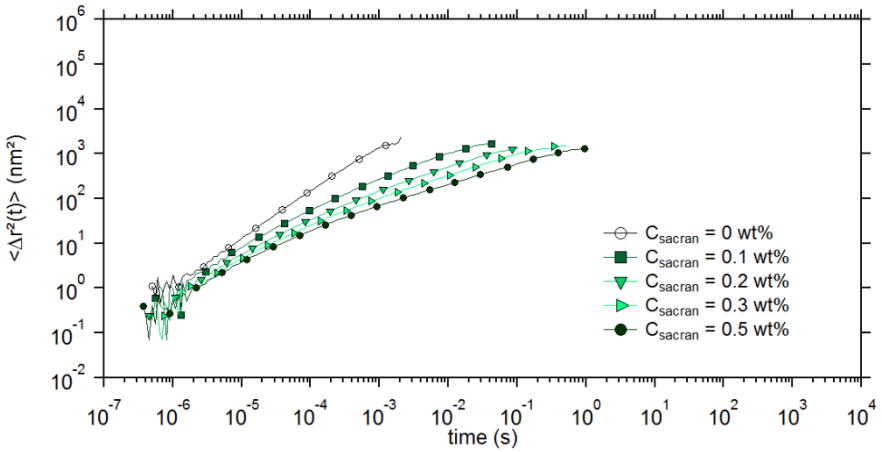

Figure 43 Mean square displacements of the microparticles in sacran solutions of different concentrations as a function of time measured by DWS.

It is worth noting that for DLS microrheology the characteristic length scale of the measurement is $1/q$, thus the measureable range of $\langle \Delta r^2(t) \rangle$ is dependent of the scattering vector as seen in eq.25: increasing the scattering angle θ (decreasing the scattering vector q) results in shifting the range to the smaller values of $\langle \Delta r^2(t) \rangle$. For DWS microrheology the characteristic length scale of the measurement is l^*, which is dependent of the probe size and concentration. In DLS/DWS microrheology, the value of average displacement $\langle \Delta r^2(t) \rangle^{1/2}$ is practically always smaller than the probe size R.

Figure 44 shows the comparison of the two techniques for sacran concentrations of 0, 0.05 and 0.2 wt%. The curves of $\langle \Delta r^2(t) \rangle$ well overlap each other without any adjustment for 0 and 0.05 wt%. By combining the two techniques a wide range of $\langle \Delta r^2(t) \rangle$ can be covered. For 0.2 wt%, the superposition is less satisfactory with a vertical shift of a factor of 2 which is acceptable for a comparison of two different rheological techniques. In general in these microrheological measurements based on dynamic light scattering

measuring the temporal fluctuations of the signals, the precisions in time are reasonably good compared to the those in the $\langle \Delta r^2(t) \rangle$ or modulus, which can be shifted by experimental artifacts such as non-fluctuating parasite light.

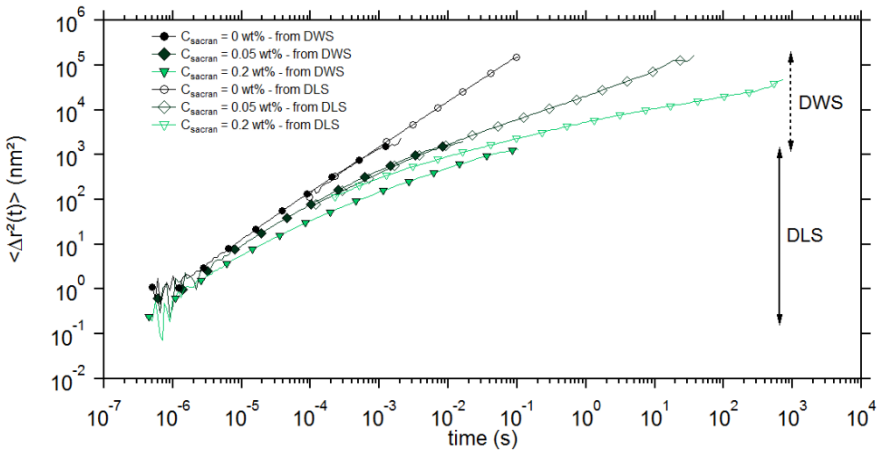

Figure 44 Superposition of mean square displacements of the particles in sacran solutions of different concentrations as a function of time measured by DLS and DWS.

3.3.3. Persistence length

The high frequencies rheological results obtained from DWS can be fitted by different modes described below. The power law of the complex modulus G^* at high frequency have been described by four regimes with a power law dependence of $G^* \sim C_n$ linked with the dynamics modes of semi-rigid chains studied.

At low frequencies, the concentrated solution have a power law dependence of $n < 1/2$ which describe the fractal mode of the network. At a concentration higher than the entanglement concentration (C_e), the network elasticity prevail over the fractal mode of the network.

When the frequency range increases, the single chain viscoelasticity starts to be measured. A regime of $n = 5/9$ describes the Zimm-Rouse mode. At this frequency range, sacran chains are considered as flexible.

At further higher frequencies, the corresponding length scale decreases and the chain rigidity start to control the viscoelasticity. The bending mode of rigid chains which corresponds to the internal dynamics of rigid rod involves with an exponent of $n = 3/4$ according to a relationship based on a statistical mechanical treatment of the single filament stress response by Gittes and MacKintosh[64–67]:

$$G^* - i\omega\eta_s = \frac{1}{15}\rho\,\kappa\, l_p \left(\frac{-2i\varepsilon}{\kappa}\right)^{\frac{3}{4}} \omega^{\frac{3}{4}} \quad , \tag{28}$$

where ρ is the volumic density of polymer, κ is the chain bending constant with a size smaller or equal to the persistence length, ε is the drag coefficient and η_S is the solvent viscosity.

The persistence length (l_p) is determined and its concentration dependence is discussed. In Figure 45, the absolute modulus G^* of the sacran solution at 0.25 wt% is plotted as a function of the frequency (the absolute modulus of the solvent, $G_s^* = -i\omega\eta$ is subtracted from that of the solution, since it cannot be negligible at high frequency for low concentrations). The local slope continues to increases thus the value of the modulus. At high frequency different dynamical modes can be identified by a power-law dependence as $G^* \sim \omega^n$. At $\omega > 10^5$ rad/s, we observe $G^* \sim \omega^1$, corresponding to the viscous mode or the Brownian diffusion at the length scale shorter than the mesh size ξ of the rigid polymer ($\xi < l_p$). In this mode the modulus is proportional to the chain concentration. Decreasing the frequency we successively detect the two mode with $n = 3/4$ and $5/9$, the bending mode and Zimm-Rouse mode. The intersection of the two modes corresponds to the longest limit of the bending mode (ω_c), thus the persistence length can be determined by:

$$\omega_c = \frac{k_B T}{8\,\eta_s\,{l_p}^3}. \qquad 29$$

where η_S is the solvent viscosity.

At further lower frequency dynamics of the entangled chains can be measured. For the sacran concentrations above 0.1 wt%, the value of n can be lower than 0.5. With small amplitude shear measurements we do not observe a terminal flow regime. We do not either observe a well-defined elastic plateau, we do not characterize the low frequency properties of the sacran solutions in this work.

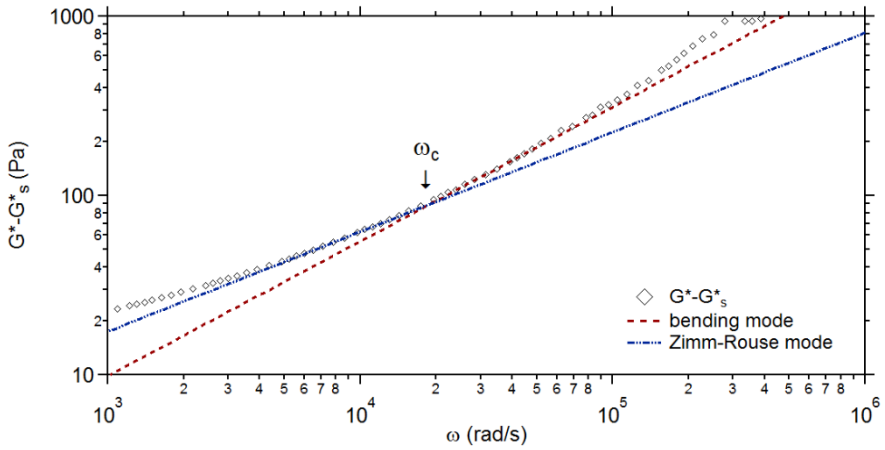

Figure 45 Complex modulus (G^*) as a function of frequency for a 0.25 wt% sacran solution. High frequency dynamics is fitted by Zimm-Rouse mode ($n = 5/9$) and bending mode ($n = 3/4$). The critical frequency, ω_c (defined previously), is determined as the junction of the Zimm-Rouse mode and the bending mode of rigid chains.

Figure 46 shows the sacran concentration dependence of the persistence length. The persistence length showed a strong concentration dependence and the value varied between about 30 and 100 nm. Compared with the values of the other semi-rigid polymers (hyanuronan[66]: 10 nm, DNA[68]: 50 nm, wormlike micelles of CPyCl-NaSal[69]: 34 nm), the sacran chain has a sufficiently high persistence length.

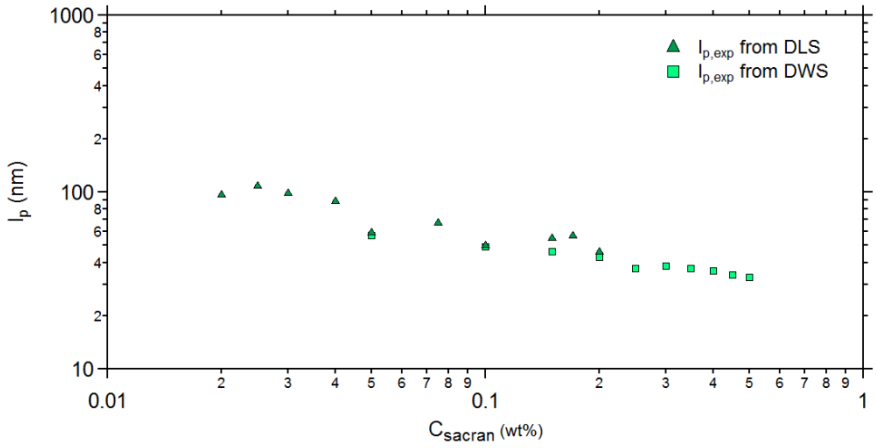

Figure 46 Variation of the persistence length of the experimentally obtained sacran chains ($l_{p,exp}$) as a function of the concentration of polysaccharides in the medium.

Care should be taken when one discusses the persistence length of polyelectrolytes, since the value of the persistence length strongly depends on the concentration. Polyelectrolyte persistence length theories of the Odijk-Skolnick-Fixman (OSF) assume that electrostatic interaction contributes to the bending stiffness of the chain independently of the other interactions. The experimentally obtained effective persistence length l_p is thus written as[70]:

$$l_p = l_{p,e} + l_{p,o} \,, \tag{30}$$

where $l_{p,e}$ is the electrostatic persistence length, and $l_{p,o}$ is the intrinsic persistence length reflecting to the rigidity of the uncharged chain.

The electrostatic persistence length is calculated by:

$$l_{p,e} = \frac{(l_B/b)^2}{4\, l_B} K^{-2} \,, \tag{31}$$

with

$$K^{-1} = \frac{1}{\sqrt{4\pi\, l_B\, C_f}} \,, \tag{32}$$

where l_B is the Bjerrum length (0.71 nm in water), b is the distance between charges on the polyelectrolyte chain, K^{-1} is the Debye-Hückel length and C_f is the ionic concentration of the solution. The distance between the charges on the sacran chain is an unknown parameter. Since 33 mol% of monosaccharide units composing of sacran is negatively charged, the average distance between the charges is assumed to be 1.5 nm (with the size of a monosaccharide: 0.5 nm).

In Figure 48 the different persistence lengths were plotted as a function of the sacran concentration. The electrostatic persistence length, $l_{p,e}$, calculated from equations above and experimental parameters, is shown as a red dashed line. It decreases with the concentration as $l_{p,e} \sim C^{-1}$, due to the counter ion (Na^+) contributing to the ionic concentration of the system. The value is lower than those measured by microrheology, indicating that the intrinsic persistence length $l_{p,0}$ is dominant at the concentration range. We adjusted the value of $l_{p,0}$ in the OSF relation (eq.30) to fit the experimental values of l_p (blue curve). With a $l_{p,0}$ of 60 nm, the prediction approaches to the experimental values for the concentration range about 0.02 – 0.1 wt%, while it cannot fit the higher concentration range whatever the value of $l_{p,0}$. The OSF equation predicts a constant persistence length at a high concentration as $l_{p,e}$ becomes negligibly low, while the experimental value of the persistence length continues to decrease with the concentration.

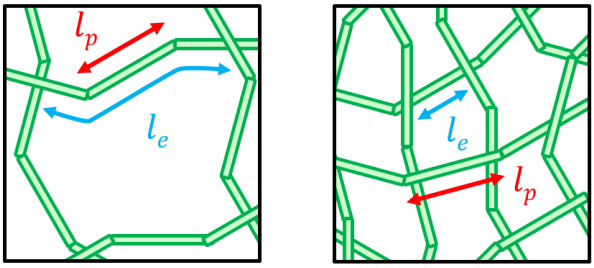

Figure 47 Left: schematic view of a polymer network where $l_p < l_e$; Right: schematic view of a polymer network where $l_p > l_e$.

This decrease in the persistence length with the concentration is explained as follows. When the rod polymer concentration increases, above a certain concentration, the distance between two entanglements points, l_e, becomes shorter than the persistence length as represented in Figure 47. In this situation, there persistence length cannot be rheologically measured, instead, the entanglement length is measured. Isambert and Maggs[71] demonstrate that l_e scales as $l_e \sim C^{-0.4}$. As shown in Figure 48, we found that the experimentally measured persistence length follows this scaling at the concentration higher than 0.1 wt%.

The origin of the high intrinsic persistence length is believed to be the helix formation. The electric conductivity of sacran solutions discontinuously decreased at around 0.1 wt% [4], which is interpreted as conformational change of sacran chain to more compact structure such as helix. X-ray scattering of sacran solutions was performed at q = 0.02 – 2 nm^{-1} and apparition of a peak in scattering curve at q= 0.23 nm^{-1}

(27 nm) was interpreted as helical pitch.[72] From our microrheological measurements it is not easy to prove the presence of helix.

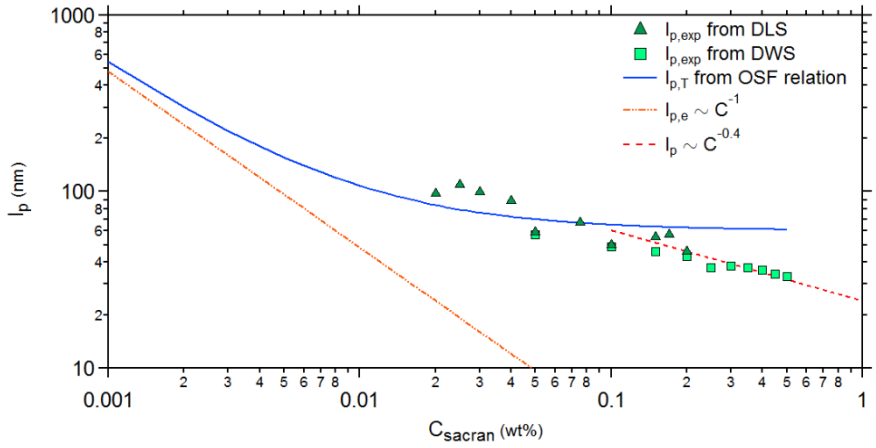

Figure 48 Variation of the persistence length of the experimentally obtained sacran chains ($l_{p,exp}$) as a function of the concentration of polysaccharides in the medium compared with the length of electrostatic persistence and the Odijk Skolnick Fixman (OSF) relation giving the theoretical evolution of persistence length.

3.3.4. Persistence length as a function of pH

Influence of pH on the persistence length was studied in acidic condition. The sacran sample used in this work is in sodium salt form, thus in acidic condition the charge density decreases and the ionic strength increases. Thus influence of the electrostatic interaction on the persistence length is expected to decrease and the intrinsic persistence length dominates the chain rigidity. Both DLS and DWS microrheology were used for two concentrations of sacran, 0.05 and 0.25 wt%. Two different acid species are used to control the pH of sacran solutions, the chloridric acid (HCl) or the gluconolactone (GL). For GL which can gradually change the pH with time, measurements were performed after stabilization of pH.

In Figure 49, the values of the persistence length of sacran determined by DLS and DWS are plotted as a function of pH. For 0.05 wt% the data are much dispersed and we do not see clear pH dependence of the persistence length, suggesting that there is no particular change in the intrinsic persistence length with pH. For 0.25 wt%, the value of the persistence length does not depend on pH. The average value is found to be 37 nm. At this concentration, as previously shown, the entanglement length is measured, suggesting that the structure of entangled chains does not change at acidic conditions.

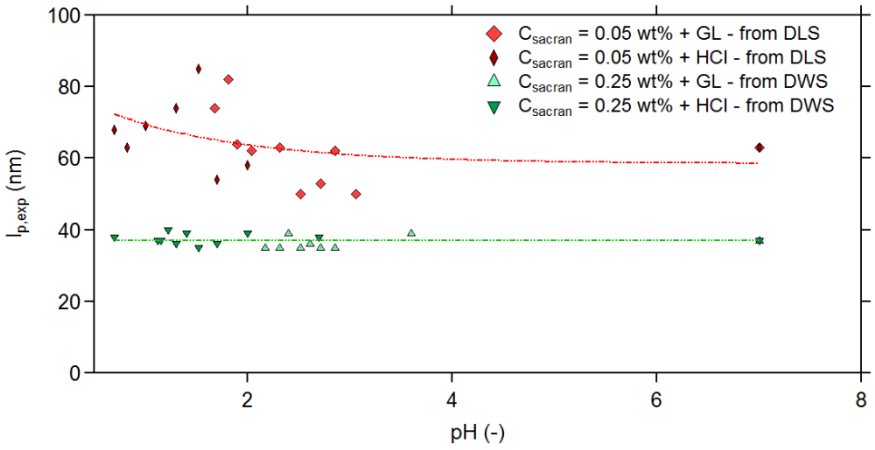

Figure 49 Persistence length (l_p) as a function of the pH of sacran solutions controlled by hydrochloric acid (HCl) or the Gluconolactone (GL), measured by DWS or DLS microrheology for sacran solutions at 0.05 and 0.25 wt%.

3.3.5. Persistence length from Static light scattering

In the preliminary work we characterized the sacran solutions with the Static light scattering (SLS), which can potentially allow us to characterize the form of the scattering object. In the case of rigid rod polymers the persistence length can be measured. In general rod-like objects and rigid polymer chains show a power-law behavior of $I \sim q^{-1}$. The persistence length can be determined from the transition from the q^{-1} mode to a q^{-2} mode (corresponding to the Gaussian coil of neutral polymers or screened polyelectrolytes) or to a q^{-4} mode (corresponding to compact domains of unscreened polyelectrolyte) with decrease in q.

Figure 50 shows the scattering intensity of a sacran solution (0.01 wt%). In the narrow accessible q range, we observe transition from a q^{-3} mode to a q^{-2} mode, however, no q^{-1} mode is observed. In fact the values of q of SLS are too small to detect the persistence length even it can be as large as 100 nm for the dilute solutions of sacran. The presence of q^{-3} mode can be classically explained by a combination of the q^{-4} mode and the q^{-2} mode, or by ill-defined size of the compact domains.[73]

While we were performing the light scattering experiments, our colleagues performed X-ray scattering experiments on sacran solutions. With a q range higher than this work (q = 0.02 – 2 nm^{-1}), q^{-3} mode was observed for a sacran solution at 0.005 wt%.[72] At 0.05 wt% a q^{-2} mode was observed. A transition from q^{-1} to q^{-2} or $q^{-3}$was observed at q^* = 0.23 nm^{-1} and the persistence length was determined: it is related to the value of q at this transition with the following equation:

$$l_p = 1.91/q^* \,. \qquad 33$$

They found a persistence length of 109 nm and claimed that it did not depend on the concentration (between 0.0025 and 0.5 wt%). The value is comparable to the OSF prediction in Figure 48.

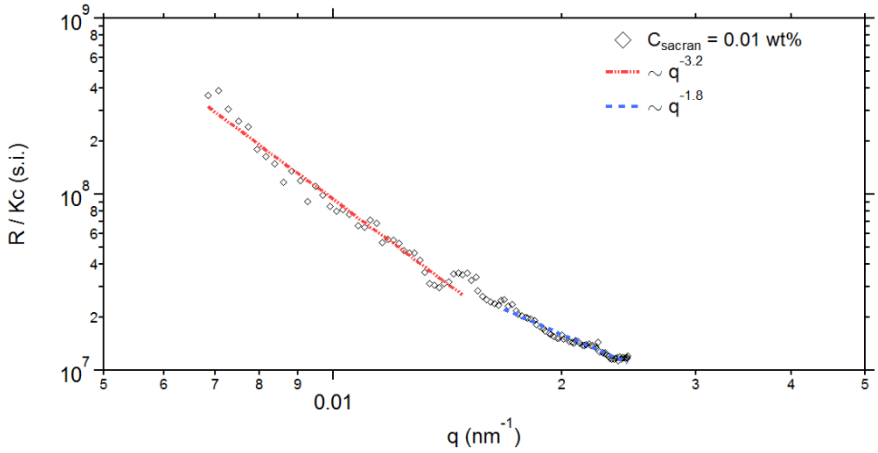

Figure 50 R/Kc as a function of q from SLS experiment performed on an aqueous sacran solution at 0.01 wt%. Red lines represent the $R/Kc \sim q^{-3.2}$ dependence observed at low q and blue lines represent $R/Kc \sim q^{-1.9}$ dependence observed at high q.

3.4. Conclusion

Firstly, the using of microrheology by DLS and DWS has been verified by varying the concentration and the diameter of the probe particles which has not occurred any change in mean square displacement level measured.

We try to measure the persistence length of sacran solutions by using SLS. A sacran solution concentrated at 0.01 wt% has been tested, but do not shown the transition between the $I{\sim}q^{-1}$ and q^{-2} modes. The range of sizes probed by SLS is too short to observe this transition for sacran solutions. Nevertheless, in the literature, X-ray scattering experiments performed on sacran solutions have shown than sacran solution at 0.05 wt% has a persistence length of 109 nm.

This persistence length has been confirm by microrheological studies by DWS and DLS performed on sacran solutions at different concentrations. These studies have shown that the persistence length of sacran chains is directly involved by the concentration of chains in solutions. The persistence length of sacran chains decreases from 109 to 33 nm when the chains concentration of solution increases from 0.02 to 0.5 wt%. The OSF relationship is verified at sacran concentrations lower than 0.1 wt%. Experimental persistence lengths measured for sacran solutions at concentrations higher than 0.1 wt% do not followed the OSF relationship but a power law of -0.4. The distance between the two entanglement points, l_e, becomes shorter than the persistence length, explaining the -0.4 deviation from the OSF relationship. The microrheological study of sacran solutions has then determined than the persistence length of sacran chains in entangled solution concentrated beyond 0.1 wt% is longer than the distance between entanglements. The crosslinking of sacran chains concentrated at more than 0.1 wt% would then be able to form rigid networks.

Finally, the evolution of persistence lengths of sacran chains as a function of the solutions pH have been followed at two sacran concentrations (0.01 wt% and 0.25 wt%). At 0.25 wt%, sacran solutions show persistence length around 40 nm independently to the pH of the solution. At 0.01 wt%, the persistence lengths measured seems to increase from 50 nm to 80 nm when the pH of the solution decreases from 3 to 1. The increase of the pH of sacran solutions seems then to increase the rigidity of sacran chains. This phenomenon could be explained by the promoting of the H-bonding. These bonding are described as the interactions causing the high rigidity of sacran chains.

4. Physical gels of sacran - Linear regime, signatures of the network rigidity

4.1. Introduction

As shown previously, sacran chains have carboxyl and sulfate functional groups and are able to form physical gels in the presence of divalent or trivalent cations. Gelation ability of sacran was tested with various cations by using a method of gel bead formation tests. We are particularly interested in the alkaline earth metals, Ca^{2+}, Sr^{2+} and Ba^{2+}. Sr^{2+} and Ba^{2+} induced gel bead formation while Ca^{2+} does not.[3] In order to better understand the interactions between sacran and the alkaline earth metal ions, rheological properties of the physical gels are studied in this work. This study will give insight on the interactions with Ra^{2+}, which cannot be investigated in our laboratory, with the view of eventual use of sacran for chemisorption of radioactive ions.

As seen in the previous chapter, the persistence length of the sacran chain is long (~ 60 nm) and the mesh size can be shorter than it. Thus the chains between the crosslinks are rigid though the sacran chain can be considered as flexible at the length scale of its contour length. Though the network formed by rigid chains can have different rheological properties than flexible chains, rheology of the rigid network has not been fully studied experimentally as gel-forming rigid polymers are rare and the number of experimental reports are limited. In this work sacran is used as model system of rigid network and its rheological properties was studied in linear and nonlinear domain.

In this chapter, we focus on the linear rheological properties of sacran physical gels crosslinked by Ca^{2+}, Sr^{2+} and Ba^{2+}. Three rheological signatures of rigid chain network are demonstrated with following three analyses.

(1) Comparison of the mesh size and the persistence length. Macrorheology and microrheology are used to accurately evaluate the mesh size and the persistence length.

(2) Effect of crosslinking ratio. The mesh size and the distance between the negative charges on the chain which are potential binding sites are characterized as a function of the crosslinking ion concentration. The role of the chain rigidity which limits crosslinking is discussed.

(3) Concentration dependence of the plateau modulus. Concentration dependence of the elastic modulus at plateau is discussed as a function of the chain rigidity. A different power-law behavior from that of flexible chains is discussed with existing models.

The difference between the three cations is also discussed.

4.2. Experimental section

4.2.1. Physical hydrogels preparation

A sacran mother solution was prepared in the same procedure as that in Chapter 3. $CaCl_2$, $SrCl_2$ and $BaCl_2$ were purchased from Sigma Aldrich and used as received. Polystyrene particles for DWS microrheology were purchased from Micromod (Germany).

The divalent cations are introduced in solution after the sacran mother dissolution by pure water. After the addition of divalent cations, the gel is gently mixed by using a vortex at low speed. The mix is stopped when the gel is totally transparent and homogeneous. The gel is then placed into the rheometer and its viscoelasticity stabilization is followed by an oscillatory time sweep (1 Hz, 1 % of strain amplitude, 25 °C).

4.2.2. Macrorheology

Macroscopic rheological measurements of sacran solutions were performed with a strain-controlled TA Instruments ARES LS1 rheometer using cone-plate geometry (diameter: 25 mm, angle 2°, gap 43 μm) with roughened surface. Frequency sweep (between 0.01 and 100 rad/s) was performed with a fixed amplitude in the linear domain.

In order to study the effect of the physical crosslinking ratio on the viscoelastic properties of sacran gels, frequency sweeps are performed from macrorheology with a cone plan geometry. Sacran gels jellify into the cone plan geometry and the gelation kinetics is observed by a time sweep test, the gelation time is fixed at 1.5 h.

4.2.3. DWS microrheology

DWS microrheological measurements were performed with the same experimental setup as that described in the previous chapter. Generally the dynamic light scattering signals from hydrogels are non-ergodic. A measurement at a fixed position does not allow to explore all the configurations of the system, thus time averaging is not equivalent to ensemble averaging. This is due to the frozen-in spatial inhomogeneity of the hydrogel network. The scattering from the probe particles trapped in the crosslinked network is also non-ergodic and ensemble averaging should be properly performed. In order to obtain ensemble-averaged autocorrelation function in our DWS measurements, a device to rotate a diffuser glass plate was placed in front of the optical fiber. Rotation at a constant speed allowed to collect scattering signals from different positions to obtain ensemble averaged $g_2(t)$ having a cut-off at about 10 s due to the rotational motion appearing at a long time range.

4.2.4. Cryo-fracturing

A small volume of gel (2-4 µL) is placed between two cups of copper and a sandwich is formed. The whole is frozen very rapidly by immersing in liquid nitrogen. The sandwich is assembled in a specific sample holder and inserted into the cryo-fracture device. This is under high vacuum (better than 10-7 mbar) and the sample is maintained at -170 °C. After fracture, a layer of 2 nm of Pt is evaporated at an angle of 45 ° and then a layer of 20 nm of carbon at an angle of 90 ° is dropped off. The whole is then returned to ambient temperature under a stream of dry nitrogen, then replicas are washed with a solution of Hellmanex at 5%. Finally the replicas are recovered on grids of 400 mesh in copper.

The observation of replicas is done using a MET Tecnai G2 operating at 200 kV and the images are obtained by a slow scan camera CCD Eagle of 2k2k.

4.2.5. Cryo-SEM

A little of gel is placed on a copper rivet, and is then frozen by rapid quenching in liquid ethane cooled by liquid nitrogen.

The rivets are mounted on the Quorum sample holder and then transferred to the preparation chamber where a fracture is performed under vacuum using a scalpel. A light sublimation is carried out at -90 ° C for 2 minutes and then a thin layer of gold is evaporated to make the surface conductive. Finally the assembly is introduced into the SEM is observed at -160 °C with an acceleration voltage of 1 kV.

4.3. Results and discussion

4.3.1. Mesh size vs persistence length

In Figure 51, viscoelastic moduli of a sacran physical gel crosslinked by Ba^{2+} are plotted as a function of the frequency measured by the macrorheology and microrheology. By combining the two methods, rheological properties are studied in a wide range of frequency. A good agreement of these two techniques was found without adjustable parameter. In general the modulus inferior to the other (in this case the loss modulus G'') superpose less satisfactorily than the other, as the inferior modulus tends to be more sensitive to experimental noises and errors. The physical gels of sacran exhibits a reasonably well-defined elastic plateau in G' at low frequencies. We did not observe relaxation in the studied frequency range in linear domain.

From the elastic modulus at plateau, G_e, the mesh size of the network is calculated. The relationship between G_e and the number of network strands per unit volume is written as[74]:

$$G_e = \frac{nkT}{V} = \frac{kT}{\xi^3}, \qquad 34$$

where n is the number of elastically active chain in the network and V is the volume of a mesh in the network. The ratio n/V is thus the number of network strands per unit volume, which is equivalent to ξ^{-3}, where ξ is the mesh size (ξ^3 corresponds to the volume per elastically active chain). For the physical gel in the figure we find 62 nm.

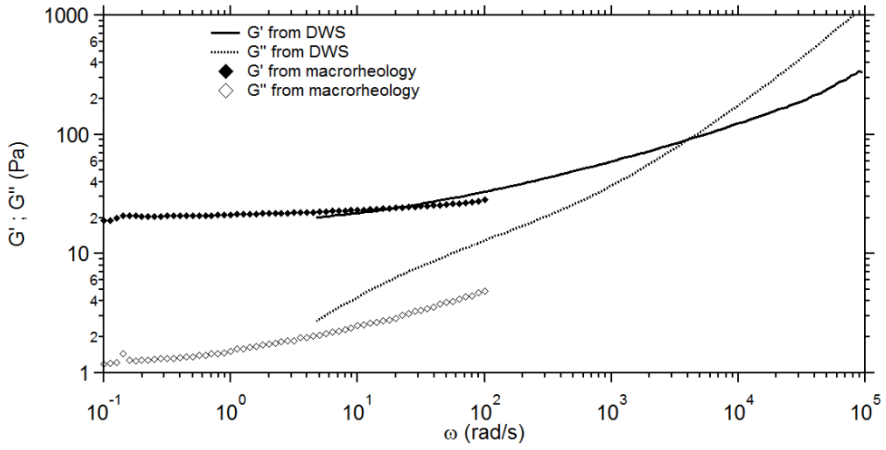

Figure 51 Viscoelastic modulus (G'; G'') as a function of frequency for a sacran gels concentrated at 0.25 wt% and crosslinked by 10^{-2} mol/L of Ba^{2+}. Diamonds: macrorheology. Lines: DWS.

At higher frequencies (typically around 10^3 – 10^5 rad/s) than those of the elastic plateau (typically < 10 rad/s), the rheological properties correspond to shorter length scales than the mesh size, thus the single

chain dynamics can be observed. Since the shear macrorheology cannot usually access to this frequency range, microrheology is used. As shown in the previous chapter, these high frequencies responses are obtained by monitoring of the motion of microscopic probes particles introduced in the sample tested. The size of the probe particles (R = 1 μm) is large compared with the mesh size of the tested network thus the particles are confined in the polymer network. The generalized Stokes-Einstein relation is valid for confined particles.

Figure 52 shows complex modulus of the sacran physical gel at high frequency. In the same way as the sacran solutions in the previous chapter, at high frequency range, the Zimm-Rouse mode ($G^* \sim \omega^{5/9}$) and the bending mode ($G^* \sim \omega^{3/4}$) are observed, and from the frequency at the transition from the Zimm-Rouse mode to the bending mode, the persistence length of the system is determined.

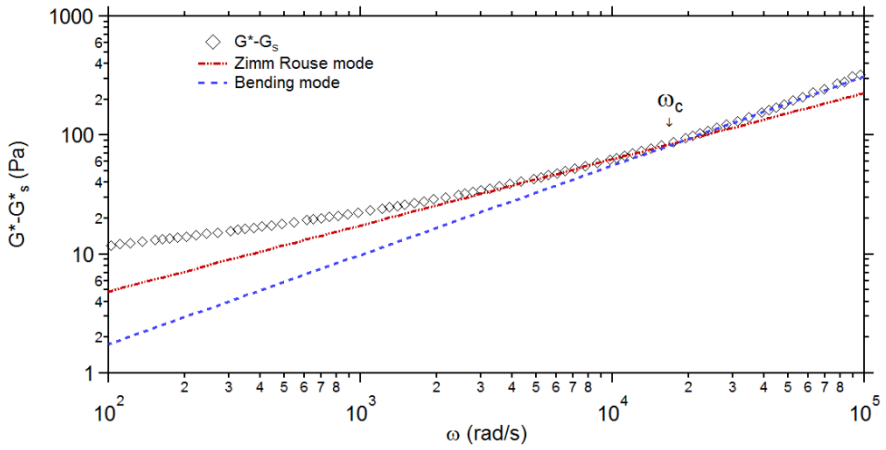

Figure 52 Complex modulus (G^*) of a sacran physical gel corrected by the complex modulus of the solvent (G_s^*) measured by DWS microrheology. Sacran concentration: 0.25 wt%. Ba^{2+} concentration: 10^{-3} mol/L.

The effects of the crosslinking ratio is studied with Ba^{2+} at a sacran concentration of 0.25 wt%. Figure 53 shows the viscoelastic moduli of the sacran crosslinked by different amounts of Ba^{2+}. Globally the superposition of the macrorheology and microrheology is satisfactory. The elastic modulus G' overlaps well. Without Ba^{2+}, the sacran solution at 0.25 wt%, G' and G'' show a power-law behavior at low frequency precisely measured by macrorheology. With an increase in Ba^{2+} concentration, the slope of G' decreases, a well-defined elastic plateau appears. The value of G'' does not change a lot, and the loss tangent $tan\,\delta = G''/G'$ reaches to about 0.05.

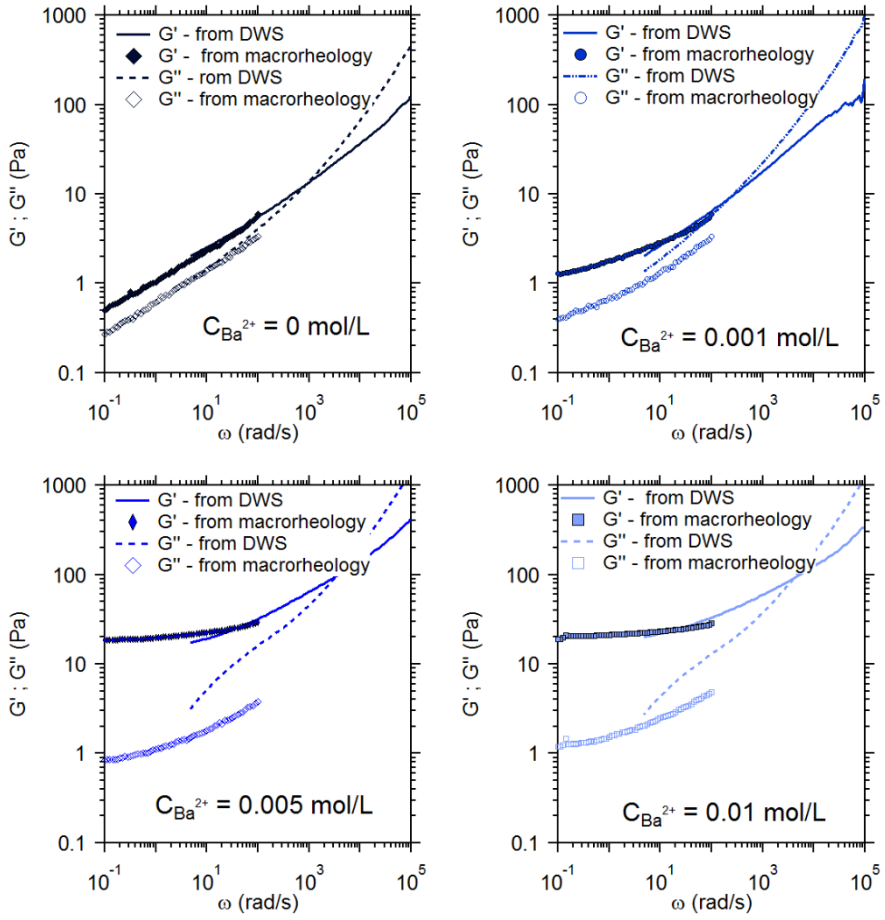

Figure 53 Viscoelastic modulus (G'; G'') as a function of frequency for sacran gels at 0.25 wt% crosslinked by different amounts of Ba^{2+} (0.001, 0.005 and 0.01 mol/L). Points: macrorheology. Lines: DWS.

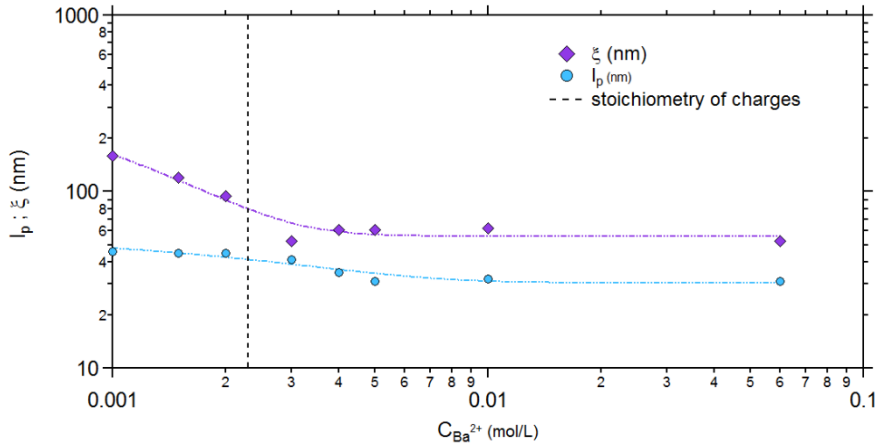

Figure 54 Mesh size (purple diamonds) and persistence length (blue circles) as a function of Ba^{2+} concentration for 0.25 wt% sacran gels. ξ is calculated from the G_e at 1 rad/s.

In Figure 54, the mesh size (ξ) and the persistence length (l_p) are plotted as a function of Ba^{2+} concentration. The dashed line indicates the stoichiometry of this ion exchange reaction: the molar ratio of the positive charges from Ba^{2+} and the negative charges on sacran chains (from sulfate and carboxylate groups) is 1. In

fact, 33 mol% of monosaccharides composing of the sacran chain are negatively charged (11 mol% of carboxyl and 22 mol% of sulfonate[75]). At 0.25 wt% of sacran, the concentration of negative charges on sacran chains is calculated as 4.6 10^{-3} mol/L. The stoichiometry of ionic crosslinking with divalent cations is then fixed at 2.3 10^{-3} mol/L.

Below the stoichiometry, ξ decreases with the increase of Ba^{2+} concentration which corresponds to an increase of the gel elasticity (note that the values of ξ are approximate as a well-defined elastic plateau is not observed at this concentration range). Beyond the stoichiometry, ξ becomes constant and around 50 nm. l_p follows a similar variation. Below the stoichiometry the value was about 45 nm, and beyond the stoichiometry it stabilized around 30 nm. The decrease in the persistence length is not explained.

Beyond the stoichiometry of this ionic gelation, these two characteristic lengths are then comparable. This result indicates that sacran networks crosslinked by more than 5 10^{-3} mol/L of Ba^{2+} form networks with semi-rigid chains segment between their crosslinking points. It should be noted that as seen for the solutions, at this concentration, we microrheologically measure the entanglement length instead of the persistence length since it is longer than the entanglement length. The intrinsic persistence length estimated from the microrheological measurement of sacran solutions is 60 nm, which is very close to the macrorheologically measured mesh size.

4.3.2. Elasticity of rigid networks, dependence of junction zones density

The effects of the crosslinking ratio on the rheological properties of sacran physical gels are further studied with macrorheology, by comparing three cations, Ca^{2+}, Sr^{2+} and Ba^{2+}. In Figure 54Figure 55Figure 56, the viscoelastic modulus of the sacran physical gels are plotted as a function of frequency (at 1 % of strain, and after 1.5 h of gelation under the rheological geometry). Results for different amounts of cations are shown. At all the concentrations tested for each ion, the elastic modulus is higher than the viscous modulus at any frequency, thus rheologically a physical gel is formed even with Ca^{2+}. The elastic modulus of the physical gels crosslinked by Ca^{2+} show rather stronger frequency dependence compared with that of the gels crosslinked by Sr^{2+} or Ba^{2+}, and the values of the moduli for Ca^{2+} are slightly lower than those for Sr^{2+} and Ba^{2+}.

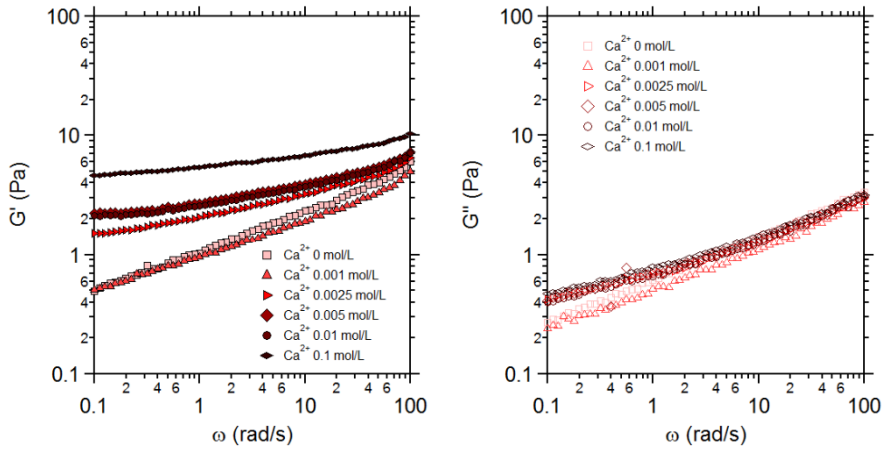

Figure 55 Viscoelastic modulus (G'; G'') as a function of the frequency for sacran gels concentrated at 0.25 wt% and crosslinked by different concentration of Ca^{2+}: 0, 0.001, 0.0025, 0.005, 0.01 and 0.1 mol/L.

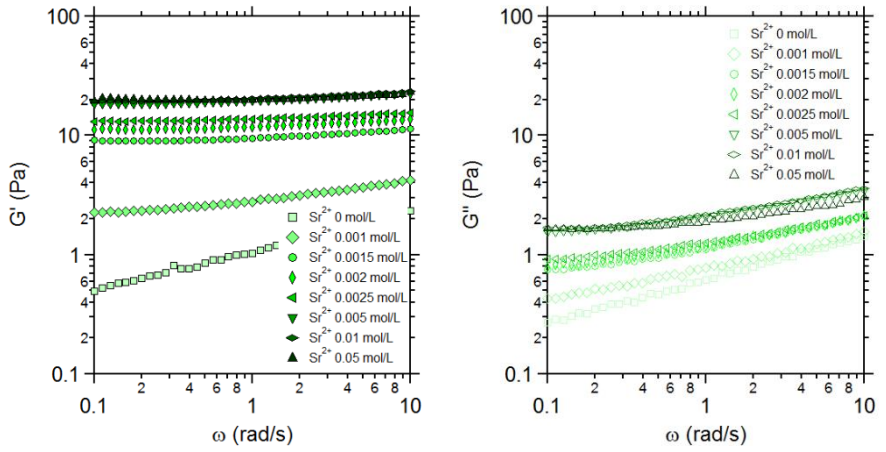

Figure 56 Viscoelastic modulus (G'; G'') as a function of the frequency for sacran gels concentrated at 0.25 wt% and crosslinked by different concentration of Sr^{2+}: 0, 0.001, 0.0015, 0.002, 0.0025, 0.005, 0.01 and 0.1 mol/L.

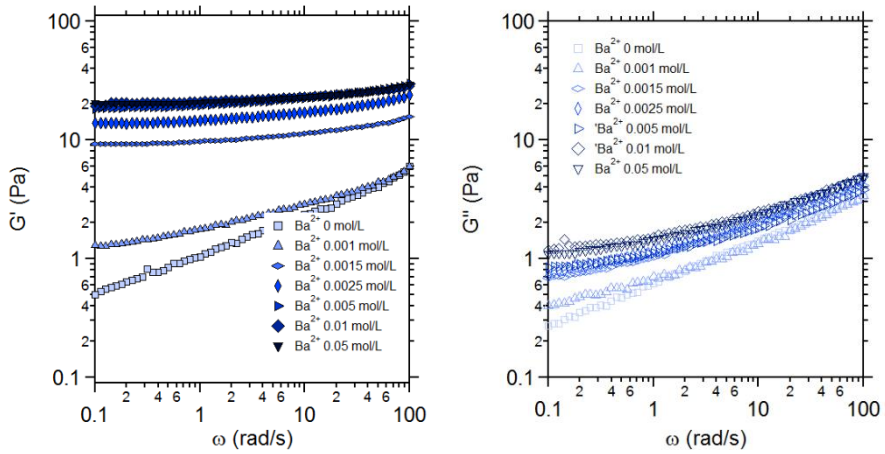

Figure 57 Viscoelastic modulus (G'; G'') as a function of the frequency for sacran gels concentrated at 0.25 wt% and crosslinked by different concentration of Ba^{2+}: 0, 0.001, 0.0015, 0.0025, 0.005 and 0.05 mol/L.

In Figure 58, G_e at 1 rad/s are plotted as a function of the ions concentration. The dashed line indicates the stoichiometry of the charges. For all the three ions species studied, the values of G_e increase with the ion concentration, and beyond the stoichiometry it becomes practically constant. For all the concentrations tested here, the same values of G_e are measured for Sr^{2+} or Ba^{2+}, around 20 Pa for cations concentrations higher than the stoichiometry. The gels crosslinked by Ca^{2+} gives G_e of several Pa. We discuss the particularity of Ca^{2+} in the next subsection (page 77).

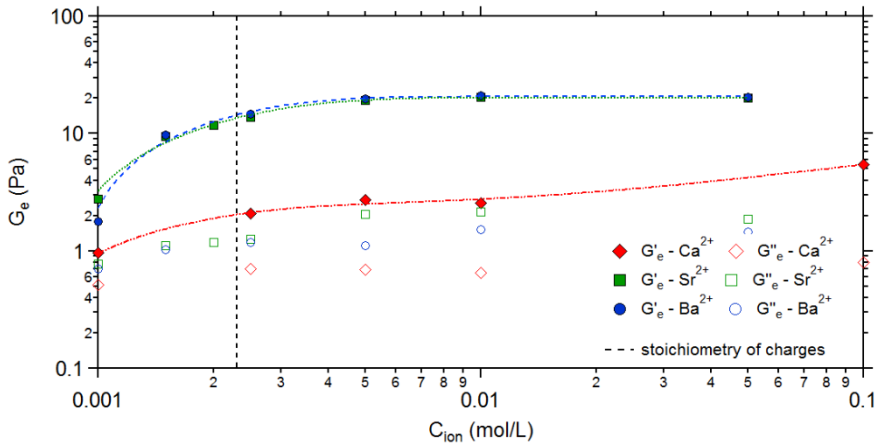

Figure 58 Elastic plateau modulus (G_e) as a function of cations concentration for 0.25 wt% sacran gels crosslinked by Ba^{2+} (blue squares), Sr^{2+} (green diamonds) and Ca^{2+} (red circles).

The mesh size of these gels is estimated from the G_e with eq.34. For an elastic modulus of 20 Pa, the corresponding mesh size is estimated to be 50 nm. As previously discussed, the average distance between negative charges on sacran chains is assumed to be 1.5 nm. The mesh size of these sacran gels is then much longer than the average distance between negative charges on sacran chain, potential crosslinking points. The ratio between these two lengths corresponds to the number of negative charges of sacran chains do not implicated in the network crosslinking per crosslinking point and is higher than 30. The comparison

between the two distances shows that all functional groups on sacran chains are not crosslinked despite the excess amount of crosslinking ions. The chain rigidity could prevent the chain from collapsing as show in Figure 59. This limit imposed by the sacran chains rigidity could be linked with the low value of the elastic plateau of sacran gels.

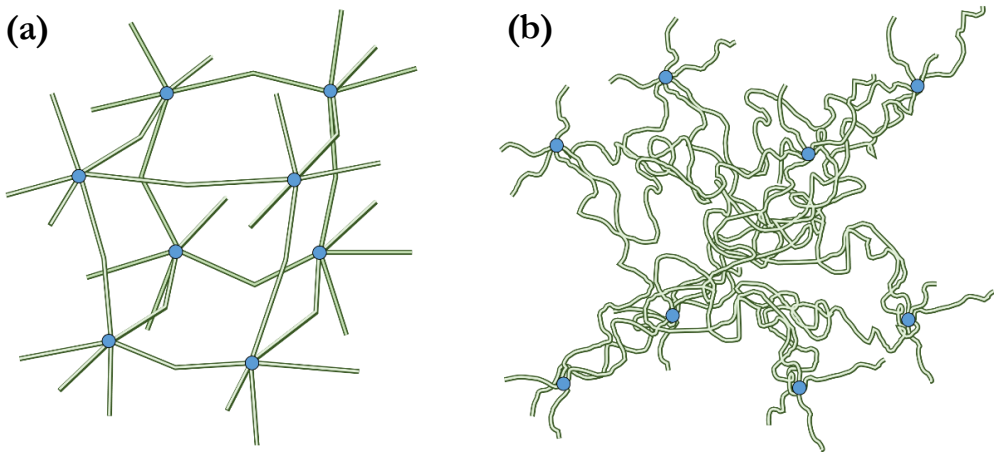

Figure 59 Schematic view of networks made of (a) a semi-rigid polymer and (b) a flexible polymer; visualization of collapsing capacity as a function of the network rigidity.

4.3.3. Sacran concentration dependence

Sacran concentration dependence of the plateau modulus was studied with the three divalent ions, Ca^{2+}, Sr^{2+} and Ba^{2+}. At a constant crosslinking ratio above the stoichiometry of the charges (440 mol%), the sacran concentration was varied and the plateau modulus G_e are measured by macrorheology. The oscillatory frequency sweeps measured from Ca^{2+}, Sr^{2+} and Ba^{2+} sacran gels are plotted in Figure 60. The value of G_e at 1 rad/s, are plotted as a function of the sacran concentration in Figure 61. For the three ions we found a power law behavior of $G_e \sim C^{1.5}$. The value of G_e of Ca^{2+} was slightly lower than those of the other two ions, as previously observed. We will discuss the particularity of Ca^{2+} in the next subsection.

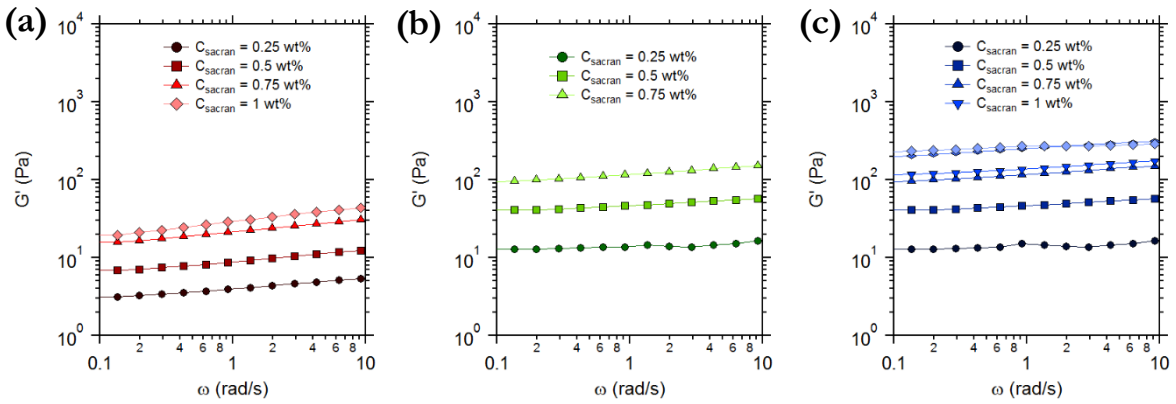

Figure 60 Evolution of elastic modulus (G') as a function of the frequency for sacran gels at different concentrations and crosslinked by a constant crosslinking ratio above the stoichiometry of the charges (4.4 mol%). (a) Sacran gels crosslinked by Ca^{2+}; (b) Sacran gels crosslinked by Sr^{2+}; (c) Sacran gels crosslinked by Ba^{2+}.

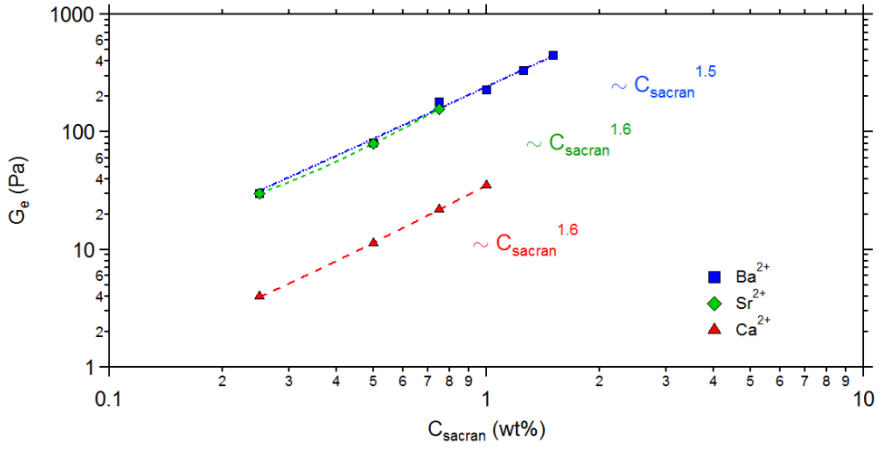

Figure 61 Elastic plateau modulus (G_e) as a function of sacran chains concentration crosslinked by Ba^{2+} (blue diamonds), Sr^{2+} (green diamonds), Ca^{2+} (red diamonds) or nothing (orange diamonds) with a constant ratio between C_{sacran} : $C_{crosslinkers}$ equal to 0.25 : 0.01.

This power law exponent of 1.5 is an indication of the network rigidity. Here we demonstrate the theoretical prediction of this power-law exponent.

This power law exponent is related to the Flory theory which describes the polymer size as a function the number of monomer with a dimensionless scaling exponent ν by the relationship[3]:

$$R_g \sim N^{\nu}, \qquad 35$$

where R_g is the radius of gyration of the elastically active chain segment and N the number of bond segments. This scaling exponent ν characterizes the chains expansion, thus the rigidity of the elastically active chain segment as shown in Figure 62. The Flory approximation of this scaling exponent ν is 3/5 for a swollen flexible chain. This scaling exponent is 1 for an ideal rigid chain.

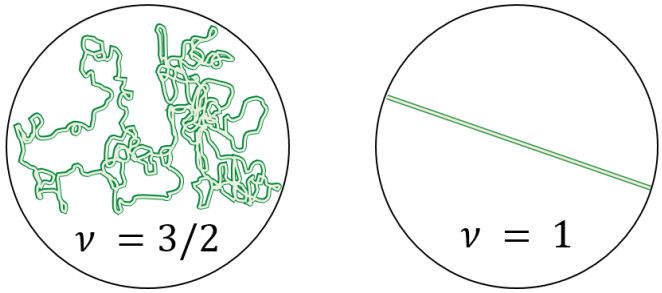

Figure 62 Schematic representation of the physical meaning of the scaling exponent.

For an athermal solvent, the plateau modulus G_e scales with the chain concentration C_s as[74]:

$$G_e \sim C_s^{\frac{3\nu}{3\nu-1}}, \qquad 36$$

where G_e is the elastic plateau modulus, C is the chains concentration.

For $\nu = 1$, G_e scales as $G_e \sim C^{1.5}$. Hinner & al.[9] verified a scaling as $G_e \sim C^{1.4}$ for strongly entangled solutions of actin and describe this deviation as due to the rigidity of the polymer.

4.3.4. Particularity of Ca^{2+} gelation

Let us comment on the difference in the absolute value of the moduli between the gels crosslinked by Ca^{2+} and those crosslinked by Ba^{2+} and Sr^{2+}. The results shown in the previous section are obtained after a gelation time of 1.5 h, which corresponded to the time where the values of modulus start to level off for sacran crosslinked by Ba^{2+} or Sr^{2+}. In order to better understand the gelation kinetics of the physical gels

crosslinked by the three ions, the time profile of the viscoelastic moduli are plotted in Figure 63 (frequency of 6.28 rad/s, strain of 1 % and temperature of 25°C). Note that G' is higher than G'' even just after the mixture with cations. It is found that the G' is higher than G'' for the sacran solution at this concentration without crosslinking cations (Figure 53). After 1.5 h, the elastic modulus obtained for sacran gels concentrated at 0.25 wt% and crosslinked by 0.05 mol/L of Sr^{2+} or Ba^{2+} is stabilized around 20 Pa. In case of Ca^{2+}, we find slow and complex evolution of the moduli. The measurement is repeated with fresh samples and the results are plotted in the left figure. Though the curves are not identical, the global tendency is the same: the values of the moduli increase with time, during the first 5 – 7 hours, reaching around 100 Pa. Then the moduli decrease slowly. This slow complex kinetics is presumably related to a large scale organization leading to the formation of a heterogeneous system.

We further investigate the ion species dependence of the viscoelasticity of the sacran physical gels in nonlinear domain in the next chapter.

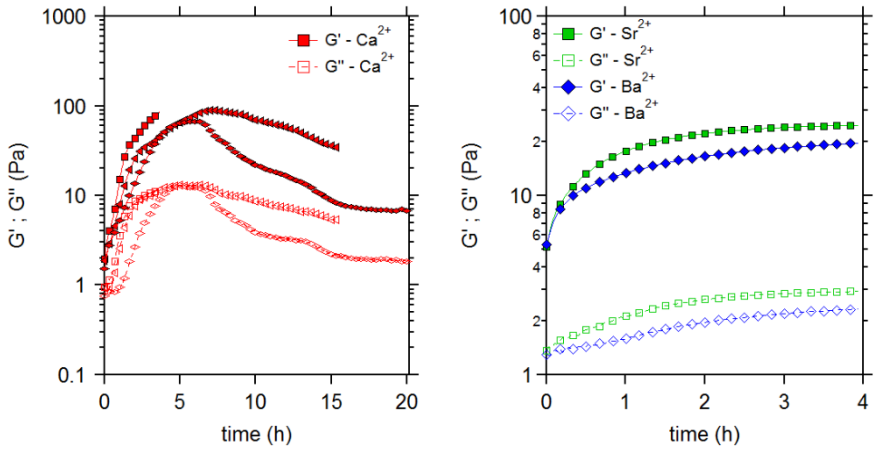

Figure 63 Right: Evolution of elastic (G') and viscous (G'') modulus as a function of time for 0.25 wt% sacran gels crosslinked by 0.05 mol/L of Ba^{2+} (blue circles) and Sr^{2+} (green diamonds) ; Left: Evolution of elastic (G') and viscous (G'') modulus as a function of time for 0.25 wt% sacran gels crosslinked by 0.05 mol/L of Ca^{2+}. Three runs at the same conditions are shown.

4.3.5. Shearing not involved in heterogeneities formation

In order to understand how the shearing could be involved on the gelation of these physical gels, the viscoelasticity of a gel with and without dynamic time sweep during its gelation is compared.

A gel concentrated at 0.25 wt% of sacran and crosslinked by 0.05 mol/L of Ca^{2+} is studied. As show in Figure 64 (a), in a first time, the gelation kinetic of the gel is followed by dynamic time sweep. The time of stabilization of the elastic modulus (called here t_{gel}) and is here equal to 1.5 h (consistent with kinetics results observed in the previous part). After this t_{gel}, a classic frequency sweep test is performed at 1 % of

strain and between 100 and 0.1 rad/s. The evolution of the G' and G'' are compared with those obtained from the same gel jellified without shearing. Basically, this second sample is introduced in the geometry gap and no shearing is applied during t_{gel}. A schematic view of these tests are shown in Figure 64 (b). The dash line represent the first test performed on the gel sheared during its gelation from which the t_{gel} is determined. The solid line describes the test performed on the second gel, 1.5 h is waited before the dynamic frequency sweep.

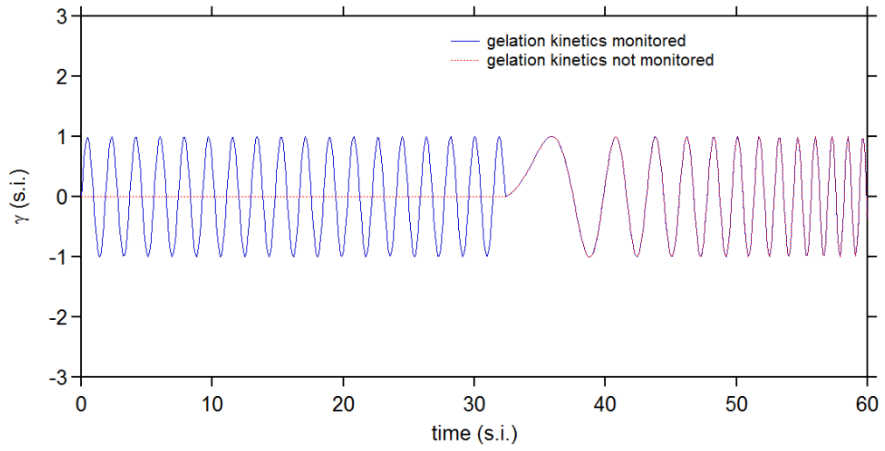

Figure 64 Schematic view of the gelation kinetics measurement where the strain is represented as a function of the time. The first time part represent the time sweep applied to one of the two identical sacran gels, the second time part represent the oscillatory frequency sweep applied to the two sacran gels.

The frequency sweep results are shown on the Figure 65. A perfect fit of these two experiments are observed. No effect of the shearing on the gelation are observed for the physical gelation of sacran at these shearing conditions. An elastic plateau is observed which described the gel elasticity. The G'' is lower than the G' than a factor ten.

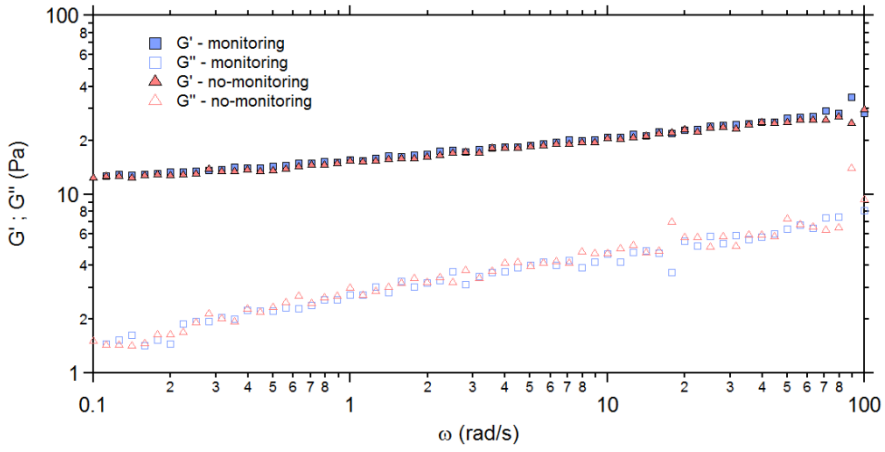

Figure 65 Elastic modulus (G') and viscous modulus (G'') as a function of frequency (1% of strain) for 0.25 wt% sacran gels crosslinked by 0.05 mol/L of Ca^{2+} with previous kinetics measurement (red triangles) and without (blue squares).

4.3.6. Imaging as final argument of the bundles formation

In order to confront rheological results previously presented, cryo-fracture and cryo-SEM have been performed and direct imaging of sacran physical gels have been obtained.

4.3.6.1. Imaging by Cryo-SEM

Cryo-SEM experiments have been performed in order to visualize the sacran organization in solution and in gels. Tree different samples are tested: a sacran solution concentrated at 0.5 wt% and two sacran gels at 0.5 wt% crosslinked by 0.1 mol/L of Ca^{2+} or Ba^{2+}.

These aqueous samples are froze and sublimated in order to be observable in SEM. This process is still new and complex. The steps of freezing and sublimation could modified the sample architecture and created bundles.

Pictures from these tree different sacran networks are compared at different observation scales. Figure 66 shows the two physical gels crosslinked by Ca^{2+} and Ba^{2+} at an observation scale around tens micrometers. The picture obtained for the sacran gel crosslinked by Ba^{2+} shows a big artefact in its right due to the sample cutting during the cryonics processing. These two pictures show some pores with pretty homogeneous sizes which seem bigger than those measured from gels rheology.

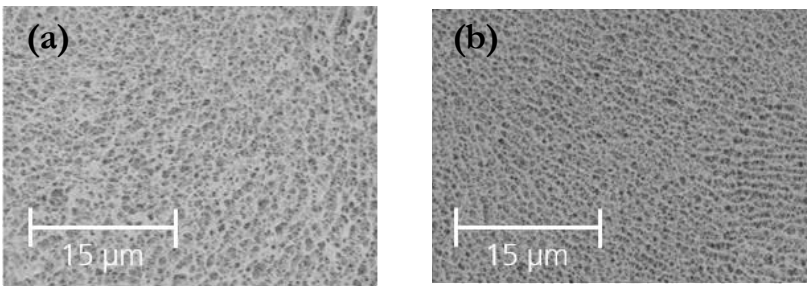

Figure 66 Cryo-SEM pictures with scales at 15 µm of 0.5 wt% sacran physical gel crosslinked by 0.1 mol/L (a) of Ca^{2+}; (b) of Ba^{2+}.

The Figure 67 shows pictures obtained from the three sacran samples. The observation scale is lowered to few microns. The pores observed on the previous pictures are also present. These pores have a diameter around the micron which is twenty times bigger than mesh sizes measured as around 50 nm from rheology.

These pores are possibly due to the processing of cryofracture which during sublimation could cause the formation of bundles for this kind of very soft matter. These pores are then not directly the evidence of the sacran network architecture. The comparison between the three pictures in Figure 67 from the three

different sacran networks which differ by their types of bonding, shows that more sample shown high linear elasticity in rheology more this bundles formation from cryonics processing is efficient.

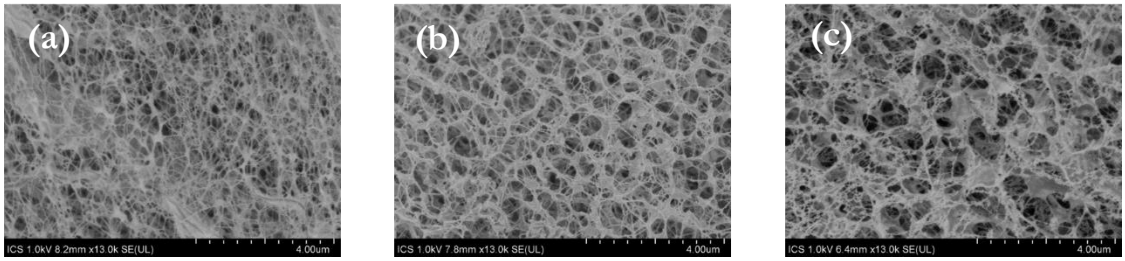

Figure 67 Cryo-SEM pictures with scales at 4 µm of 0.5 wt% sacran physical gel crosslinked by 0.1 mol/L (a) Ba^{2+}, (b) Ca^{2+} and (c) nothing observation of sacran fibrils between water bags.

The pictures in Figure 68 represent the same samples observed at shorter scales than previously, here around the micron. Two different kind of networks are observable in each of these pictures.

In the foreground, the bundling phenomena described previously is observed more finely. The link between the elasticity of the network before cryonics (measured previously by rheology) and the bundling efficiency is observed.

The sample of sacran solution without ionic crosslinker does not show these bundles surrounding the foreground pores. The physical gels crosslinked by divalent cations show these foreground pores and some large bundles surrounding them. As previously discussed, sacran gels crosslinked by Ba^{2+} show, compared which sacran gels crosslinked by Ca^{2+}, higher linear elasticity, faster gelation kinetics, lower activation energy and no strain-hardenings. During the cryonics process, Ba^{2+} ions conduce to a faster formation of crosslinked sacran chains which are subjected to a deformation. Ca^{2+} ions stabilize them more efficiently the conformation of sacran chains and then disadvantage the formation of bundles surrounding the pores formed during the cryonics process.

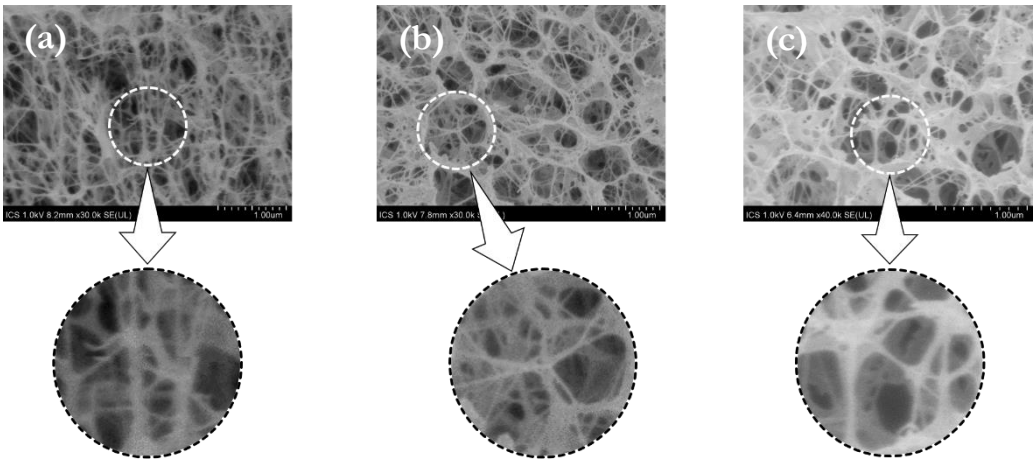

Figure 68 Cryo-SEM pictures with scales at 1 µm of 0.5 wt% sacran physical gel crosslinked by 0.1 mol/L (a) Ba^{2+}, (b) Ca^{2+} and (c) nothing observation of sacran fibrils between water bags.

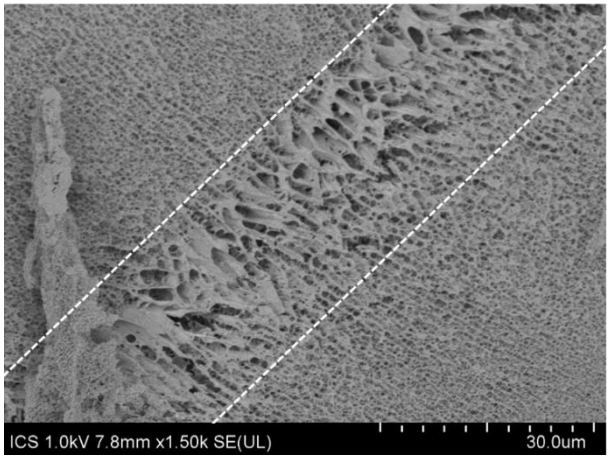

Figure 69 Cryo-SEM picture of a sacran gel concentrated at 0.5 wt% and crosslinked by 0.1 mol/L of Ca^{2+}.

In Figure 69, large pores are observed in a specific zone in the center of the picture of sacran gel crosslinked by Ca^{2+}. This zone of larger pores describes the presence of a zone of high water concentration (corresponding to a low chains density) in the gel pre-cryonics. This picture is then the evidence of heterogeneities presence in sacran gels.

4.3.6.2. Imaging by Cryo-fracture

In order to obtain imaging more precise and potentially able to validate the formation of complex bundles as the origin of the particular non-linear behaviors of these biological hydrogels, cryo-fracture pictures have been made.

Cryo-fracture pictures of sacran physical gels are performed in order to observe directly the single sacran chain organization. This technique is still in development and requires a special expertise to realize correctly the fracture of the micrometric cryogenically frozen sample.

Pictures obtained by cryo-fracture are not precise enough to clearly explain the large persistence lengths of sacran chains. However, an anisotropy is seen in these pictures realized in sacran gel crosslinked by Sr^{2+} ion. This anisotropic structures composed from pretty large bundles ($D_{bundles}$ ~ 10 µm) observed in cryo-fracture are consistent with the potential strain-hardening origin defined from rheological measurements. The strain-hardening observation was defined in sacran physical gels as dependent of the formation of large bundling zones which are able to be oriented and stretched under a nonlinear strain amplitude. The cryo-fracture pictures are obtained from the mold made from the fractured surface of the cryogenically frozen sacran gel. Thus, the sacran gel observed from cryofracture has been deformed in its nonlinear regime before the mold made.

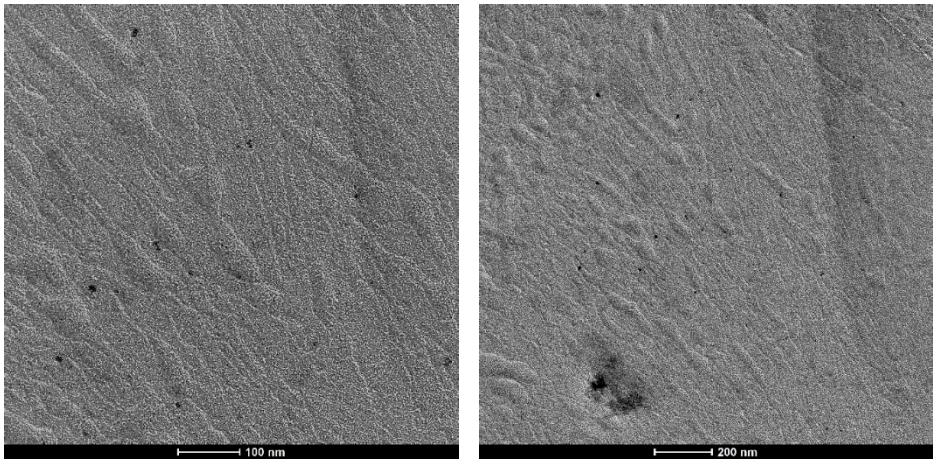

Figure 70 Cryo-fracture pictures of 0.5 wt% sacran physical gel crosslinked by 0.1 mol/L of Sr^{2+}, observation of sacran fibrils between water bags.

4.4. Conclusion

In this part, we successfully prepared physical gels of sacran crosslinked by divalent ions, Ca^{2+}, Sr^{2+} and Ba^{2+}, and we characterized linear rheological properties of these gels by macrorheology and microrheology. We showed three physical signatures of the rigid network (the chain between two crosslinking points is rigid).

(1) The mesh size estimated from the plateau modulus is much longer than the fixed charge distance on the sacran chain, suggesting that the chain rigidity prevent the chain from collapsing upon crosslinking.

(2) The mesh size was found to be comparable to microrheologically determined persistence length.

(3) At a constant crosslinking ratio, the plateau modulus scaled as $C_{sacran}{}^{1.5}$.

The physical gels crosslinked by Sr^{2+} and Ba^{2+} behaved similarly, while those crosslinked by Ca^{2+} showed lower moduli. The kinetics of gelation induced by Ca^{2+} are slower and more complex than those induced by Ba^{2+} and Sr^{2+}, suggesting formation of larger structure of sacran chains with Ca^{2+}.

Different influences of macrorheological measurements on the sacran network architecture are investigated. If shearing frequencies between 1 and 5 Hz are not influenced the elasticity of sacran gels.

The multi-scales rheological study in the linear regime of sacran physical gels have determined precisely the microscopic architecture of network which composed them. The rigidity of segments of sacran chains between two consecutive junction zones of these physical gels have been proved.

5. Physical gels - Non-linear regime, network rigidity and heterogeneities

5.1. Introduction

As reviewed in Chapter 1, filament-forming proteins playing important roles in cell mechanics and motility commonly show strain-hardening under large strain[77]. The rigidity-induced strain-hardening can be promising in the context of mechanical reinforcement of hydrogels, still, it is a challenge to synthesize a model system. The relation between viscoelastic properties and network architecture of gels made of rigid chains is not well experimentally studied. In the previous chapter, we have shown that the sacran physical gels are made of rigid chains at the length scale of the mesh size. It is interesting to correlate this description of the nanometric architecture of sacran networks with their nonlinear rheological behaviors.

In this chapter, we study the nonlinear rheological properties of the sacran physical gels. The three divalent cations, Ca^{2+}, Sr^{2+} and Ba^{2+} are used and compared each other. In order to clarify the effects of these cations as crosslinker to bridge two anions on sacran chains and as ions to change the ionic strength and the interactions of the charged polysaccharide, comparison with Mg^{2+} and Na^{+} are also done.

5.2. Experimental section

5.2.1. Physical gel preparation

A sacran mother solution was prepared according to the usual procedure described in the chapter 3. $CaCl_2$, $SrCl_2$, $BaCl_2$, NaCl and $MgCl_2$ were purchased from Sigma Aldrich and used as received.

The various salts are beforehand solubilized in pure water. The right quantity is added into the sacran mother solution in order to obtain the desired concentrations both in cations and sacran. After the addition of divalent cations, each sample is mixed by using a vortex at low speed. The mix continues during one minute and the gel becomes totally transparent and homogeneous. The fresh gel is then placed into the geometry of the rheometer and its viscoelasticity stabilization is followed by an oscillatory time sweep (1 Hz, 1 % of strain amplitude, 25 °C).

5.2.2. Rheological measurement

Macroscopic nonlinear rheological measurements of sacran physical gels were performed with a strain-controlled TA Instruments ARES LS1 rheometer using cone-plate geometry (diameter: 50 mm, angle 2°, gap 50 µm) with a roughened surface and an oil bath to prevent the gel from drying. Three kind of sweeps are systemically and consecutively performed on each sample tested by macrorheology at 25 °C: (1) an oscillatory time sweep (1 %, 1 Hz) in order to study the gelation kinetics of the gel, (2) an oscillatory frequency sweep (1 %, 25 °C) in order to characterize the linear viscoelastic properties of the chemical gels characterized by an elastic plateau (the results are shown in the previous chapter), and (3) an oscillatory strain sweep (1 Hz, 25 °C) in order to probe the rheological behaviors of gels in their nonlinear regimes. The strain amplitude was varied between 1 and 150 %.

5.3. Results and discussion

5.3.1. Dependence of the ion species

As seen in the previous chapter, the gelation kinetics show a strong ion species dependence. Gelation kinetics of sacran networks at 0.25 wt% crosslinked by 0.05 mol/L of Ca^{2+} is slower and much complex than those of gels crosslinked by the same amount of Sr^{2+} or Ba^{2+}, Figure 71 (a), and presumably larger structures slowly develop. In this chapter we use physical gels after a gelation time of 1.5 h (when the moduli practically stabilize) in order to evaluate the effects of eventual larger structures on the nonlinear rheological properties.

Time profiles of the macrorheological viscoelastic moduli for sacran physical gels crosslinked by Ca^{2+}, Sr^{2+} or Ba^{2+} are shown in Figure 71 (a). The concentration of sacran is 0.25 wt% and the ion concentration is 0.05 mol/L. As shown in the previous chapter, the gelation kinetics by the Ca^{2+} gelation is slower and more complex than those by the Sr^{2+} and Ba^{2+}. When gelation by Sr^{2+} and Ba^{2+} stabilize after 1.5 h, the G' from the gelation by the Ca^{2+} starts to stabilize and decrease after 10 h. The evolution of elasticity of sacran gels crosslinked by Ca^{2+} is not understood. After the time sweep, strain sweeps are performed in order to characterize the nonlinear rheological behaviors.

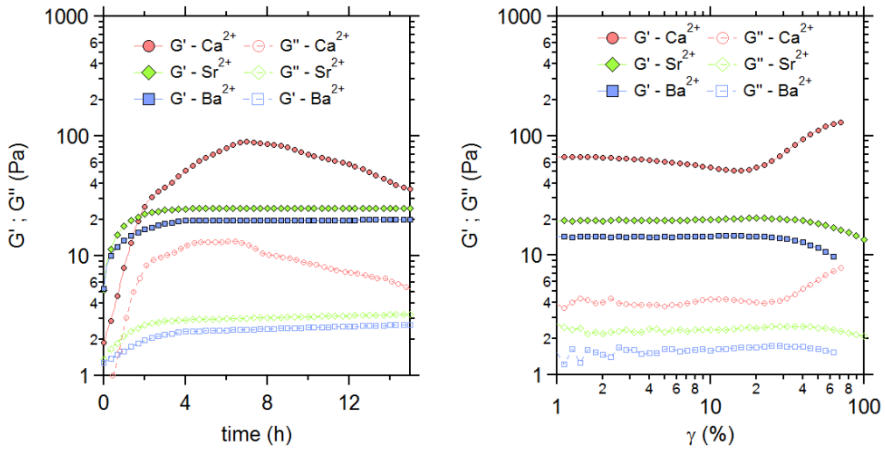

Figure 71 Viscoelastic modulus (G' ; G'') from time profiles and oscillatory strain sweeps performed on sacran physical gels crosslinked by Ba^{2+}, Sr^{2+} and Ca^{2+}. Elastic modulus (filled symbols) and viscous modulus (open symbols). Sacran concentration: 0.25 wt%. Ion concentration: 0.05 mol/L.

Figure 71 (b) shows the evolution of viscoelastic moduli of 0.25 wt% sacran physical gels crosslinked by the three different cation species as a function of the strain amplitude. After this gelation time, the moduli of the gel crosslinked by Ca^{2+} is higher than those of the gels crosslinked by Sr^{2+} or Ba^{2+}. The gels crosslinked by Ba^{2+} and Sr^{2+} show a similar strain-softening behavior. Above a certain strain amplitude (about 40 %), the elastic modulus falls. On the contrary, the gel crosslinked by Ca^{2+} shows a strain-hardening behavior.

The value of G' slightly decreases when the strain increases, then it starts to raise at a strain of about 20 %. This increase of gel elasticity is followed by a sharp decrease (data points for this decrease not shown), presumably when the sample is ejected from the geometry or fractured. Here we define two parameters characterizing a strain-hardening behavior. The strain-hardening ratio (Q) is defined as the ratio of the maximum value of G' to G_e (G' at the linear domain). The strain at which the modulus starts to breakdown is defined as γ_{max}. For the 0.25 wt% sacran gel crosslinked by 0.05 mol/L of Ca^{2+}, we find Q = 2 and γ_{max} is approximatively 99 %.

The same tests are performed on physical gels of a higher sacran and ion concentrations (C_{sacran} = 0.5 wt%, C_{ion} = 0.1 mol/L) keeping the crosslinking ratio (above the stoichiometry). In Figure 72, time profiles of the viscoelastic moduli are shown. Interestingly, at this concentration the evolution of the modulus for the gel crosslinked by Ca^{2+} is less complex and similar to that for gels crosslinked by Sr^{2+} and Ba^{2+}; the moduli gradually increase then level off. The kinetics are slower than those at 0.25 wt% and the absolute value of moduli for the gel crosslinked by Ca^{2+} is lower than that by Sr^{2+} and Ba^{2+}.

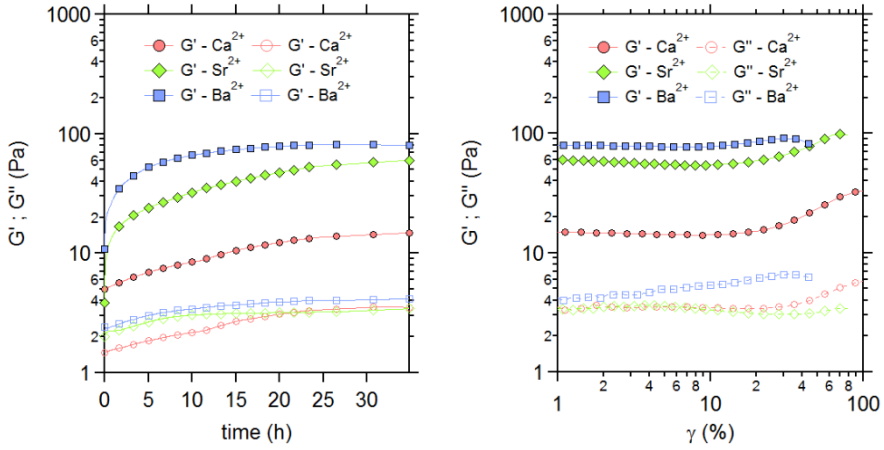

Figure 72 Elastic modulus (G') as a function of strain for 0.5 wt% sacran gels crosslinked by 0.1 mol/L of Ba^{2+} (blue squares), Sr^{2+} (green diamonds) and Ca^{2+} (red circles).

Strain sweep tests are performed after the gelation time of 35 hours. The values of G_e for the gels crosslinked by Sr^{2+} and Ba^{2+} are close (60 Pa for Sr^{2+}, 80 Pa for Ba^{2+}). The G_e of the gel crosslinked by Ca^{2+} is around 15 Pa and showing a well-defined elastic plateau. This value is lower than that for 0.25 wt%, suggesting the presence of heterogeneous structure at 0.25 wt%. We observe a strain-hardening behavior dependent of the ion species. For the gel crosslinked by Ca^{2+}, the behavior is similar to that of the gel at 0.25 wt%: the moduli start to increase at about 30 % and the strain-hardening ratio Q is found to be 2.3. At this concentration we observe similar strain-hardening for the gel crosslinked by Sr^{2+}, with a Q of 1.6. For the gel crosslinked by Ba^{2+}, the value of Q is about 1.1, though it is difficult to say strain-hardening occurs for this gel, at least the strain softening behavior observed for the 0.25 wt% gel is not observed. The γ_{max} observed for these same sacran gels crosslinked by Ba^{2+}, Sr^{2+}, and Ca^{2+} are respectively about 30, 70, and 100 %. Apparently, with increase in the elasticity, the breakdown of the moduli appears at lower strain amplitude.

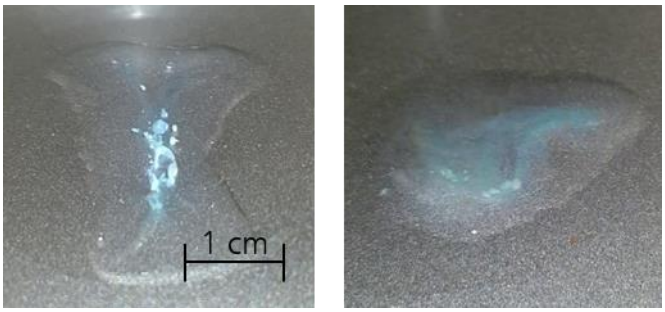

Figure 73 Pictures of sacran gels at 0.5 wt% after the oscillatory strain sweep crosslinked by 0.1 mol/L of Ca^{2+}(left) and by 0.05 mol/L of Ba^{2+} (right).

Another interesting observation is done with the gel samples after the rheological measurements when the samples were unloaded from the geometry (Figure 73). For the gel crosslinked by Ca^{2+}, we observed millimetric white large structures visible with even naked eyes. For the gel crosslinked by Ba^{2+}, these large structures are also observed, though the size seems less pronounced. The same phenomenon is observed for the Sr^{2+} gelation. This result suggests again that the sacran chains can form large structures in the presence of the ions, especially Ca^{2+}, and that these structures are presumably related to the strain-hardening behavior.

These large structure formation could be correlated with the ionic radius of the cation used. The ionic radius of Ca^{2+}, Sr^{2+} and Ba^{2+} are respectively equal to 100, 113 and 136 pm. The kosmotropic effect is related to the capacity of an ionic species to stabilize bio-macromolecules aggregates[78]. A kosmotrope causes the solvent molecules to organize around the molecule and stabilizes the interactions. This phenomenon is called "salting-out". A "salting-out" ion induces an increase in the viscosity and a decrease in the rotational decay of water[79]. The kosmotropic effect is classified by the empirical Hofmeiser series which describes the ranking of the (salting-out and salting-in) ions to precipitate macromolecules. This Hofmeiser series consider all the alkaline earth metal divalent ions used in this study as kosmotropes. Thus these ions are expected to be capable to structure the sacran chain organization. This kosmotropic effect is directly linked with the water dipole theory developed in order to explain the salting effect produced by a polar cosolute. The higher the charge density of the ion is, more ordered the structure of water around is. And stabilized polymer chains tend towards a precipitation. In the case of sacran helix formation might be involved. The ions studied in this work are listed in order of their charges densities:

$$Na^{+} > Mg^{2+} > Ca^{2+} > Sr^{2+} > Ba^{2+}.$$

Considering the kosmotropic effect, Mg^{2+} should be the more disposed to stabilized sacran chains and produced crystallizations domains within the network.

The effect of addition of salts on the rheological properties of sacran entangled gels is further studied in order to better evaluate the ion species dependence of the physical gelation of sacran. Time sweep experiments are performed by macrorheology (1 %, 1 rad/s, 25°C) in order to compare the gelation ability of the five ions: Na^{+}, Mg^{2+}, Ca^{2+}, Sr^{2+} or Ba^{2+} (in Cl salt form). And the result is shown in Figure 74. The gels crosslinked by Na^{+} and Mg^{2+} show further slower evolution than that crosslinked by Ca^{2+}, and the

moduli stabilize after 40 h around an elastic modulus around 20 Pa. Since there is no difference between the systems with Na^+ and Mg^{2+}, it is suggested that Mg^{2+} does not crosslink the sacran chain by divalent charges, and there are other mechanisms of modulus increase induced by the salts. The ionic strength of $MgCl_2$ and NaCl is not identical, thus the slow kinetics are presumably controlled by the dynamics of the long sacran chains. The values of G_e for the system with Na^+ and that with Mg^{2+} are about 19 Pa, much lower than that of the gel crosslinked by Ba^{2+} (85 Pa), close to that of the gel crosslinked by Ca^{2+} (16 Pa), suggesting that Ca^{2+} does not ionically crosslink either.

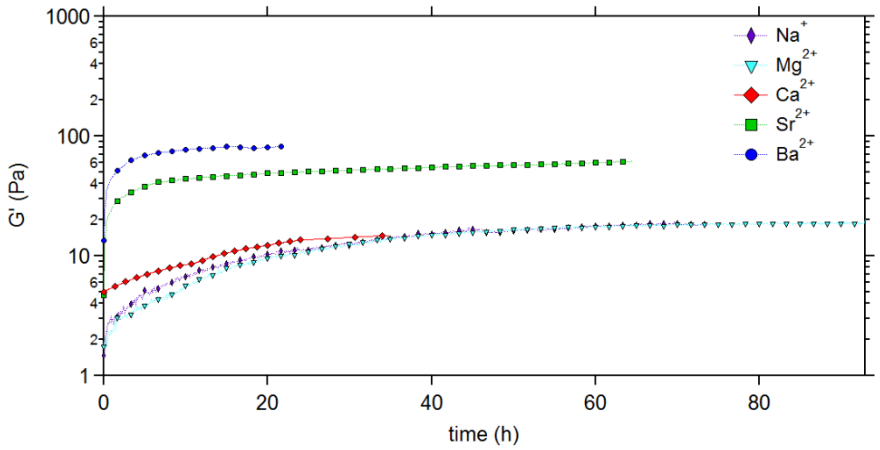

Figure 74 Elastic modulus (G') as a function of time during a time sweep performed at 1 %, 1 rad/s and 25°C for sacran gels at 0.5 wt% and crosslinked with 0.1 mol/L of different salts.

Nonlinear rheological properties are studied and the viscoelastic moduli are plotted as a function of strain in Figure 75. In the non-linear domain observed at strains higher than 10 – 30 %, measurements show strong ion species dependence. The gels in the presence of Na^+ and Mg^{2+} show a pronounced strain-hardening behavior. The strain-hardening starts to appear from 10 % of strain, and the ratio Q is about 12 for Na^+ and 15 for Mg^{2+}. For this batch of samples, the gels crosslinked by Ca^{2+} and Sr^{2+} showed also strain-hardening of weak intensities, and that crosslinked by Ba^{2+} exhibits strain-softening, the moduli decrease in the nonlinear regime and no hardening is observed.

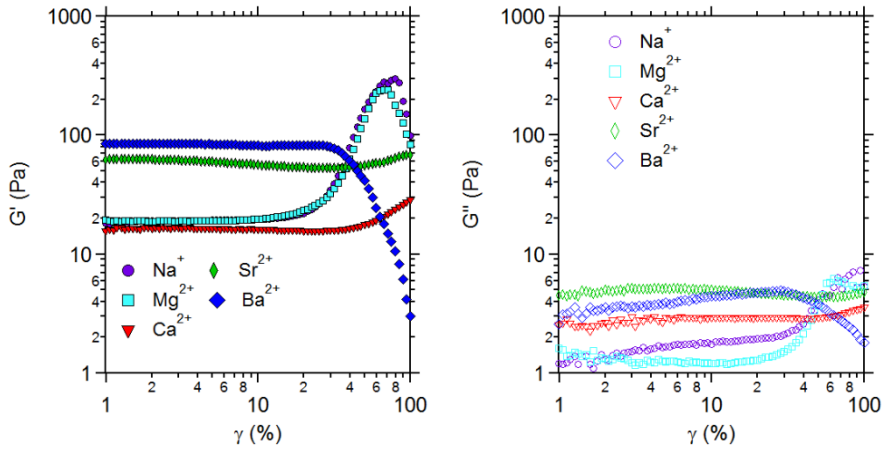

Figure 75 Elastic modulus (G') and viscous modulus (G'') as a function of strain during a strain sweep performed at 1 rad/s and 25°C for sacran gels at 0.5 wt% and crosslinked with 0.1 mol/L of different salts.

These results suggest that there are two effects of these ions on the network structure and consequently on the viscoelasticity of sacran solutions/gels: (1) the divalent cations are potentially able to crosslink sacran chains by electrostatic interactions, and (2) they change the ionic strength of the solution and influence the inter-chain interactions between the sacran chains. The first crosslinking effect seems increasing in the following order, $Ba^{2+} > Sr^{2+} > Ca^{2+} \geq Mg^{2+}$, since the value of G_e increases and the gelation time decreases in this order. The crosslinking ability seems to increase with the ionic size of the cations. Therefore, the higher the charge density of the crosslinking cation is, the slower the gelation kinetics is, the less elastic the formed physical gel is and the more favorable for a strain-hardening behavior. This phenomenon could be explained by the kosmotropic effect which increases with the charge density of the ion. The stronger the kosmotropic effect of the cation is, the more water molecules are organized near the cations which decreases the affinity of the ion with the negative charges on the sacran chains.

Since Mg^{2+} does not show any particular differences with Na^{+}, we assume that this divalent cation does not ionically crosslink the sacran chain, however, very slow evolution of moduli occurs and the strain-hardening is observed. The difference in G_e between Ca^{2+}, Mg^{2+} and Na^{+} is weak, thus Ca^{2+} may not ionically crosslink the sacran chains either. These ions presumably induce the association of sacran chain by unidentified interactions. The moduli of the corresponding sacran solution without added salt do not evolve at this time scale (data not shown). This result suggests that the sacran chains can associate each other in the presence of salt, presumably the screening of the electrostatic repulsion plays a role in the chain association.

The effect of salt concentration on non-linear rheological properties of sacran is studied with NaCl which do not ionically crosslink sacran chains. Figure 76 shows the time profiles of the elastic modulus of 0.25 wt% sacran solutions containing NaCl at different concentrations. The modulus increases with time though the evolution is not monotonic, the modulus evolution is irregularly and irreproducible with time. This kinetics are presumably related to the heterogeneous network structure of the weakly associating sacran network. The modulus seems stabilized after 20 – 40 h depending on the salt concentration. One can say that the initial rate of modulus change increases with the salt concentration, as well as the value of modulus after a long time (60 h), indicating the effect of the salt on the moduli evolution. The values of the elastic modulus of the gels are between 6 and 18 Pa.

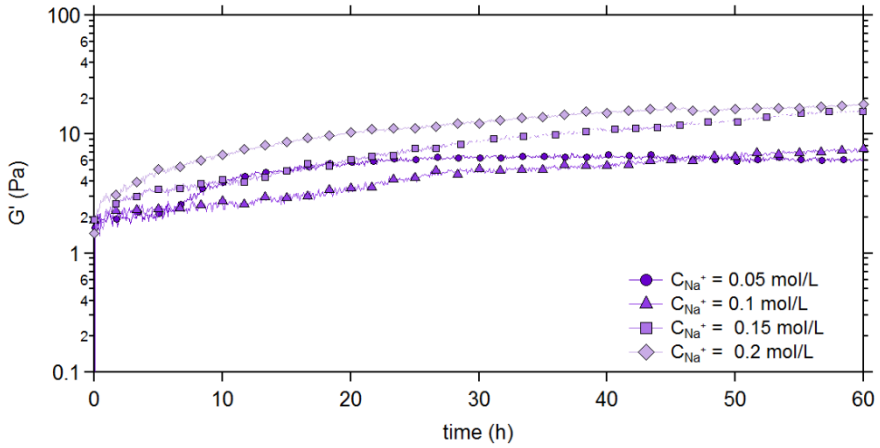

Figure 76 Viscoelastic modulus (G'; G'') as a function of time obtained from oscillatory time sweeps performed on sacran gels at 0.5 wt% in presence of different NaCl concentrations.

Figure 77 shows the strain amplitude dependence of the viscoelastic moduli for the 0.5 wt% sacran gels in the presence of NaCl at different concentrations. For all the NaCl concentrations studied, the strain-hardening behavior is observed. With an increase in the salt concentration, the strain-hardening becomes more pronounced. The moduli slightly increases at a small strain range about a few per cents. The reason is not known.

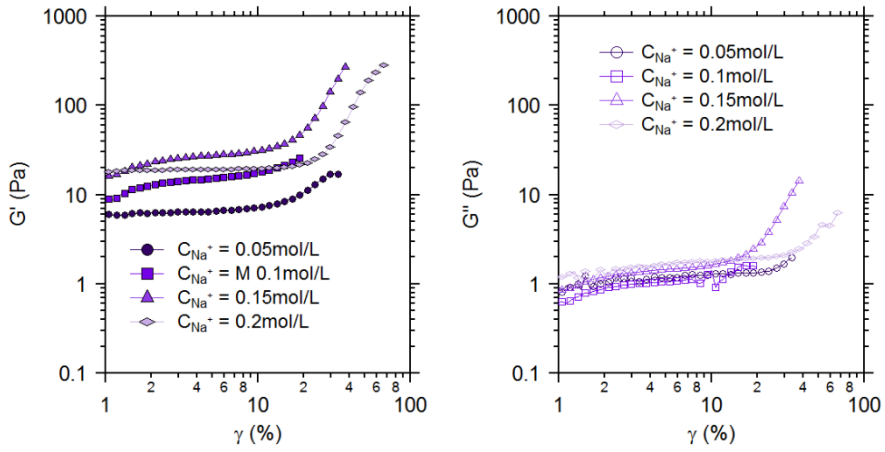

Figure 77 Elastic modulus (G') and viscous modulus (G'') as a function of strain amplitude obtained from oscillatory strain sweeps performed on sacran gels at 0.5 wt% in presence of different NaCl concentrations.

The three parameters characterizing the sacran gels in the presence of NaCl are summarized in the Figure 78 as a function of the salt concentration in the medium. The elastic plateau modulus increases with the salt concentration, suggesting that the number of association points of sacran chains increases with a decrease in the electrostatic repulsion between the charged chains. The strain-hardening ratio Q increases sharply from 3 to 15 between 0.1 and 0.15 mol/L of NaCl, suggesting that some structural change occurs at this concentration range. The γ_{max} shows a more complex evolution: with an increase in the NaCl concentration from 0.05 to 0.1 mol/L, γ_{max} decreases from 30 to 20 %, then it increases from 20 to 66 % when the salt concentration increases from 0.1 to 0.2 mol/L. Though this change is presumably related to the network structure, we do not have enough experimental data to conclude, as the gelation time is too long to repeat

the same experiments. The value of γ_{max} can depend on fracturing or slipping of the gel under large deformation which are not in general very reproducible.

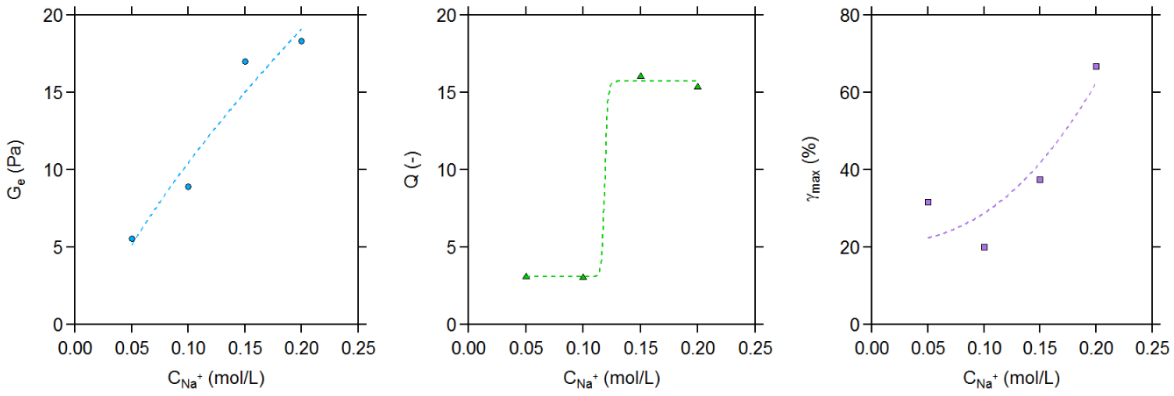

Figure 78 G_e (blue circles), Q (green triangles), and γ_{max} (purple squares) as a function of C_{NaCl} obtained from oscillatory strain sweeps performed on sacran gels at 0.5 wt% in presence of different NaCl concentrations.

This salt effect which lead the association of sacran can be observed with the other divalent cations, in competition with the ionic crosslinking effect. The salt effect induces slower modulus increase, strain-hardening and presumably larger structure formation. The ionic crosslinking effect induces formation of a gel in a relatively short time scale having strain softening behavior. For Mg^{2+}, we do not have evidence of ionic crosslinking with this cation, it behaves practically similarly to Na^{+}. The salt effect induces the noticeable strain-hardening with the ratio Q of about 15. For Ca^{2+} and Sr^{2+}, both effects competes with one another and depending on the conditions one of the two dominates the other. For Ca^{2+} the salt effect is more dominant with an Q around 2. This might explain the absence of bead formation (gelation time is too short to form a gel bead). For Sr^{2+} the ionic crosslinking effect is more dominant and only at certain conditions strain-hardening can be observed. For Ba^{2+}, the ionic crosslinking effect is dominant at all the conditions studied in this work.

5.3.2. Strain-hardening, cycle tests

The effects of strain amplitude stimulus on strain-hardening properties observed for physical gels of sacran crosslinked by Ca^{2+} are studied. 20 cycles of strain sweep tests are performed at 6.28 rad/s by increasing the maximum amplitude by a step of 5 %. For 20th cycle, the strain is varied from 1 % to 100 %. The sweeps are performed by macrorheology with a cone-plane geometry. Here we study the gel at 0.25 wt% crosslinked by Ca^{2+} (0.1 mol/L), which shows a strain-hardening behavior. After a dynamic time sweep during 48 hours (in order to confirm the stabilization of the moduli), these oscillatory strain sweep tests are performed. A schematic view of the strain sweep steps (1 Hz, 25 °C) is shown in Figure 79. Each step begins at 1 % of strain, the strain amplitude of each step goes to a strain amplitude 5 % higher than the previous one without waiting time between the steps.

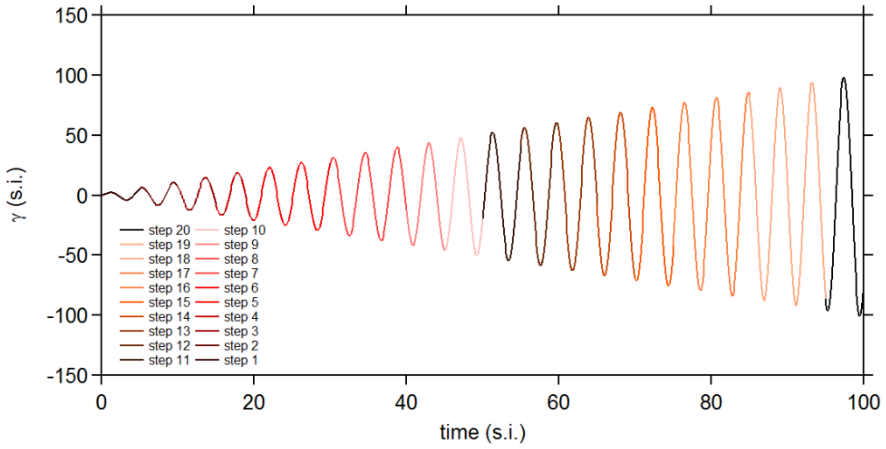

Figure 79 Schematic view of oscillatory strain sweep test from 1 % to 100 % performed by step of 5 % at 6.28 rad/s, 25 °C; representation of the strain amplitude applied to the sample as a function of the experiment time.

In Figure 80, the strain dependence of the viscoelastic moduli of a sacran gel at 0.5 wt% crosslinked by 0.1 mol/L of Ca^{2+} is plotted for each strain step. Strain-hardening behavior is commonly observed at the strain amplitude higher than 10 %. The value of G_e gradually decreases at each strain step from 170 Pa to 50 Pa. This decrease of the linear viscoelasticity could correspond to a partial breaking of the physical crosslinks. The strain-hardening behavior is still observed even at the cycles with the decreased plateau modulus. G'' shows the same tendency: its value decreases with increase in the maximal amplitude, a small strain hardening is observed.

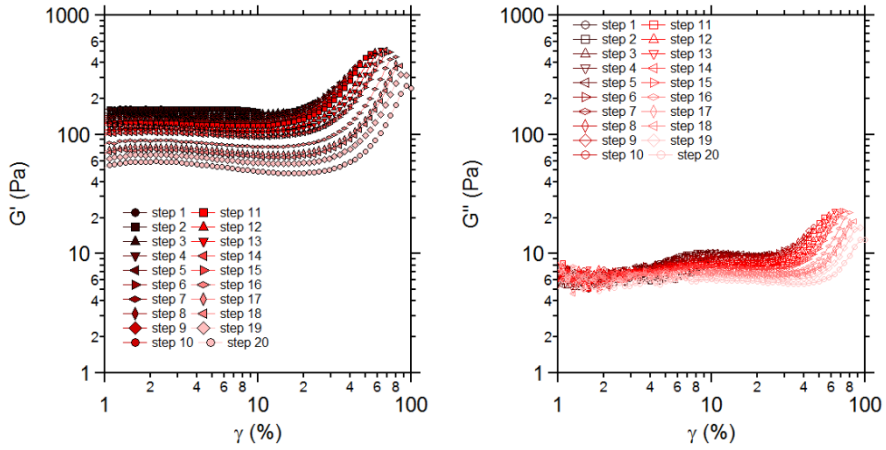

Figure 80 G' (solid marks) and G'' (open marks) as a function of strain from 1 % to 100 % with a step of 5 % for a sacran gel at 0.5 wt% and crosslinked by 0.1 mol/L of Ca^{2}.

In order to better compare the evolution of the strain hardening behavior, the values of G' are normalized by the value at the strain of 1 % are plotted as a function of the strain in Figure 81. The hardening is shifted to higher strain as imposed strain increases: at the maximal values of G' the values continue to follow the curve of the previous step. A slight strain softening is observed at a strain range of 5 – 30 %.

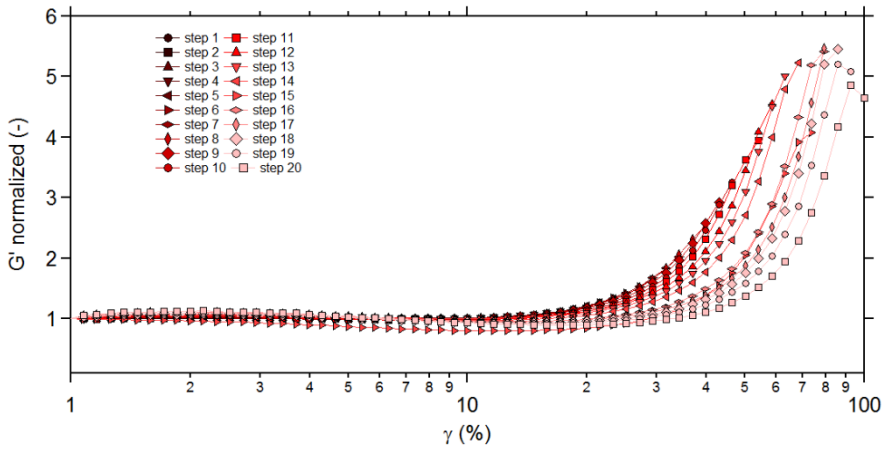

Figure 81 G' normalized by the G' of each step at 1 % of strain amplitude as a function of strain from 1 % to 100 % with a step of 5 % for a sacran gel at 0.5 wt% and crosslinked by 0.1 mol/L of Ca^{2+}.

Figure 82 shows the maximum strain amplitude dependence of the plateau elastic modulus G_e and the strain-hardening ratio, Q. The linear domain is up to 10 % of strain, then the value of G_e decreases with the maximal strain amplitude. The value of Q increases to about 5 with the increase in γmax up to 60 %, then the value of Q levels off.

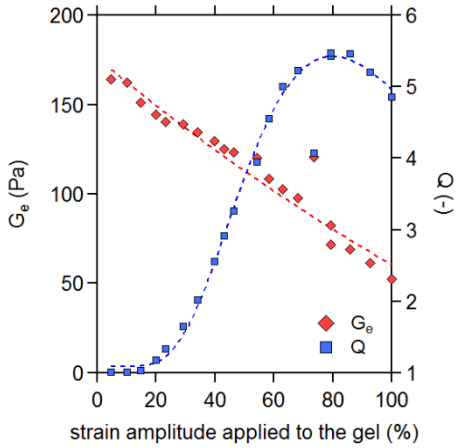

Figure 82 Elastic modulus at 1 % and 6.28 rad/s considered as G_e (blue circles), and Q (red diamonds) as a function of the maximum strain amplitude applied on the sacran gel (at 0.5 wt% and crosslinked by 0.1 mol/L of Ca^{2+}).

It is known that many associating polymer solutions show strain-hardening which is attributed to the increase in the number of elastically active chains and/or to the non-Gaussian chain stretching. The sacran physical gels can be considered as transient network associating polymers. At the strain amplitude from 20 to 80 %, the strain-hardening increases at each strain step when the linear elasticity decreases. If these strain-hardenings are caused by an increase of the number of elastic active chains, G_e would be expected to increase, while we observe its decrease. The decrease in G_e suggests that the physically crosslinked sacran network is reorganized under shear above a certain strain. The physical crosslinks are transient and can break under shear. Though they are also reversible thus can reform, in our experiments without waiting time between cycles, recovery of G_e is not complete. The non-Gaussian chain stretching seems to be more probable for the rigid sacran chains.

Rigid chains can be aligned under large deformation and when they are associative and crosslinkable, bundle-like structure may be formed, as schematically illustrated in Figure 83. As previously discussed, between two crosslinking points, there are many negative charges with an excess amount of Ca^{2+}, and aligned rigid chains can have more contact points which can be crosslinked. Such bundle formation can decrease the number of the elastically active chains and may decrease the linear elasticity of the sacran gel. In the next chapter, we continue to investigate on the non-linear elasticity by using chemical gels of sacran.

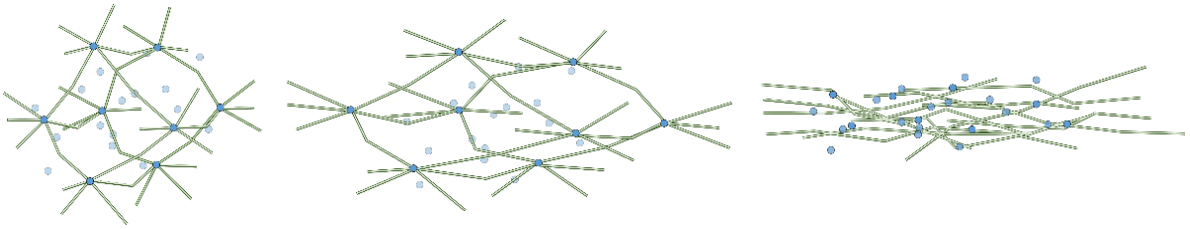

Figure 83 Schematic view of possible sacran network reorganization during submitted to an increase (from left to right) of the strain amplitude: from the ideal rigid network to the bundle formation, sacran chain rigid segments are represented by green rectangles and ionic crosslinking agents by blue circles.

5.3.3. Strain rate frequency superposition (SRFS)

In order to better characterize the strength of the crosslinking divalent cations, the dynamics of the physical crosslinking is studied from rheological relaxation process. Though the ionic crosslinking is expected to be reversible, we do not observe the terminal flow in the sacran physical gel at as low frequency as 10^{-3} rad/s even at high temperatures (Figure 84). In order to characterize the dynamics of the physical gels which do not flow in linear domain, a series of strain rate frequency superposition (SRFS) experiments is performed. This method, where the frequency is swept at a fixed strain rate, allows us to evaluate slow relaxation process of viscoelastic media which is too slow to be observed with a classical frequency sweep test (at a fixed strain amplitude)[56]. From this relaxation time obtained at different temperatures, the activation energy of the relaxation of the sacran gel is calculated by an Arrhenius plot. Note that the time–temperature superposition is not successful for this system.

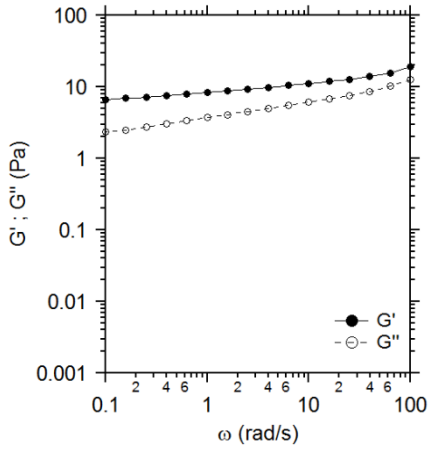

Figure 84 Viscoelastic modulus (*G'*; *G''*) as a function of frequency for 0.5 wt% sacran gels crosslinked by 0.1 mol/L of Ca^{2+} (1%, 25 °C).

SRFS tests are performed for strain rates between 7.5 10^{-3} and 1 s^{-1} for frequencies between 0.01 and 10 rad/s (data for the frequency higher than 1 rad/s were not used as they contain a lot of noises). As an example, the viscoelastic moduli of a 0.5 wt% sacran gel crosslinked by 0.1 mol/L Ca^{2+} as a function of frequency are plotted in Figure 85. Compared to the curve for the constant strain amplitude frequency sweep which shows an elastic plateau at this frequency range, the curves for constant strain rates show flowing at low frequency. At this condition, we do not observe strain-hardening.

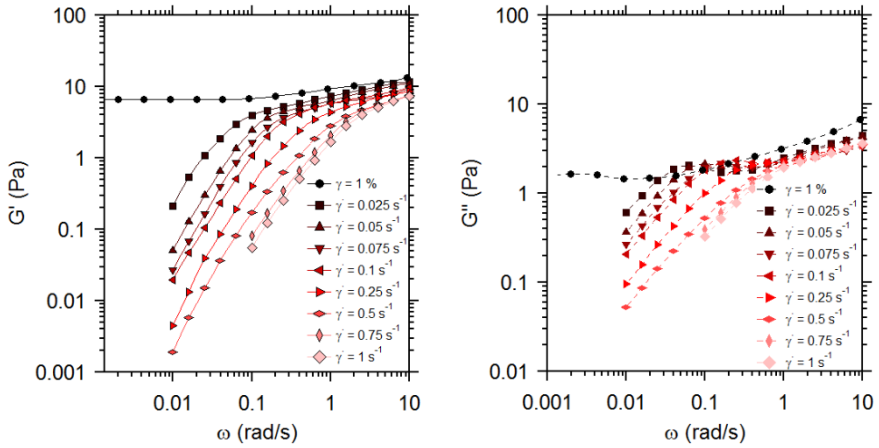

Figure 85 Elastic modulus (G') and viscous modulus (G'') as a function of frequency for 0.5 wt% sacran gels crosslinked by 0.1 mol/L of Ca^{2+} for different constant strain rate from 2.5 10^{-2} to 1 s^{-1}.

These curves at different strain rates are horizontally and vertically shifted to superpose on a reference curve. The curve at $\dot{\gamma} = 7.5\ 10^{-3}\ s^{-1}$ is chosen as reference. The horizontal and vertical shift factors a and b are respectively determined, and shifted viscoelastic moduli bG' and bG'' are plotted as a function of the shifted frequency $a\omega$ (Figure 86). G' and G'' master curves are obtained covering an extended frequency range. At the high frequency range, G' is higher than G'', then they show a crossover and G'' becomes higher than G', thus the physical gel shows terminal flow. Superposition is less satisfactory for G' after the crossover. From the master curves, we obtain values of $\tau_c = 1/a\omega_c$ as the relaxation time of the network relaxation.

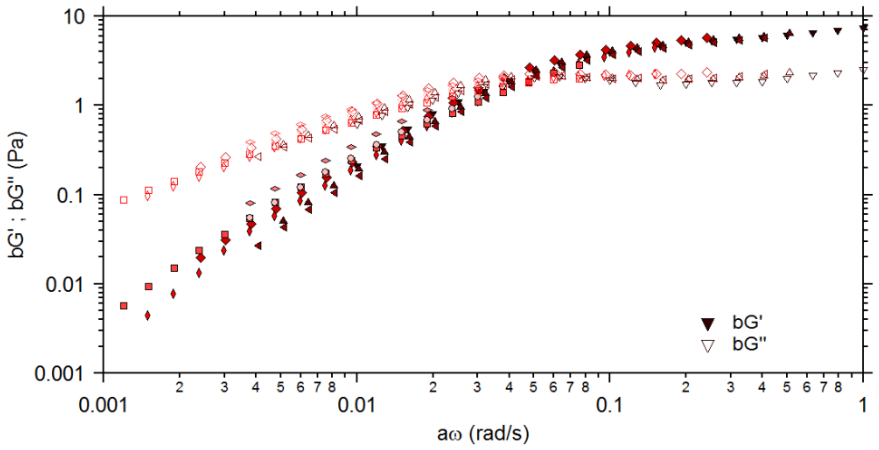

Figure 86 Viscoelastic modulus (G'; G'') rescaled by SRFS factors as a function of frequency for 0.5 wt% sacran gels crosslinked by 0.1 mol/L of Ca^{2+} for different constant strain rate from 2.5 10^{-2} to 1 s^{-1}.

The values of a and b are plotted as a function of $\dot{\gamma}$ in Figure 87. The horizontal shift factor a decreases with an increase in $\dot{\gamma}$ as $a \sim \dot{\gamma}^{-1}$, while the vertical shift factor b is practically constant, as often observed for SRFS.

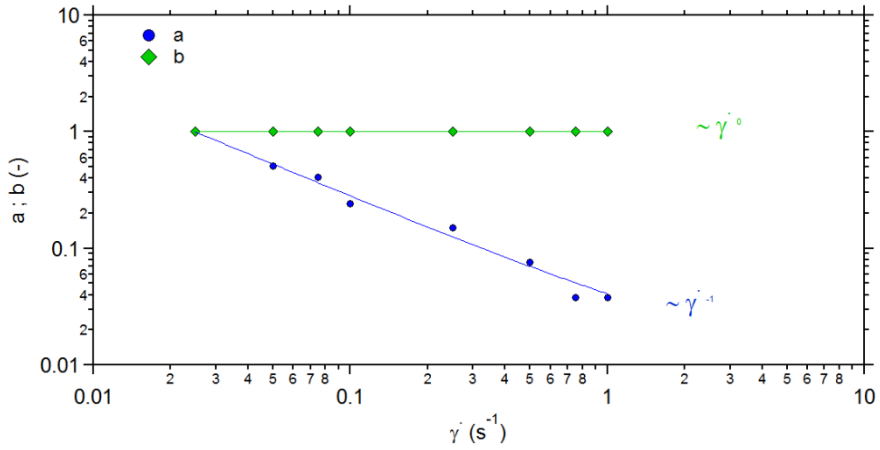

Figure 87 SRFS factors a (blue circles) and b (green diamonds) which respectively rescale the frequencies and the modulus (G' and G'') of frequency sweeps as a function of the strain rate of the rescaled sweep. Example of sacran gel at 0.5 wt% crosslinked by 0.1 mol/L of Ca^{2+}.

The same SRFS experiments are performed at 5 temperatures (15, 25, 35, 45 and 55 °C) to determine the relaxation time τ_c for the physical gels of 0.5 wt% of sacran, crosslinked by Ca^{2+}, Sr^{2+} or Ba^{2+} at 0.01 or 0.1 mol/L (above the stoichiometry concentration). As the relaxation time is determined, now we estimate the activation energy.

In chemical kinetics, the Arrhenius law allows to describe the variation in the rate of a chemical reaction as a function of the temperature. This law was enunciated by Svante August Arrhenius in 1889 in his article "On the reaction velocity of the inversion of cane sugar by acids". Indeed, the Arrhenius law has been verified experimentally for a large number of chemical reactions. However, not all reactions follow this law (especially enzymatic reactions). The Arrhenius law is therefore an empirical law. The Arrhenius equation can be given in the form:

$$1/\tau_c = A\, e^{-E_a/RT}, \qquad 37$$

where $1/\tau_c$ is the kinetic constant, E_a the activation energy, R the gas constant, T the temperature. In general $ln(1/\tau_c)$ is plotted as a function of $1/T$ to obtain a linear relation, then the value of E_a is determined from the slope of the linear regression.

The values of $ln(1/\tau_c)$ are plotted as a function of $1/T$ in Figure 88 and Figure 89 for all sacran gels tested. The results demonstrate that the relaxation time increases in the following order: $Ba^{2+} > Sr^{2+} > Ca^{2+}$, thus the sacran gels crosslinked by Ca^{2+} flow faster than those crosslinked by Sr^{2+} or Ba^{2+}. With the increase in the ion concentration from 0.01 to 0.1 mol/L, the relaxation time increases for all the three ions.

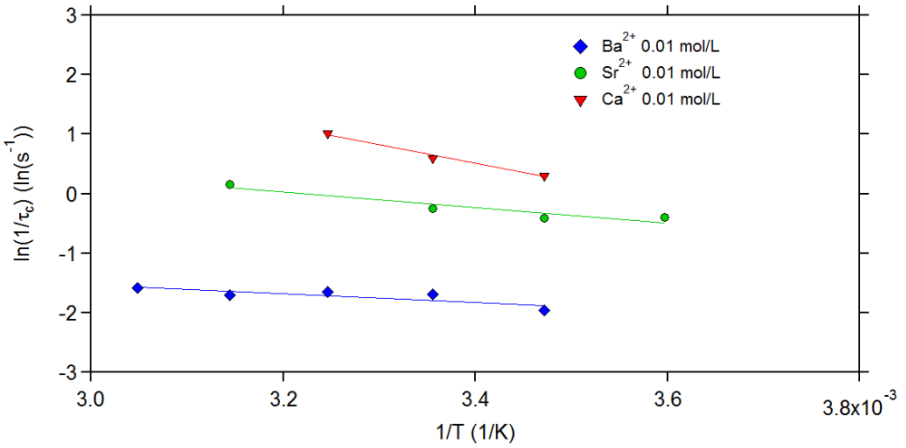

Figure 88 $Ln[1/\tau_c]$ as a function of $1/T$ for 0.5 wt% sacran gels crosslinked by 0.01 mol/L of Ba^{2+} (blue diamonds), Sr^{2+} (green circles) and Ca^{2+} (red triangles), the activation energies of these physical gelation are calculated from the slope of these curves.

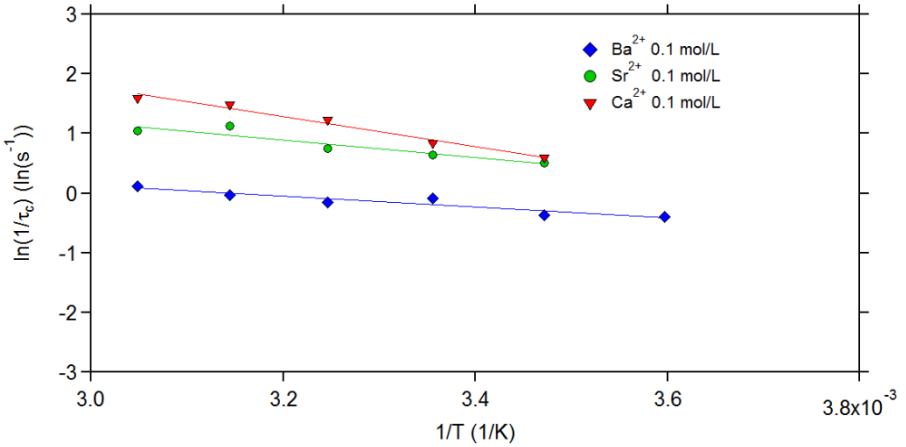

Figure 89 $Ln[1/\tau_c]$ as a function of $1/T$ for 0.5 wt% sacran gels crosslinked by 0.1 mol/L of Ba^{2+} (blue diamonds), Sr^{2+} (green circles) and Ca^{2+} (red triangles), the activation energies of these physical gelation are calculated from the slope of these curves.

$ln(1/\tau_c)$ is found linear to $1/T$ within experimental errors. From the slope of $ln(1/\tau_c)$ vs $1/T$, we obtained the value of $-E_a/RT$ and the values of activation energy are calculated and reported in Table 1. The value of E_a increases in the following order, Ca^{2+} > Sr^{2+} > Ba^{2+}, respectively equal to 21, 12 and 8 kJ/mol for crosslinkers concentration of 0.01 mol/L and 26, 11 and 6 kJ/mol for crosslinkers concentration of 0.1 mol/L. The activation energy of calcium alginate gelation is around 20 kJ/mol[80] which is comparable with results obtained for the calcium sacran gelation. These activation energies obtained for sacran physical gels are low thus the dynamics are not strongly influenced by the temperature.

Crosslinking ion	C_{ion} (mol/L)	E_a (kJ.mol^{-1})
Ca^{2+}	0.01	21
	0.1	26
Sr^{2+}	0.01	12
	0.1	11
Ba^{2+}	0.01	8
	0.1	6

Table 1 Activation energies of sacran crosslinking as a function of crosslinking ion species and its concentration.

5.4. Conclusion

In this chapter the nonlinear properties of the sacran physical gels crosslinked by Ca^{2+}, Sr^{2+} and Ba^{2+} are studied. For the systems with a 0.25 wt% of sacran, a strain hardening behavior is observed only for the system with Ca^{2+}. For a sacran concentration of 0.5 wt%, the systems with Ca^{2+} and Sr^{2+} showed the strain hardening behavior. The strain hardening ratio Q is about 2. No evident strain hardening is observed in the presence of Ba^{2+}, strain softening is observed. In the presence of Ca^{2+}, the evolution of the moduli is slower than in the presence of the two other ions, giving a lower value of the elastic plateau.

We find that these divalent ions have two effects on the viscoelasticity of the sacran solution.

(1) These divalent ions jellify sacran by bridging charges supported by sacran chains.

(2) These cations serve as ions to change the ionic strength and the interactions of the sacran chains.

In order to better understand the ion effect, systems with Na^{+} or Mg^{2+} are studied. The increase in the modulus is slower than that of the other three ions, giving a gel as soft as that crosslinked by Ca^{2+}. A pronounced strain hardening behavior is observed with a ratio of about 12 – 15. Since we do not observe any differences between the systems in the presence of Mg^{2+} and Na^{+}, Mg^{2+} does not crosslink the sacran ionically. The value of the elastic plateau for Ca^{2+} system is similar to the Mg^{2+} system, Ca^{2+} does not presumably ionically crosslink sacran chain either. These gels contain large structure after shear tests, which is supposed to be the origin of the strain hardening.

The relaxation of the gels crosslinked by the three divalent ions are compared by using SRFS to observe their relaxation times at low frequency at constant strain rates. Master curves of shifted G' and G'' as a function of the shifted time are constructed and the relaxation time is determined for the three ions at different temperatures. The relaxation time increases in the following order, $Ba^{2+} > Sr^{2+} > Ca^{2+}$. These ion species dependence might be explained by the kosmotropic effects of the ions. With a decrease in the radius of the ions, the charge density increases and more water molecules are organized around the ions to decrease the affinity with the ions. The activation energy is calculated from the Arrhenius plot of the relaxation time. We obtain for Ca^{2+}, Sr^{2+} and Ba^{2+} respectively around 21, 12 and 8 kJ/mol. These values are low thus indicates that the relaxation time does not strongly depend on the temperature.

6. Chemical gels of sacran

6.1. Introduction

In the previous chapter, we have studied the nonlinear properties of sacran physical gels. The strain hardening behavior has been demonstrated. The strain hardening ratio Q is found to be around 2 for the gels crosslinked by Ca^{2+}, about 16 for the gels crosslinked by Na^{+} or Mg^{2+}. Though the latter two ions induced the pronounced strain hardening behavior, the preparation time is rather long (more than 72 hours) and experiments are difficult to reproduce. The physical crosslinking is basically reversible and the structures can evolve under large strain as observed from the evolution of the plateau modulus. In this chapter, nonlinear rheological properties of sacran chemical gels are studied. With permanent crosslinks, the network structures are expected to be more stable at large deformations, allowing to characterize the nonlinear properties until eventual rupture of the bonds.

Sacran is a polysaccharide possessing many hydroxyl groups on its monosaccharide residues. Hydroxyl groups can be used to chemically crosslink the polysaccharide with divinyl sulfone (DVS) as crosslinker[81,82]. Crosslinking reaction is based on Oxa-Michael addition between a DVS molecule and two alkoxide groups generated from hydroxyl groups on the polysaccharide (around 250 mol% of monosaccharide residue) at basic conditions. Figure 90 shows the schematic of the crosslinking reaction by DVS taken from literature[82]. In this reference the crosslinking reaction with hyaluronic acid is studied. In this work the same reaction is used for sacran. In Figure 91 the expected chemical crosslinking structure of sacran is shown.

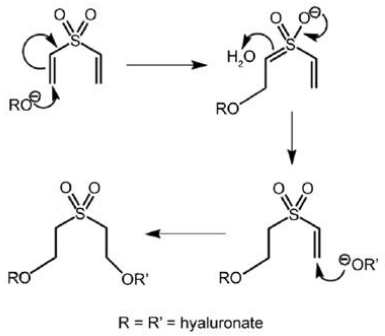

Figure 90 Oxa-Michael addition mechanism of the crosslinking of hyaluronic acid with divinyl sulfone.[82]

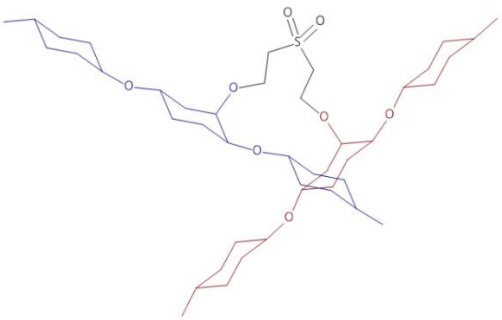

Figure 91 Schematic view of chemical bonding by a DVS molecule (black) between two sacran chains (blue and red) performed by Oxa-Michael addition mechanism.

In this chapter, first we study the gelation diagram of sacran by DVS as a function of the sacran and DVS concentrations. Secondly their macro- and micro-rheological properties are briefly characterized. The persistence length is determined from the high frequency dynamics and compared with that of the solutions. Finally the linear and nonlinear macrorheological properties of the sacran chemical gels are studied. In this part the sacran concentration is fixed at 0.5 wt% and the DVS concentration or pH (adjusted by addition of NaOH) are varied in order to control the crosslinking ratio of the gels. The nonlinear stress-strain relation is further studied by a nonlinear network elasticity model which relates the network elasticity to molecular parameters of the single chains composing of the network. Comparison of the model with the experiments allows us to discuss the rigidity of the chain.

6.2. Experimental section

6.2.1. Chemical gel preparation

A sacran mother solution was prepared according to the usual procedure described in the chapter 3.

Divinylsulfone (DVS) and NaOH are purchased from Sigma Aldrich.

Mixture of sacran, NaOH and DVS at controlled concentrations is prepared in a small plastic vial. This mixture is homogenized at each addition step by using a vortex at low speed for 1 min. The mixture is let jellified in the vial for gelation diagram and swelling tests. For rheological tests the mixture is immediately placed into the measurement geometry of the rheometer.

6.2.2. Rheological measurement

Rheological measurements of sacran chemical gels are performed in the same way as the physical gels. We use a strain-controlled TA Instruments ARES LS1 rheometer using cone-plate geometry (diameter: 50 mm, angle 2°, gap 50 μm) with a roughened surface and an oil bath to prevent the gel drying. Three kind of sweeps are systemically and consecutively performed on each sample tested by macrorheology at 25 °C: (1) an oscillatory time sweep (1 %, 1 Hz) in order to study the gelation kinetics of the gel, (2) an oscillatory frequency sweep (1 %, 25 °C) in order to characterize the linear viscoelastic properties of the chemical gels characterized by an elastic plateau, and (3) an oscillatory strain sweep (1 Hz, 25 °C) in order to probe the rheological behaviors of gels in their nonlinear regimes. The strain amplitude was varied between 1 and 100 %.

6.2.3. DWS microrheology

DWS microrheological measurements were performed with the same experimental setup as that described in the previous chapter. Generally the dynamic light scattering signals from hydrogels are non-ergodic. A measurement at a fixed position does not allow to explore all the configurations of the system, thus time averaging is not equivalent to ensemble averaging. This is due to the frozen-in spatial inhomogeneity of the hydrogel network. The scattering from the probe particles trapped in the crosslinked network is also non-ergodic and ensemble averaging should be properly performed. In order to obtain ensemble-averaged autocorrelation function in our DWS measurements, a device to rotate a diffuser glass plate was placed in front of the optical fiber. Rotation at a constant speed allowed to collect scattering signals from different positions to obtain ensemble averaged $g_2(t)$ having a cut-off at about 10 s due to the rotational motion appearing at a long time range.

6.3. Results and discussion

6.3.1. Diagram of chemical gelation

First of all, a gelation diagram of the chemical gelation of sacran by DVS is drawn, as a function of the sacran and DVS concentrations in the presence of 0.2 mol/L of NaOH, with a gelation time of 72 h. To check the gelation, the test tube tilting method is often used: when a sample in a test tube or other vials is tilted, if the sample flows, it is considered as sol, and when it does not flow, it is considered as gel. However, in the case of the sacran chemical gels prepared at low concentrations, the modulus can be as low as several Pa and the gels can flow (typically at the sacran concentrations lower than 0.5 wt% and the DVS concentrations lower than 0.15 mol/L) as the modulus is not sufficiently high to sustain its own weight. Therefore, in this work we check insolubility of the chemical network: the samples are immersed in a large quantity of water to observe if the samples totally dissolve after 48 hours. If the sample is gel, it does not dissolve in water. To better visualize the gels having very low polymer concentration, a tracer amount of polystyrene particles (same as those used for the microrheological measurements, at 0.01 wt%) are dispersed prior to the gelation in order to increase the contrast between water and gels whose refractive index is very close to that of water .

Figure 92 shows the chemical gelation diagram of the sacran gel crosslinked by DVS. We find sol-gel transition limits between 0.2 and 0.3 wt% of sacran for a constant DVS concentration at 0.15 mol/L, and between 0.001 and 0.005 mol/L of DVS for a constant sacran concentration at 0.5 wt%. When the polymer concentration decreases, there is a site-percolation limit, where the concentration of the available binding sites on the polymer chains decreases and gelation does not occur. It is worth noting that that the gelation limit we found (0.2 – 0.3 wt%) is much higher than C^* of the sacran solution (0.004 wt%). When the crosslinker concentration decreases, there is a bond-percolation limit, where the concentration of the crosslinker is not sufficient to percolate the chains. In the case of physical gels discussed in Chapters 4 and 5, above the divalent ion concentration of about 0.003 mol/L no ion concentration dependence of the plateau modulus is observed. Though the chemical crosslinking occurs with -OH groups and not with negative charges on sacran chains, the limit of gelation controlled by the chain rigidity might impose the bond percolation limit around this concentration.

At high concentrations of sacran and/or DVS, turbid white gels are obtained without particles, which scatter the visible lights. This suggests that there are large aggregates of the polymers scattering visible lights. Generally gelation and precipitation are competitive, and especially for rigid chains, bundle formation can be favored. We do not study the aggregates which can be in very small quantity but can scatter a lot of lights.

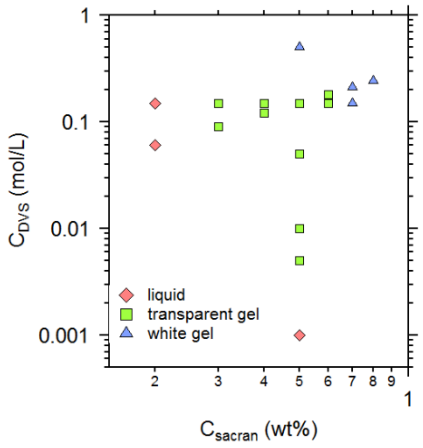

Figure 92 Gelation diagram (C_{DVS} vs C_{sacran}) of sacran. Blue circles: liquid samples (sols); green squares: transparent gels; red triangles: white turbid gels. The NaOH concentration is fixed at 0.2 mol/L for all the tests.

Figure 93 shows pictures of sacran gels at a sacran concentration of 0.5 wt% crosslinked by different amounts of DVS immersed in water for the solubility test. The gels crosslinked at the high DVS concentrations (0.05 and 0.1 mol/L) keep the shape of the test tube in which the gels were crosslinked. We do not observe a significant swelling of the gels, presumably due to the rigidity of the chain. Since the gels are very soft and the polymer concentration is low, an accurate measurement of equilibrium swelling is difficult. The gels crosslinked at lower DVS concentrations (0.01 and 0.005 mol/L) are too soft to support their own weight to keep their cylindrical shape even in water, the gels are compressed by the gravity.

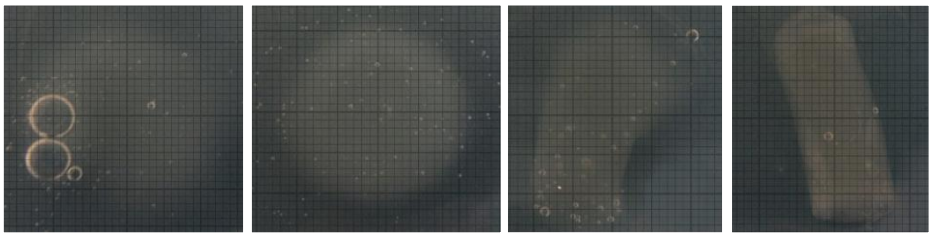

Figure 93 Pictures of sacran chemical gels at a concentration of 0.5 wt% crosslinked by different amount of DVS at fixed basic conditions (0.2 mol/L of NaOH). From left to right: C_{DVS} = 0.005, 0.01, 0.05 and 0.1 mol/L. The white color of these gels is obtained by addition of 0.01 wt% of microparticles of polystyrene (radius: 1 µm). The scale of the grid in the background is 1 mm.

6.3.2. Persistence length

In order to characterize the chain rigidity of the sacran chemical gels, microrheological measurements are performed. Figure 94 shows the viscoelastic moduli of a 0.5 wt% sacran chemical gel crosslinked by DVS at 0.15 mol/L in the presence of 0.2 mol/L of NaOH, measured by macrorheology and microrheology. By comparing the two techniques we observe a difference in absolute value of modulus. The macrorheology gives higher values of moduli than those by microrheology, with a factor of 2 – 3. This difference is believed to arise from the heterogeneity of the chemical network giving a more pronounced non-ergodicity of the scattering signal. In the gels there are frozen-in concentration gradients, or the concentration gradients are statically fixed by crosslinks. The scattered light from these static gradients does not fluctuate with time, depending on the measurement positions in the sample. Thus it is more difficult to evaluate the fluctuation of the dynamic components from the gels, and the absolute value of the mean-square displacement ($\langle \Delta r^2(t) \rangle$), thus the modulus, can be affected. Irreversible chemical crosslinks can induce more heterogeneity in the gel than the physical gels by the reversible crosslinks. In fact the physical gels of sacran are transparent at all the conditions studied, while the chemical gels can be turbid, suggesting the spatial heterogeneity of the chemical gels. Here we use the macrorheological results to calculate the mesh size of the network from the plateau modulus, while the microrheological results are used to estimate the persistence length since the persistence length is calculated from the transition frequency of the bending mode but not from the absolute value of the moduli.

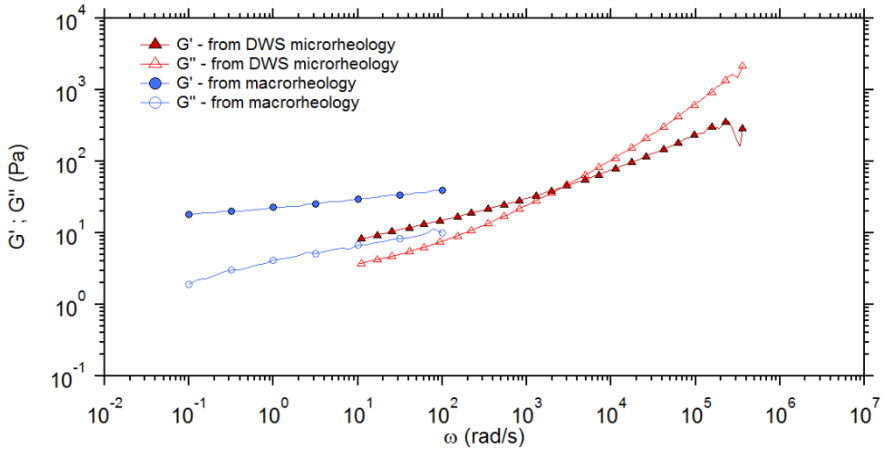

Figure 94 Viscoelastic moduli of a sacran chemical gel measured by macrorheology and DWS microrheology. Sacran concentration: 0.5 wt%, DVS concentration: 0.15 mol/L, NaOH concentration: 0.2 mol/L.

Figure 95 shows the viscoelastic moduli of the sacran chemical gels at various sacran concentrations crosslinked by DVS at a concentration of 0.1 mol/L in presence of 0.2 mol/L of NaOH. At the measured frequency range, the elastic modulus strongly increases with the concentration though we do not observe a well-defined elastic plateau. The microrheology can measure the single chain dynamics at high frequencies

where the moduli are supposed to increase proportionally to the sacran concentration. The noise level is rather high for G' above 2×10^5 rad/s.

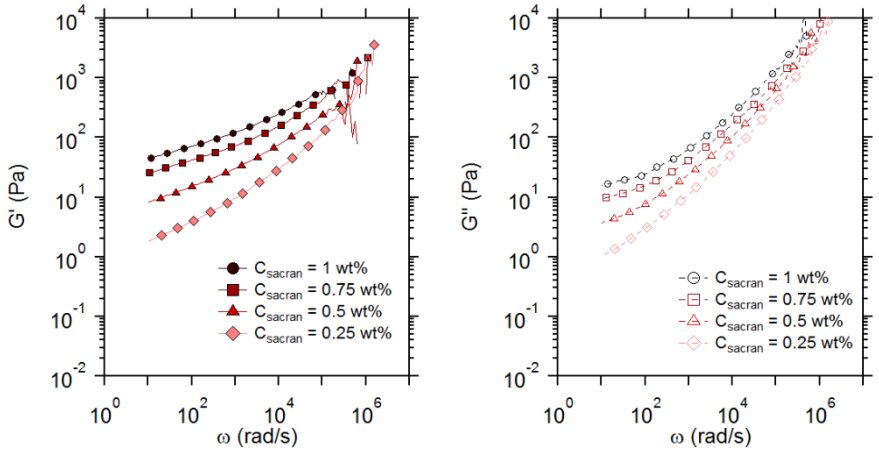

Figure 95 Viscoelastic moduli measured by DWS as a function of frequency for sacran chemical gels at different sacran concentrations crosslinked by 0.1 mol/L of DVS in presence of 0.2 mol/L of NaOH.

In Figure 96, the complex modulus is plotted as a function of frequency. The values of G^* at 10^5 rad/s (frequency arbitrary chosen as representative of high frequencies rheological responses of the gels) increase proportionally to the chain concentration as shown in the figure. The relatively large value for 1 wt% is presumably due to the turbidity of the system which disturb the multiple scattering measurements.

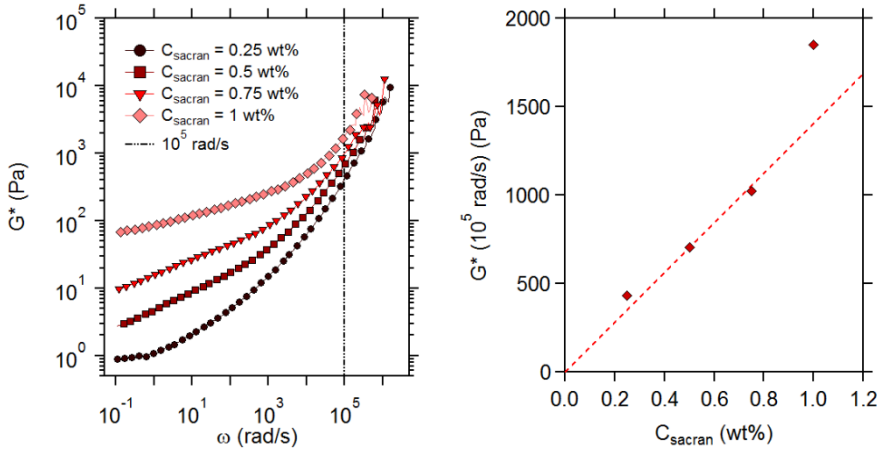

Figure 96 Left: Complex modulus (G^*) as a function of frequency of sacran gels at different sacran concentrations crosslinked by 0.1 mol/L of DVS in presence of 0.2 mol/L of NaOH. The dashed line represents the frequency 10^5 rad/s chosen to represent the evolution of the sacran single chain dynamics traced in the right figure. Right: Complex modulus (G^*) at 10^5 rad/s as a function of the sacran concentration.

In the same way as for the physical gels, at high frequencies, the Zimm-Rousse mode and the bending mode are identified. From the intersection of the two modes a critical frequency is determined to calculate the persistence length of the system. From the value of the elastic modulus at the plateau, the mesh size is

determined, and these two characteristic lengths are plotted in Figure 97 as a function of the sacran concentration. The values of the persistence length decrease with the sacran concentration: as previously discussed (Chapter 3) at this high concentration range the persistence length is not properly determined by this method but the entanglement length is estimated. Thus the variation of the persistence length from 45 nm to 20 nm corresponds to the decrease in the entanglement length. The values of the mesh size obtained from the macrorheological measurements of the elastic plateau are found higher than that of the persistence length (entanglement length) with a factor of about 2. The same factor is found for the physical gels crosslinked by Ba^{2+} at different concentrations. At 1 wt% the two lengths are approaching, presumably due to the inaccurate microrheological measurement at this concentration which overestimate the persistence length (entanglement length).

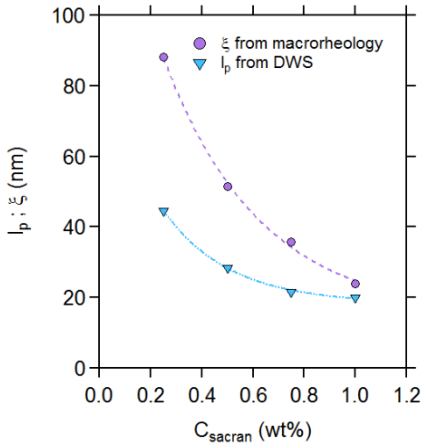

Figure 97 Persistence length (cyan triangles) and mesh size (purple circles), respectively measured by DWS microrheology and macrorheology, as a function of the sacran concentration. The gels are crosslinked by 0.1 mol/L of DVS in the presence of 0.2 mol/L of NaOH.

C_{sacran} (wt%)	ξ_{macro} (nm)	$l_{p,DWS}$ (nm)
0.25	88	45
0.5	52	29
0.75	36	22
1	24	20

Table 2 Mesh size and persistence length respectively measured from macrorheology and DWS as a function of the sacran concentration in gels crosslinked by 0.1 mol/L of DVS in the presence of 0.2 mol/L of NaOH.

The values of persistence lengths of the chemical gels are plotted as a function of the sacran concentrations in Figure 98. For comparison those of the sacran solutions are plotted as well as the corresponding Odijk-Skolnick-Fixman (OSF) prediction shown in Chapter 3. The values for the chemical gels and solutions are very close and follow the same scaling law, $l_p \sim C_{sacran}{}^{-0.4}$, corresponding to the scaling of the

entanglement length. This result indicates that at the high frequencies corresponding to the single chain dynamics, the chemically crosslinked networks have rigid chains between the crosslinking points in the same way to the entangled solutions.

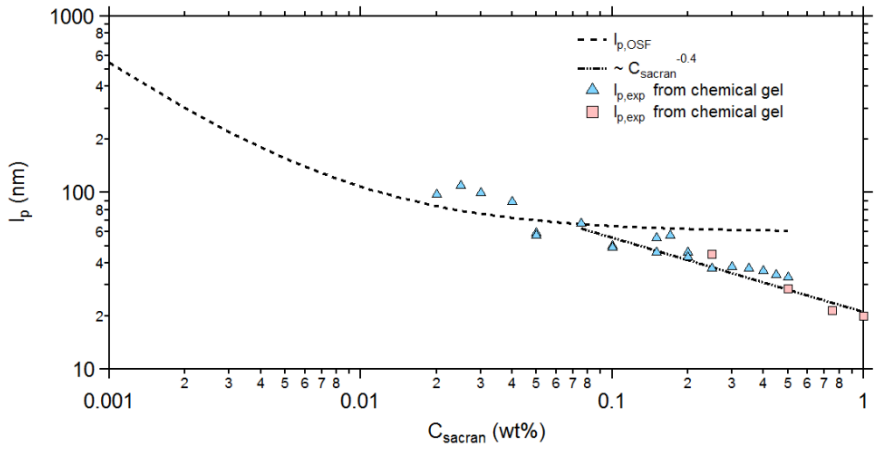

Figure 98 Persistence length as a function of the sacran concentration of chemical gels (cyan squares) and solutions (blue triangles) measured by DWS compared with the theoretical prediction of the OSF relation (dash line).

The same DWS measurements are performed for sacran chemical gels at a concentration of 1 wt% crosslinked by different amount of DVS at a fixed NaOH concentration (0.2 mol/L). In Figure 99, the viscoelastic moduli of the gels are plotted as a function of frequency. In the high frequency range, the values of moduli are expected to be proportional to the polymer concentration and independent of the crosslinker concentration. Here we find a strong DVS concentration dependence for both G' and G'' above C_{DVS} = 0.2 mol/L. This result suggests that the microrheological measurements are inaccurately performed due to the turbidity of the gels above this critical sacran concentration.

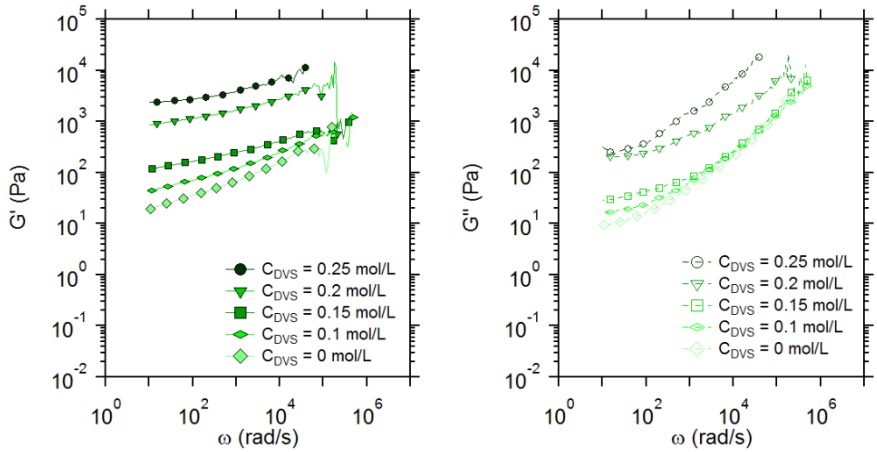

Figure 99 Microrheologically measured G' and G'' as a function of frequency for sacran gels at a concentration of 1 wt% crosslinked by DVS at different concentrations. NaOH concentration: 0.2 mol/L.

6.3.3. Linear regime and gelation kinetics

We study the linear and nonlinear rheological properties of the sacran chemical gels. Firstly the linear rheological properties are characterized to evaluate the plateau modulus. We intensively study the chemical gels at a sacran concentration of 0.5 wt% as we did for the physical gels. In order to finely control the crosslinking ratio, the crosslinker concentration and the pH are used as parameters. Two series of gels are synthesized: (1) the DVS concentration is changed at a constant NaOH concentration (0.2 mol/L) and (2) the NaOH concentration changed for a constant DVS concentration (0.15 mol/L). Using the plateau modulus as an indication of the effective crosslinking ratio (bond between two polymer chains), the properties of the two series are compared.

6.3.3.1. DVS series

In order to determine the gelation time t_{gel} of the chemical gels, the evolution of the moduli is monitored at a strain amplitude of 1 % and a frequency of 1 Hz. In Figure 100, the viscoelastic moduli are plotted as a function of time for 0.5 wt% sacran chemical gels crosslinked by DVS at different concentrations at C_{NaOH} = 0.2 mol/L. The value of G' for a 0.5 wt% sacran solution is around 3 Pa which is slightly lower than those of the chemical gels at t_o. The value of G' is higher than that of G'' from the beginning of the chemical crosslinking reaction, thus as gelation time, the time at which the value of G' starts to level off is taken as t_{gel} for convenient sake. Within 1 hour G' stabilizes and t_{gel} does not show a strong DVS concentration dependence, suggesting that there are sufficient amount of activated crosslinking points (alkoxide groups) on the sacran chains and the rate-limiting process is the contact of the two chains whose dynamics are supposed to be slow. The value of G'' is much lower than G' and time evolution seems very little.

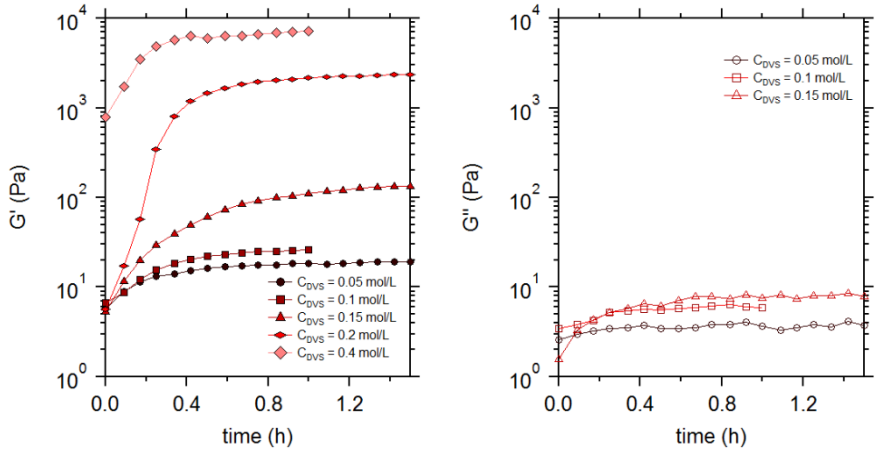

Figure 100 Elastic modulus (G') and viscous modulus (G'') as a function of time for 0.5 wt% sacran chemical gels crosslinked by different concentrations of DVS in basic condition (0.2 mol/L of NaOH).

After 1.5 hours of reaction, frequency sweep is performed between 0.1 and 100 rad/s in order to characterize the linear rheological properties of the chemical gels. Figure 101 shows the viscoelastic moduli of the chemical gels as a function of frequency. We observe a well-defined elastic plateau showing a strong DVS concentration dependence. For all the DVS concentrations tested, the values of G'' are much lower than those of G', indicating that the sacran gels are highly elastic as it is often the case for chemically crosslinked network without dissipative mechanism.

The elastic plateau modulus G_e as a function of the DVS concentration is also plotted in Figure 101. G_e increases with the DVS concentration, and at C_{DVS} = 0.15 mol/L, it reaches about 150 Pa which is very close to the value for the physical gels at same sacran concentration crosslinked above the stoichiometry. Interestingly the value of Ge continues to increase with increase in C_{DVS}, can be as high as 8000 Pa. The concentration of hydroxyl groups on sacran at 0.5 wt% is about 0.8 mol/L. Thus the theoretical stoichiometry of this chemical gelation is around C_{DVS} ~ 0.4 mol/L. It is unlikely that the chemical crosslinking would occur at this high crosslinking ratio. At this stoichiometry, gels would be very elastic with very short entanglement length. De-swelling of gels would occur due to their high elasticity and the loss of hydroxyl groups. We do not observe macroscopic shrinkage of the chemical gel, while the gel is turbid at the DVS concentration above 0.2 mol/L. This result suggests that highly crosslinked large structures which can support large stresses are formed during chemical crosslinking.

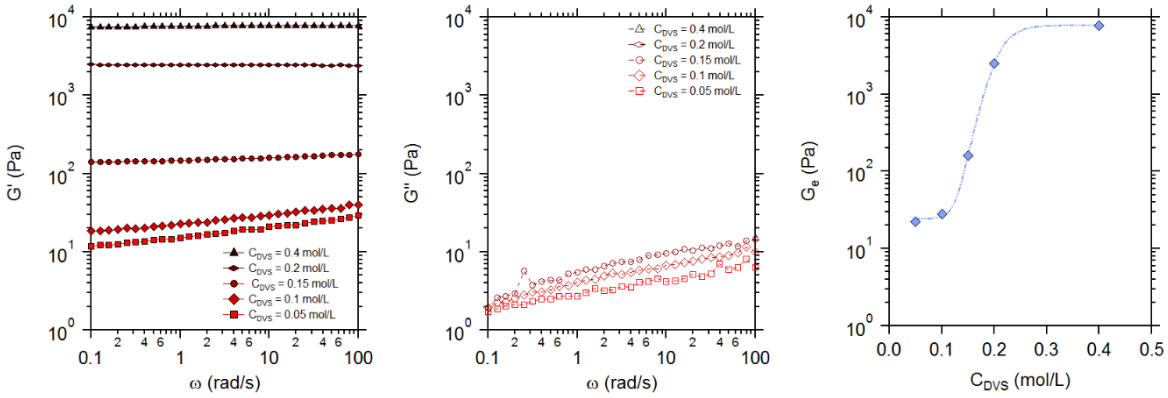

Figure 101 Left: G' as a function of the frequency for sacran chemical gels at 0.5 wt% and crosslinked by DVS at different concentrations at fixed pH by 0.2 mol/L of NaOH; Middle: G'' as a function of the frequency for these sacran chemical gels; Right: G_e (obtained at 6.28 rad/s) as a function of the DVS concentration of these sacran chemical gels.

6.3.3.2. NaOH series

We studied the effect of the pH on the chemical gelation of sacran by DVS. The value of pH is adjusted by addition of NaOH in the solutions. Since the hydroxyl groups are turned into reactive alkoxide groups at basic conditions for the reaction with DVS, the value of pH can control the number of available binding

sites on sacran chains, thus the crosslinking ratio. A series of sacran chemical gels at a concentration of 0.5 wt% crosslinked by DVS at 0.15 mol/L are synthesized at various NaOH concentrations, and their linear rheological properties are studied.

The gelation kinetics of chemical gelation is studied as a function of the NaOH concentration. In Figure 102, the gelation kinetics of sacran gels crosslinked in different NaOH concentrations are shown as the viscoelastic moduli as a function of time at a strain amplitude of 1 % and a frequency of 1 Hz. The value of pH influences the gelation time t_{gel}. The gelation time are practically independent of pH at the NaOH concentrations higher than 0.1 mol/L, while at lower concentrations it increases with decrease in the NaOH concentration (or pH). At the lowest NaOH concentration tested (0.03 mol/L), the gelation time is over 3 hours. This result suggests that the rate-limiting process is the creation of alkoxide groups from OH- at the low NaOH concentrations, then the contact of the sacran chains at high NaOH concentrations. The values of G'' are less than 10 Pa and slightly depend on the pH.

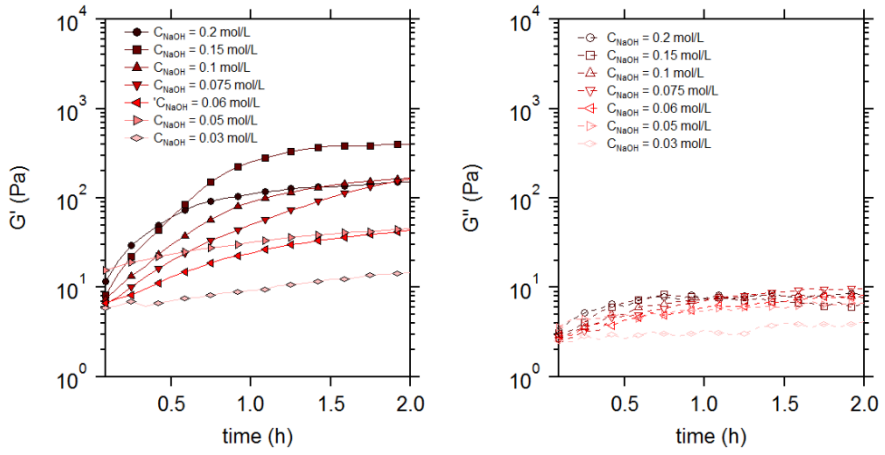

Figure 102 Left: Elastic modulus (G') as a function of time for 0.5 wt% sacran chemical gels crosslinked by 0.15 mol/L of DVS in different basic conditions; Right: Viscous modulus (G'') as a function of time for 0.5 wt% sacran chemical gels crosslinked by 0.15 mol/L of DVS in different basic conditions.

The frequency sweeps are performed for the chemical gels after the reaction time of 3 hours, and the results are shown in Figure 103. At the concentrations tested here, which are higher than 0.03 mol/L, a well-defined elastic plateau is observed. The value of G_e reaches about 300 Pa. the values of G'' are less than 20 Pa, and the gels are elastic with the value of $tan\ \delta$ ranging 0.1 – 0.01. The values of G_e at 6.28 rad/s are also plotted as a function of C_{NaOH}. Two regimes are observed: G_e increase rapidly with the NaOH concentration below 0.075 mol/L, G_e becomes independent of C_{NaOH}.

From this rheological study of the linear regime of sacran chemical gels, it is demonstrated that the plateau modulus can be tuned over two decades by adjusting pH. For both of the two series of experiments (DVS concentration dependence and NaOH concentration dependence), the effective crosslinking ratio is not

directly measured. In order to compare the two series, in the following sections, the value of G_e is chosen as indication of the crosslinking ratio.

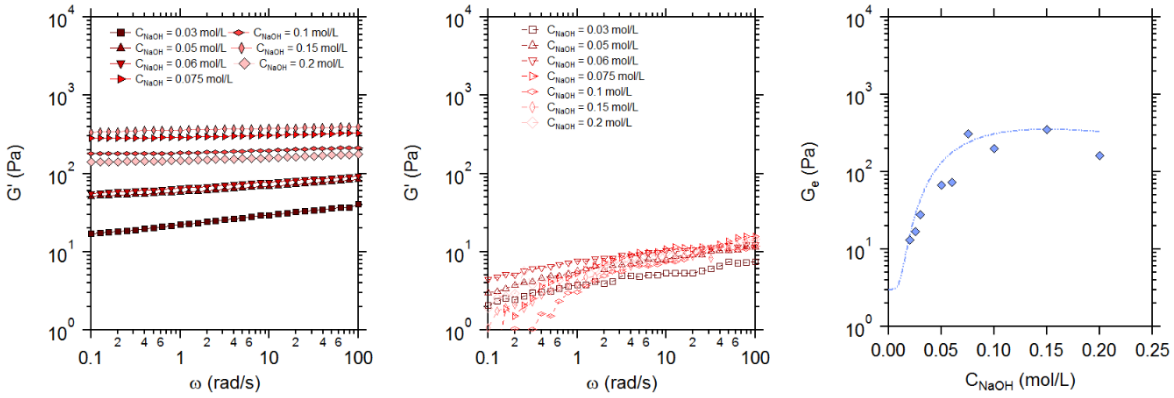

Figure 103 Left: G' as a function of the frequency for sacran chemical gels at a concentration of 0.5 wt% crosslinked by 0.15 mol/L of DVS at different NaOH concentrations. Middle: G'' as a function of the frequency for these sacran chemical gels. Right: G_e (obtained at 6.28 rad/s) as a function of the NaOH concentration of these sacran chemical gels.

6.3.4. Nonlinear regime and strain-hardening

The nonlinear rheological properties of sacran chemical gels are studied for the two series of the chemical gel samples, those prepared at a fixed NaOH concentration varying the DVS concentration, and those prepared at a constant DVS concentration varying the NaOH concentration.

6.3.4.1. DVS series

We rheologically study the non-linear regime of sacran chemical gels at a concentration of 0.5 wt% crosslinked by different DVS concentrations with 0.2 mol/L of NaOH. Strain sweep tests are performed after the gelation time of 3 hours in order to characterize the non-linear rheological properties.

The Figure 104 shows the value of G' as a function of the strain γ for the chemical gels crosslinked at different DVS concentrations. At the DVS concentrations higher than 0.1 mol/L, a strain-hardening behavior is commonly observed. The value of G' increases with strain then dramatically decreases after the peak of G' (data points after the peak are not shown in the figure). This behavior is believed to be due to the breaking or slipping of the sample in the geometry. For gels crosslinked at a DVS concentration of 0.05 mol/L, strain softening is observed after 10 % of strain. At 0.05 mol/L of DVS, the sacran gel shows a strain softening at strain of 10 %, then a strain hardening is observed at a strain of 50 %. This phenomenon is presumably related to the very heterogeneous network structures at this low crosslinking ratio.

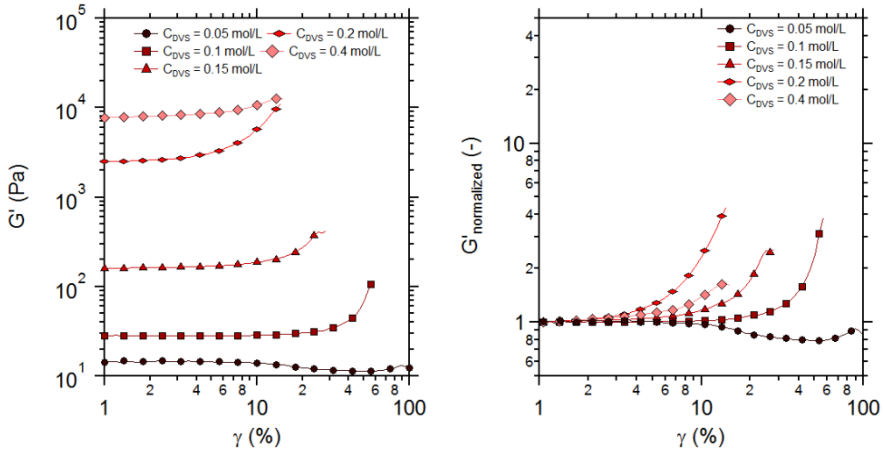

Figure 104 Left: Elastic modulus (G') as a function of strain for 0.5 wt% sacran chemical gels crosslinked by different amount of DVS in basic condition (0.2 mol/L of NaOH); Right: Evolution of the G' normalized by the elastic plateau moduli as a function of the strain for the same sacran gels.

In order to better compare the strain hardening behavior, the values of G' normalized by those of G_e are plotted as a function of strain in Figure 105 right. The strain-hardening is characterized by the strain hardening ratio, Q, equivalent to the maximal value of normalized G'. Q varies with the DVS concentration,

between 2 and 5 at the given condition. The value of Q is expected to be controlled by the fracture/slip process, thus to be rather irreproducible. The nonlinear behaviors of networks are also characterized by the value of the maximal strain at the peak, γ_{max}, thus the extensibility of the gel decreases with chemical crosslinking. The value of γ_{max} is shifted to lower strain as the DVS concentration increases from 90 % (for 0.05 mol/L) to 15 % (for 0.2 mol/L).

In Figure 105, the DVS concentration dependence of the elastic plateau G_e, of the strain hardening ratio Q and of the flow strain γ_{max} are summarized. For the DVS concentration between 0.05 and 0.2 mol/L, the value of Q increases and that of γ_{max} decreases with the DVS concentration. This result suggests that the chain extensibility decreases with the increase of the chemical crosslinking ratio. The gel crosslinked at the DVS concentration of 0.4 mol/L does not follow these tendencies, presumably this turbid gel has high heterogeneity of the structure and the network is elastic but brittle.

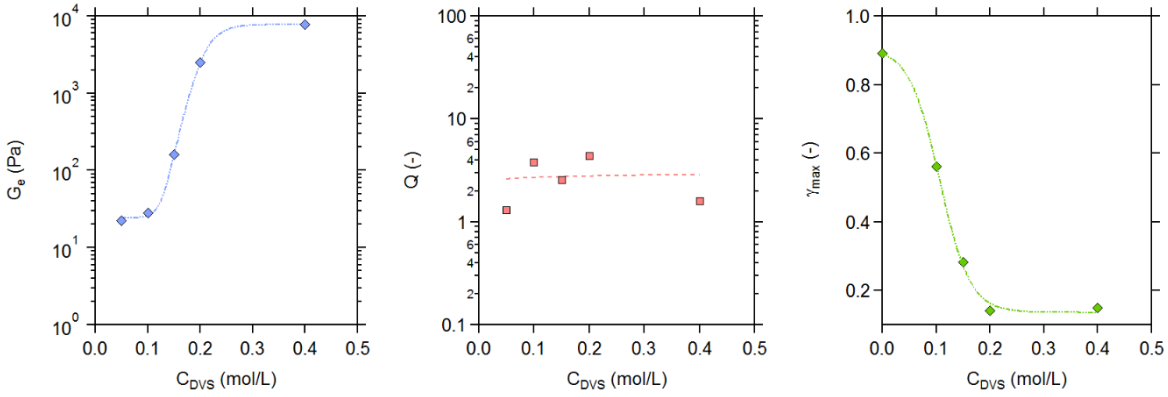

Figure 105 Left: Elastic plateau modulus (G_e), Center: strain-hardening ratios (Q), Right: γ_{max}, as a function of the C_{DVS} for sacran gels (0.5 wt%) prepared at a NaOH concentration of 0.2 mol/L.

6.3.4.2. NaOH series

Nonlinear rheological experiments are performed for the sacran chemical gels at a concentration of 0.5 wt% crosslinked by 0.15 mol/L of DVS at different NaOH concentrations. In Figure 106 (left), the evolution of G' of sacran gels crosslinked at different NaOH concentrations are shown as a function of the strain amplitude. A pronounced strain hardening behavior is observed for the gels crosslinked at the NaOH concentration higher than 0.03 mol/L. The plateau modulus increases with the NaOH concentrations and stabilizes around 150 – 350 Pa. In Figure 106 (right), the normalized G' is plotted as a function of strain. For the gel crosslinked at 0.03 mol/L of NaOH, the strain hardening ratio can be around 20. With increase in the NaOH concentration, the strain hardening start to occur at lower strain.

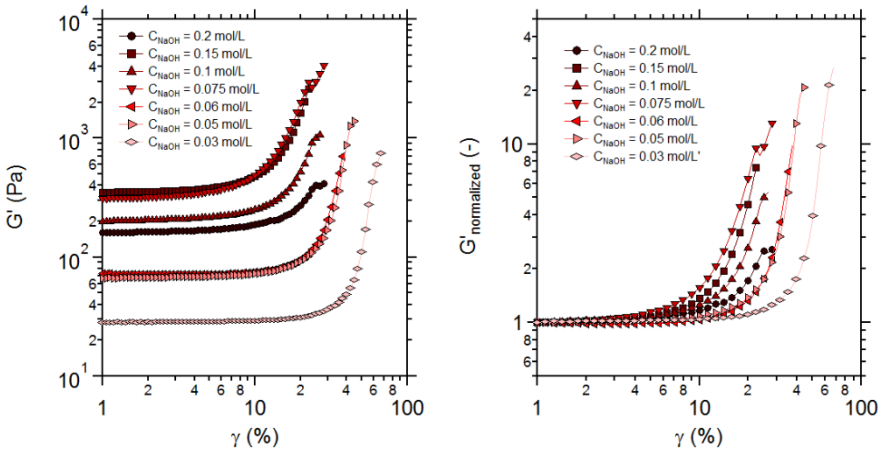

Figure 106 Left: Elastic modulus (G') as a function of the strain amplitude applied to the sacran chemical gels (C_{sacran} = 0.5 wt%) crosslinked by 0.15 mol/L of DVS at different NaOH concentration. Left: normalized G' as a function of the strain amplitude.

In Figure 107, the NaOH concentration dependence of the plateau modulus G_e, the strain hardening ratio Q and the maximal strain amplitude γ_{max} are shown. One can distinguish two ranges of NaOH concentration. G_e increases with CNaOH up to 0.075 mol/L, then it levels off, suggesting that the effective chemical crosslinking ratio given by the fixed DVS concentration saturates above 0.075 mol/L. The values of Q as well as γ_{max} decrease with the NaOH concentration below 0.075 mol/L; then they levels off.

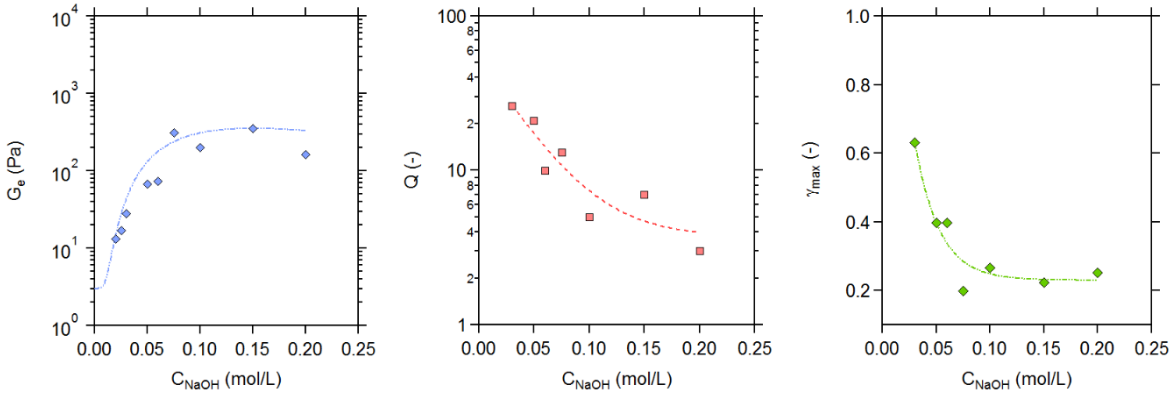

Figure 107 Elastic plateau modulus (G_e), the strain hardening ratio Q and the maximal strain γ_{max} as a function of NaOH for sacran chemical gels. Sacran concentration: 0.5 wt%, DVS concentration: 0.15 mol/L.

Let us comment on the result of a cycle test. 14 cycles of strain sweep tests are performed at 6.28 rad/s by increasing the maximum amplitude by 5 % for each cycle. Figure 108 shows the viscoelastic moduli as a function of strain for the 14 cycles. The curves perfectly superpose even at the strain hardening. For the physical gels crosslinked by Ca^{2+}, the same test is performed and the decrease in the plateau modulus is found (Chapter 5). This result indicates that no detectable rupture of the chemical bonds or the chains occur except at the largest strain inducing the dramatic decrease of the moduli.

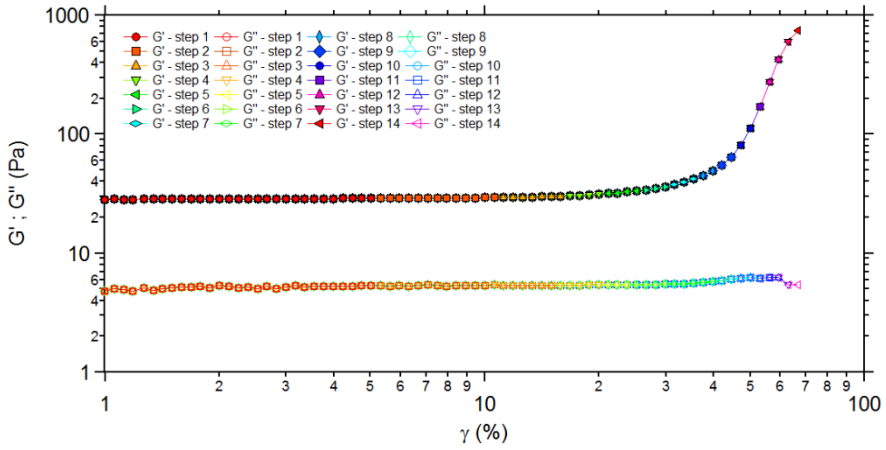

Figure 108 Viscoelastic moduli as a function of strain. For a sacran gel at a concentration of 0.5 wt% crosslinked by 0.15 mol/L of DVS in the presence of 0.03 mol/L of NaOH. For each cycle the maximal strain amplitude increases from 5 % to 80 % with a step of 5 %

6.3.4.3. Comparison

Here we compare the two series of chemical gels, one prepared at different DVS concentrations with a fixed NaOH concentration, and the other prepared at a fixed DVS concentration with different NaOH concentrations. We use the plateau modulus as an indication of the chemical crosslinking ratio of the gels prepared at different conditions. Figure 109 shows the values of Q and γ_{max} as a function of the plateau modulus G_e for the two series of gels. For the values of Q, the data are very dispersed, especially at low G_e values. The series of gels prepared at various DVS concentrations gives lower values of Q. These values are sensitive to many factors as it is related to the fracturing of the gel. Thus it is difficult to conclude the G_e dependence of Q, though Q globally seems decreasing with G_e. For the value of γ_{max}, data dispersion is less significant compared to Q values, and we can clearly see that γ_{max} decreases with increase in G_e and the two series of the gels show the same trend. This result suggests that as the crosslinking ratio increases, the length between two crosslinking points becomes shorter, which means that the chain is certainly more rigid.

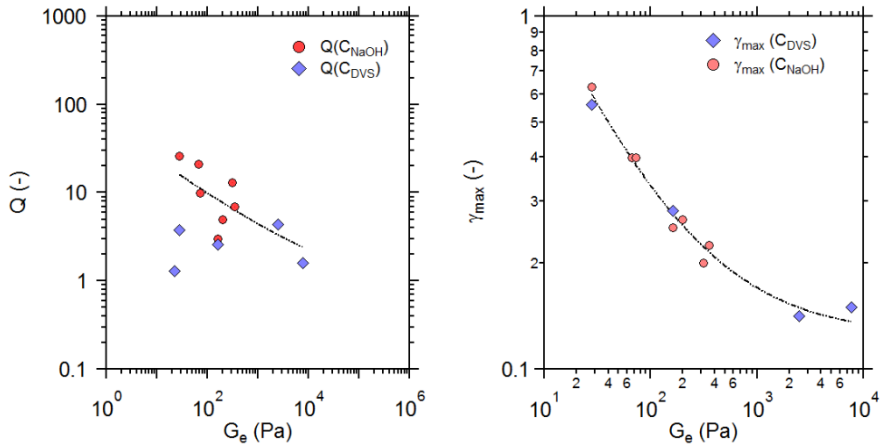

Figure 109 Q and γ_{max} as a function of the elastic plateau moduli of the sacran chemical gels. Circles: gels crosslinked by 0.15 mol/L of DVS at different NaOH concentrations. Diamonds: gels crosslinked at various DVS concentrations at 0.2 mol/L of NaOH. The sacran concentration is 0.5 wt%.

6.3.5. Comparison with the model

We further characterize the nonlinear behavior of the sacran chemical gels with an existing model[5] of network deformation which can describe nonlinear mechanical properties of gels by relating their macroscopic strain-hardening behavior to molecular parameters of the elastically active chains.

The model describes the shear stress as a function of the strain γ, chain extensibility parameter β, chain bending constant κ, and the network shear modulus G. β is defined as the ratio of the mean-square distance between the crosslinks in the undeformed chain and the square of the end-to-end distance of the fully stretched chain. The bending constant is proportional to the bending modulus (thus to Young's modulus) of the chain. The characteristics of the network (chain concentration, crosslinking ratio) are included in the value of the shear modulus G. By using two dimensionless parameter, β and κ, nonlinear deformation of the network can be classified into three deformation regimes, the network deformation regime, the bending deformation regime and the bond stretching regime, covering from flexible chains to rods, from entropic deformation to enthalpic bond stretching.

With this model the shear stress $\sigma(\gamma)$ is written as:

$$\sigma_{xy}(\gamma) = \frac{G_0(1-\beta)^2\gamma}{2}\left(3 + \frac{2b_K}{b}\sqrt{\kappa^2 + \left(1 - \frac{\beta(\gamma^2+3)}{3}\right)^{-2}} - \frac{2b_K}{b}\sqrt{\kappa^2+1}\right), \qquad 38$$

where G_0 is the shear modulus at small deformations $G_0 \approx 2G/3(1-\beta)^2$, β is the elongation ratio, b_K is the Kuhn segment length, b is the monomer length, κ is the chain bending constant. Figure 110 shows the values of σ calculated with this equation for three sets of parameters (see the caption). The value of σ diverges at $\gamma_c = \sqrt{3(1-\beta)/\beta}$. Thus with an increase in β, the strain hardening occurs at lower value of strain. This value is expected to be close to the experimental value of γ_{max}. Nevertheless, since σ increases very rapidly near this critical strain, failure of the sample is likely to occur near this critical strain and the experimental precision for σ might be very low. The decrease of κ, observed from the green curve to the red curve, induces an increase of σ in the linear domain. The decrease of β, observed from the blue curve to the red curve, induces a decrease of the σ in the linear domain.

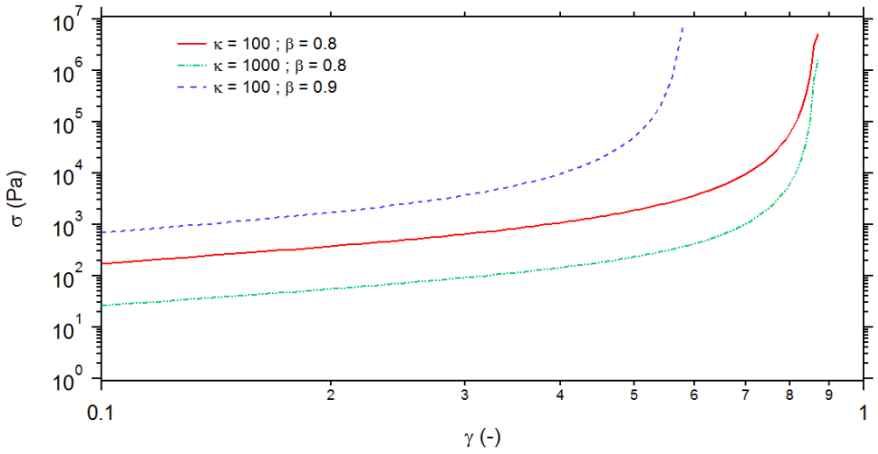

Figure 110 Stress – strain curves calculated with the model (eq.38). The following parameters are used: G_0 =100 Pa, b_k =100 nm, b =0.5 nm, and κ =100 with β =0.8 for the red curve, κ =1000 with β =0.8 for the green curve and κ =100 with β =0.9 for the blue curve.

The experimental data of the shear stress $\sigma(\gamma)$ for the sacran chemical gels, prepared in the two series of conditions, are fitted by this model with three free parameters to determine: β, κ and b_K/b. For G_0, the experimental value of the shear modulus in linear domain is used.

6.3.5.1. DVS series

First the chemical gels prepared at different DVS concentrations at a fixed NaOH concentration are studied. In Figure 111 the experimental values of σ are plotted as a function of strain, fitted with the model. The model fits well the linear domain likewise the beginning of the strain hardening, while at large strain amplitude a deviation is observed. The measured stress is lower than the model prediction, except for the gel crosslinked at C_{DVS} = 0.1 mol/L. The reason why the experimental value can be higher is not clear.

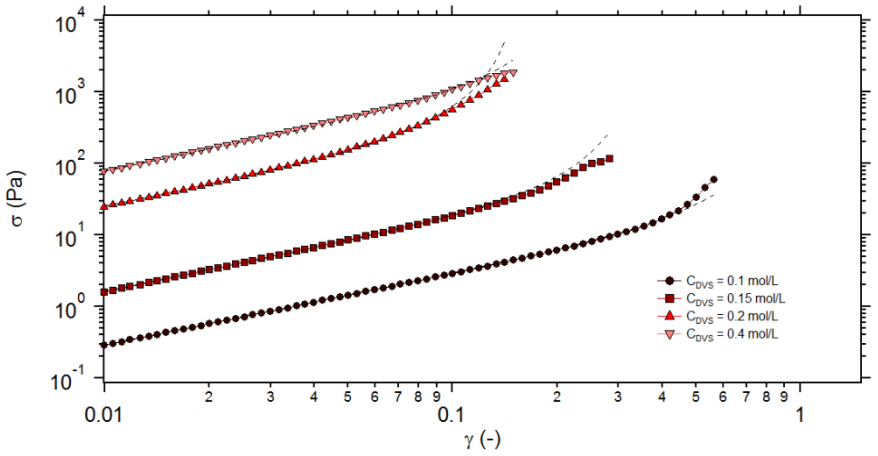

Figure 111 Stress – strain curves fitted by eq.38 for sacran chemical gels crosslinked at different DVS concentrations. Sacran concentration: 0.5 wt%, NaOH concentration: 0.2 mol/L.

In Figure 112, the two parameters β and κ obtained from the fit are plotted as a function of the DVS concentration. We find very high values of β, varying from 0.84 to 0.99. These values close to 1 indicates that the sacran chains between the chemical crosslinks are very rigid (the mean-square distance between the crosslinks in the undeformed chain is very close to the square of the end-to-end distance of the fully stretched chain). The values of κ are constant around 200 except for the gel crosslinked by 0.4 mol/L of DVS showing much higher value around 600.

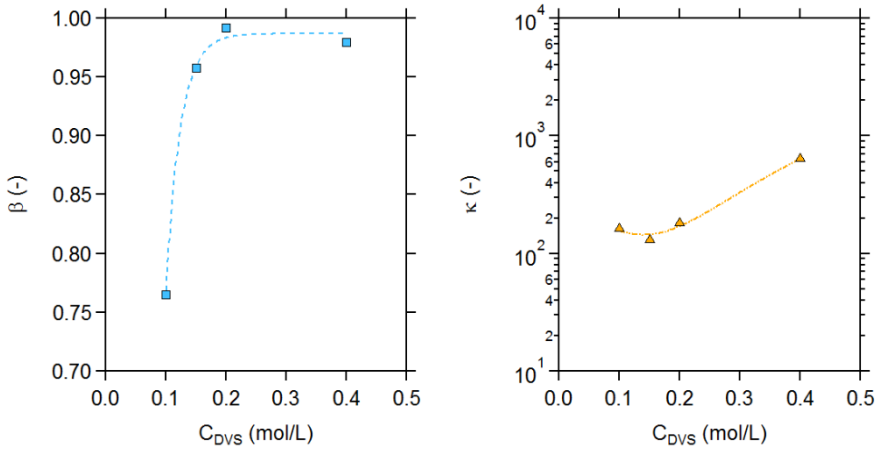

Figure 112 Elongation ratio (β) and the chain bending constant (κ) determined by fitting the experimental data with the model (eq.38) as a function of C_{DVS}. Sacran concentration: 0.5 wt%, NaOH concentration: 0.2 mol/L.

6.3.5.2. NaOH series

Also for the series of the chemical gels crosslinked by 0.15 mol/L of DVS at various NaOH concentrations, the experimental data of the stress are fitted with the model. In Figure 113, the experimental data fitted by the model are shown. The model fits well the experimental data in the linear domain and the beginning of the strain hardening, deviations are observed at large deformation. Similarly to the other series of the gels crosslinked at different DVS concentrations, the model prediction gives higher values of σ than the experiments except for the gels with lower modulus having relatively larger extensibility.

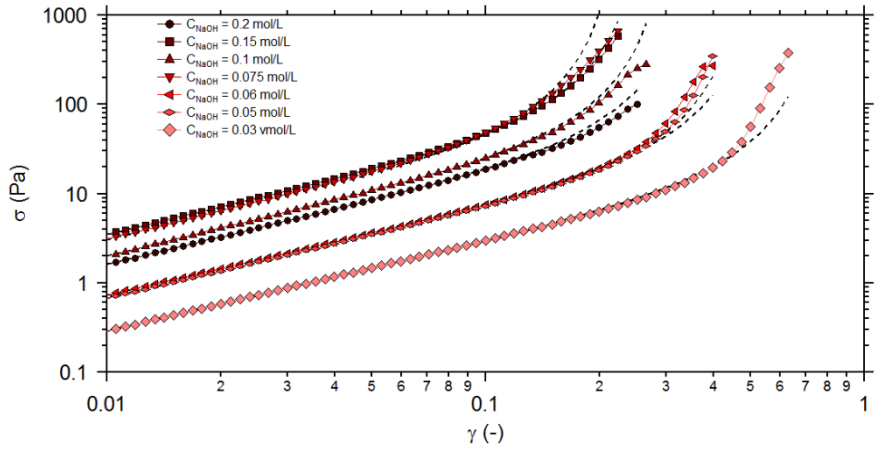

Figure 113 Stress – strain curves for sacran chemical gels crosslinked by 0.15 mol/L of DVS at different NaOH concentrations. Sacran concentration: 0.5 wt%.

In Figure 114, the values of β and κ are plotted as a function of C_{NaOH}. The value of β varies from 0.82 to 0.97, increases with C_{NaOH}. Up to 0.075 mol/L. The value of κ is almost constant, about 140. This result suggests that the change in pH at this range does not change the chain rigidity, no structural change affecting the rigidity occurs.

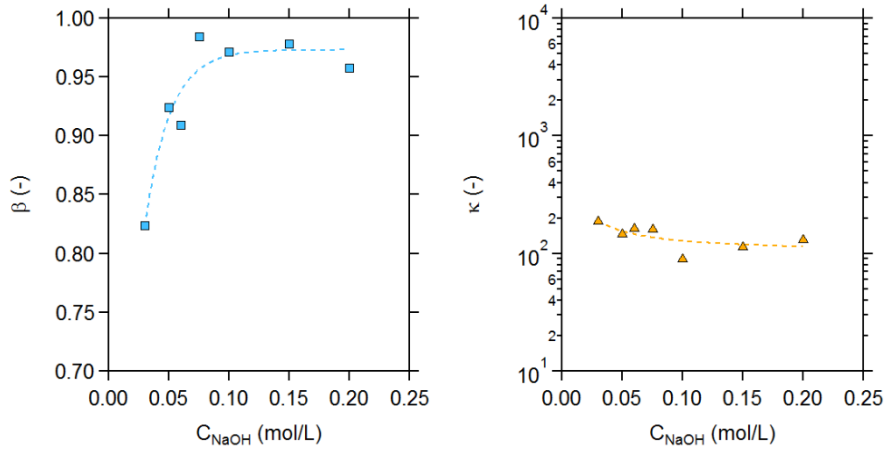

Figure 114 Elongation ratio (β) and chain bending constant (κ) as a function of the C_{NaOH}. Sacran concentration: 0.5 wt%, DVS concentration: 0.15 mol/L.

6.3.5.3. Comparison

The same trend of β and κ are observed for the two series of the chemical gel preparation conditions. Now we compare them as a function of the elastic plateau modulus, G_e. In Figure 115, the values of β and κ for the two series of the gels are plotted as a function of G_e. The values from the two series can be rescaled to collapse on a same tendency. The value of β increases with G_e and stabilizes around 0.99. The value of κ does not depend on G_e, except for the sacran gel with a G_e = 7.8 kPa (C_{DVS} = 0.4 mol/L, C_{NaOH} = 0.2 mol/L). For all the other gels studied the values of κ are around 140 and are not dependent of the gel elasticity. The chain bending constant κ characterizes the single chain rigidity, but is not related to the length of the chain between the crosslinks.

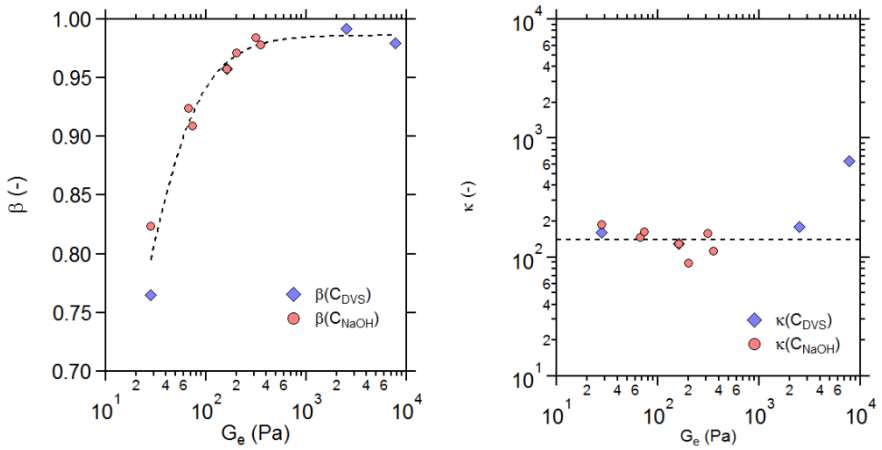

Figure 115 β and κ as a function of the elastic plateau modulus (G_e) of the sacran chemical gels. Tested by an oscillatory strain sweep. Circles: sacran gels crosslinked by DVS at different DVS concentration, diamonds: gels crosslinked at various NaOH concentrations.

The last free parameter of the fit, the ratio between the Kuhn length on the bond length, b_K/b, is plotted as a function of the G_e in Figure 116. This ratio is constant on the range of G_e measured, for the two series of the gels, expect for the gel at G_e = 600 Pa. This result confirms that the Kuhn length, which is $2\ l_p$ in the wormlike chain model, does not depend on the network elasticity.

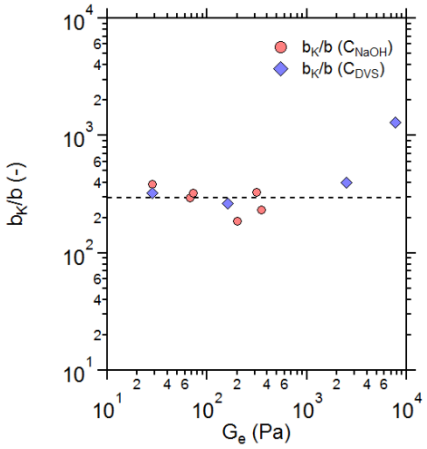

Figure 116 b_K/b as a function of Ge for the sacran chemical gels. The circles represents the sacran gels concentrated at 0.5 wt% and crosslinked by 0.15 mol/L of DVS in presence of different amount of NaOH. The diamonds represents the sacran gels concentrated at 0.5 wt% and crosslinked by different amount of DVS in the presence of 0.2 mol/L of NaOH.

The relation between b_k and κ is given as:

$$b_K = \frac{b(1+\langle cos(\theta)_0\rangle)}{1-\langle cos(\theta)_0\rangle} = \frac{b(1+coth(\kappa)-\kappa^{-1})}{1-coth(\kappa)+\kappa^{-1}} \qquad 39$$

where θ is the rotation angle of the Kuhn segment. This relation indicates $b_K = 2\kappa b$ for $\kappa \gg 1$. The sacran chemical gels studied in this work show $\kappa \sim 140$, thus the deformations of the gels are described as the bending of wormlike chain. The value of b_K/b is plotted as a function of κ in Figure 117. Note that both are free parameters of the fit. As shown in Figure 117, the value of b_K/b is well proportional to κ, all the data points (including that for G_e = 600 Pa) collapse on a linear regression with a slope of 2. This result indicates that the nonlinear properties of the sacran chemical gels can be described by the bending of wormlike chain.

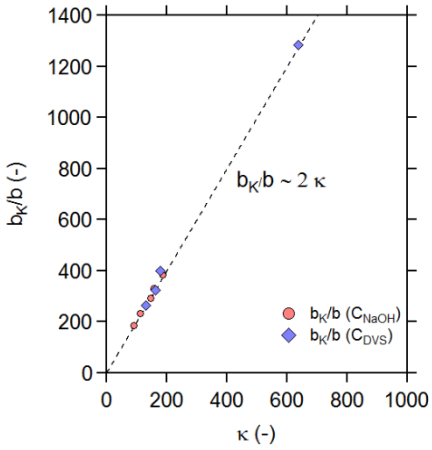

Figure 117 Comparison between the modelling parameters b_K/b and κ obtained from the fitting of the stress-strain experimental curves.

In order to evaluate the experimentally determined maximal extensibility, γ_{max}, we compare the values of γ_{max} with those theoretically predicted by the model.

As a consequence of the bending deformation, the stress diverge to infinity at the critical strain amplitude γ_c:

$$\gamma_c = \sqrt{\frac{3(1-\beta)}{3}}. \qquad 40$$

γ_c depends only on β. By using the values of b determined by fitting, we estimate the value of γ_c.

In Figure 118 the value of γ_{max} is compared with the value of γ_c. We observe that γ_{max} is very closed to γ_c, showing slightly lower values than the theoretical prediction, about 0.7 times lower than the γ_c. This means that the extensibility of the gels is lower than the model prediction. Also we remark that the difference between γ_{max} and γ_c seems more pronounced at high γ_c thus low β. These results are reasonable, since the chemically crosslinked network structure is supposed to be heterogeneous as at high strain amplitude, and certain weak zones can be broken before the chains are full stretched.

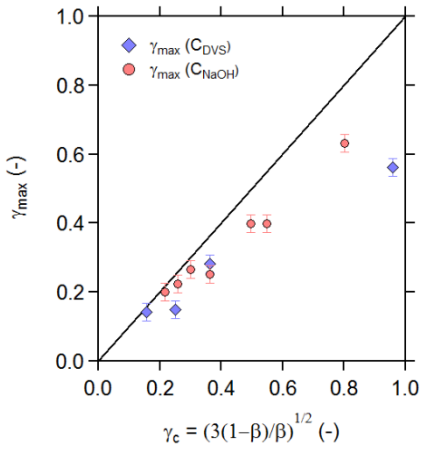

Figure 118 γ_{max} as a function of $\gamma_c = \sqrt{3(1-\beta)/\beta}$. The solid line correspond to $y = x$ and the dashed line correspond to linear fitting of our points (y =0.7 x).

6.4. Conclusion

Sacran chemical gels have been studied by macrorheology in order to characterize the strain-hardening capacity of the sacran gels. The sacran chemical gels are prepared by reacting with a chemical crosslinker divinyl sulfone (DVS) which interacts with hydroxyl groups on the polysaccharide in basic condition. The pH (adjusted by addition of NaOH) and the C_{DVS} are used as parameters to control the crosslinking ratio in sacran chemical gels. A chemical gelation diagram as a function of the DVS and sacran concentrations is made. The obtained chemical gels are elastic and transparent, except at high crosslinking ratio. The turbidity of the gel at high crosslinking ratio suggests formation of large structure presumably bundles.

Two series of gelation conditions are tested: at a fixed NaOH concentration (0.2 mol/L) with various DVS concentrations, and at a constant DVS concentration (0.15 mol/L) with various NaOH concentrations. In linear domain the moduli of the sacran chemical gels from the two series show a well-defined elastic plateau.

In nonlinear domain we observed a strain hardening behavior for all the gels (above 0.05 mol/L of DVS or 0.03 mol/L of NaOH). The strain-hardening ratio Q can be as large as 25. The amplitude of the strain-hardening, such as the minimal strain amplitude applied to the gel when a failure occurs (γ_{max}), are correlated with the gel elasticity G_e. The more the sacran gel is chemically crosslinked and elastic, the less the strain hardening ratio Q and the strain at rupture occurs γ_{max}. The two series of the gels varying of C_{DVS} or C_{NaOH} show the identical tendency, suggesting that no structural changes occur at high pH.

A nonlinear network elasticity model developed by McKintosh et al. is used to fit the stress – strain curves experimentally obtained from the sacran chemical gels. This model describes the linear and nonlinear stress – strain relation of polymer networks with two parameters: the chain bending constant (κ) and the chain elongation ratio (β). These parameters are determined by fitting the experimental curves with the model. For the two series of the sacran chemical gels, the value of κ is independent of the elasticity of the gels: it depend on the single chain elasticity of the polymer. The β increases dramatically with the increase of the crosslinking ratio in the sacran gels approaching to the critical value of 1 corresponding to totally rigid rod between crosslinking points. The elongation ratio of polymer chain between crosslinks seems then be the key parameter of strain-hardening observation from semi-rigid polymer networks. A mechanism of strain-hardening has been then proposed for sacran gels.

It is noticed that strain-hardening amplitudes observed from sacran gels (Q up to 26) are large compare with those for protein filament gels such as fibrins found in literature. In regards to these large strain-hardening observed from sacran gels and the biocompatibility of this polysaccharide, sacran could then be interesting for reinforce hydrogels with aimed biomedical applications

Conclusion

Sacran solutions

By passive microrheology based on DLS and DWS, the persistence length (l_p) of the sacran chain has successfully been determined from the transition between the Zimm-Rouse mode and the bending mode. The value of l_p shows a sacran concentration dependence, it decreases with an increase in the concentration. This decrease is partly explained by the theory of Odijk-Skolnick-Fixman which describes the contribution of the electrostatic interaction on the persistence length. The intrinsic persistence length is estimated to be 60 nm. At higher concentration above 0.1 wt% at which the theory fails to describe the decrease in l_p, we measure the entanglement length l_e, the chain length between the crosslinks, instead of the persistence length, since the latter is longer than the former at this concentration range and the microrheological determination of l_p fails. We find a scaling law of $l_e \sim C^{-0.4}$ as predicted by Isambert and Maggs[71]. Beyond 0.1 wt%, sacran chains seem then enough entangled to form rigid network.

Sacran physical gels – linear regime

We have studied the gelation of sacran by divalent cations in the alkaline earth metal elements: Ca^{2+}, Sr^{2+} and Ba^{2+}. These physical gels crosslinked by reversible ionic interactions have also been studied by microrheology, the persistence length is measured. The values of the viscoelastic modulus were found by microrheology and macrorheology agree well. The persistence length of the sacran gels at 0.25 wt% determined by microrheology is comparable to the mesh size of the gels determined by macrorheology.

Above the stoichiometry of the charges, the value of the elastic plateau G_e is independent of the cation concentration. For the sacran gels at 0.25 wt%, the mesh size is around 60 nm. This value is much larger than the distance between charges on the sacran chains estimated at 1.5 nm. This result suggests that a large quantity of charges on the sacran chains are not involved in the interchain crosslinks, presumably due to the chain rigidity.

Finally, the plateau modulus is studied as a function of the sacran concentration. We find a power law as $G_e \sim C_{chains}^{\ 1.5}$ for the three different cations. This power law exponent is predicted by Rubinstein and Colby as $G_e \sim C_{chains}^{\ 3\upsilon/(3\upsilon-1)}$ with $\upsilon = 1$ for the caser of rigid chains.

The kinetics of gelation induced by Ca^{2+} are slower and more complex than those induced by Ba^{2+} and Sr^{2+}, suggesting formation of larger structure of sacran chains with Ca^{2+}.

Sacran physical gels – nonlinear regime

These physical gels of sacran have been studied in their nonlinear regime. Strain-hardening behaviors are observed for certain conditions, principally in the presence of Ca^{2+}. The gelation by Ca^{2+} induces formation of sacran gels more heterogeneous than those obtained by Sr^{2+} and Ba^{2+}.

In order to separate the ionic crosslinking of sacran chains by the divalent cations and the salt effect of these cations, the viscoelastic moduli of sacran in the presence of NaCl is tested. After very slow evolution of the moduli, a pronounced strain hardening behavior is observed. Presumably in the presence of salts screens the electrostatic repulsions between the charged sacran chains.

Sacran chemical gel

Sacran chemical gels have been then studied by macrorheology in order to characterize the strain-hardening behavior of the sacran chemical gels.

The sacran chemical gelation is prepared by crosslinking abundant hydroxyl groups (in alkoxide form in basic conditions) with divinyl sulfone (DVS). The value of pH controlled by NaOH concentration and the DVS concentration are varied to control the crosslinking ratio in the sacran chemical gels. Transparent elastic gels are obtained, except for the gels prepared at high DVS concentrations which are turbid. Presumably large structures are formed.

The sacran chemical gels show in their nonlinear regime large amplitude strain-hardenings behaviors. The strain hardening ratio can reach 25. The amplitude of these strain-hardenings, such as the strain amplitude at the failure (the gel is broken or slips in the geometry), γ_{max}, decreases with an increase in the plateau modulus of the gels. It is noticed that strain-hardening amplitudes observed from sacran gels (Q up to 26) are large compared with known biopolymers.

A nonlinear elasticity model is used to fit the stress – strain curves experimentally obtained for the chemical gels of sacran. This model describes the stress – strain relationship of polymeric networks as a function of the rigidity and extensibility of the chains. These parameters are determined by fitting the experimental data of stress. The chain bending constant (κ) is independent of the elasticity of the sacran chemical gels. The constant value of κ indicates that in the nonlinear domain the sacran chain strands behave as worm-like chains, and bending of the chain is dominant in nonlinear elasticity. The elongation ratio (β) increases dramatically with the increase of the crosslinking ratio in the sacran gels approaching to 1 which corresponds to rigid rods.

Perspectives

Physical gels of sacran could be interesting as decontamination agents. Sacran chains are able to be crosslinked by the barium which let us think that radium could also create gels with sacran. In this way, the sacran could be used as decontamination agent for radioactive wastes.

Chemical gels of sacran are able to form very soft networks. These gels are interesting for their elasto-capillarity properties due to their high surface tension.

Finally, the reinforcement of hydrogels by using rigid networks is limited by their brittleness. This brittleness is due to the elongation ratio of chains which limits the deformability of rigid networks. This brittleness could be bypassed by manufacturing nanocomposites hydrogels composed of sacran.

References

1. Storm, C., Pastore, J. J., MacKintosh, F. C., Lubensky, T. C. & Janmey, P. A. Nonlinear elasticity in biological gels. *Nature* **435,** 191–194 (2005).
2. Okajima, M. K., Kaneko, D., Mitsumata, T., Kaneko, T. & Watanabe, J. Cyanobacteria That Produce Megamolecules with Efficient Self-Orientations. *Macromolecules* **42,** 3057–3062 (2009).
3. Okajima, M. K., Miyazato, S. & Kaneko, T. Cyanobacterial Megamolecule Sacran Efficiently Forms LC Gels with Very Heavy Metal Ions †. *Langmuir* **25,** 8526–8531 (2009).
4. Mitsumata, T. *et al.* Ionic state and chain conformation for aqueous solutions of supergiant cyanobacterial polysaccharide. *Phys. Rev. E* **87,** (2013).
5. Carrillo, J.-M. Y., MacKintosh, F. C. & Dobrynin, A. V. Nonlinear Elasticity: From Single Chain to Networks and Gels. *Macromolecules* **46,** 3679–3692 (2013).
6. *Encyclopedic Dictionary of Polymers | Jan W Gooch | Springer*.
7. Drury, J. L. & Mooney, D. J. Hydrogels for tissue engineering: scaffold design variables and applications. *Biomaterials* **24,** 4337–4351 (2003).
8. Hoffman, A. S. Hydrogels for biomedical applications. *Adv. Drug Deliv. Rev.* **64,** 18–23 (2012).
9. Wichterle, O. & Lím, D. Hydrophilic Gels for Biological Use. *Nature* **185,** 117–118 (1960).
10. Ratner, B. D. & Hoffman, A. S. Synthetic Hydrogels for Biomedical Applications. in *Hydrogels for Medical and Related Applications* (ed. Andrade, J. D.) **31,** 1–36 (AMERICAN CHEMICAL SOCIETY, 1976).
11. COVALENT BINDING OF BIOMOLECULES TO RADIATION-GRAFTED HYDROG... : ASAIO Journal. *LWW* Available at: http://journals.lww.com/asaiojournal/Fulltext/1972/04000/COVALENT_BINDING_OF_BIOMOLECULES_TO.3.aspx. (Accessed: 7th June 2017)
12. *Poly(Ethylene Glycol) Chemistry - Biotechnical and | J. Milton Harris | Springer*.
13. Noda, Y., Hayashi, Y. & Ito, K. From topological gels to slide-ring materials: Review. *J. Appl. Polym. Sci.* **131,** n/a-n/a (2014).

14. Braun, P. V., Wiltzius, P. & others. Electrochemical fabrication of 3D microperiodic porous materials. *Adv. Mater.* **13,** 482–485 (2001).
15. The Polyrotaxane Gel: A Topological Gel by Figure-of-Eight Cross-links - Okumura - 2001 - Advanced Materials - Wiley Online Library. Available at: http://onlinelibrary.wiley.com/doi/10.1002/1521-4095(200104)13:7%3C485::AID-ADMA485%3E3.0.CO;2-T/full. (Accessed: 21st June 2017)
16. Edwards, S. F. & Vilgis, T. The effect of entanglements in rubber elasticity. *Polymer* **27,** 483–492 (1986).
17. de Gennes, P.-G. Sliding gels. *Phys. Stat. Mech. Its Appl.* **271,** 231–237 (1999).
18. Zhao, C. *et al.* Sliding mode of cyclodextrin in polyrotaxane and slide-ring gel. *J. Phys. Condens. Matter* **17,** S2841 (2005).
19. Karino, T., Shibayama, M. & Ito, K. Slide-ring gel: Topological gel with freely movable cross-links. *Phys. B Condens. Matter* **385–386, Part 1,** 692–696 (2006).
20. Novel Cross-Linking Concept of Polymer Network: Synthesis, Structure, and Properties of Slide-Ring Gels with Freely Movable Junctions - ProQuest. Available at: http://search.proquest.com/openview/8c842dbecc26b4799ae6f431b26030f5/1?pq-origsite=gscholar&cbl=546295. (Accessed: 21st June 2017)
21. Ito, K. Slide-ring materials using topological supramolecular architecture. *Curr. Opin. Solid State Mater. Sci.* **14,** 28–34 (2010).
22. Mayumi, K., Tezuka, M., Bando, A. & Ito, K. Mechanics of slide-ring gels: novel entropic elasticity of a topological network formed by ring and string. *Soft Matter* **8,** 8179–8183 (2012).
23. Sakai, T. *et al.* Design and Fabrication of a High-Strength Hydrogel with Ideally Homogeneous Network Structure from Tetrahedron-like Macromonomers. *Macromolecules* **41,** 5379–5384 (2008).
24. Kurakazu, M. *et al.* Evaluation of Gelation Kinetics of Tetra-PEG Gel. *Macromolecules* **43,** 3935–3940 (2010).
25. Sakai, T. *et al.* Highly Elastic and Deformable Hydrogel Formed from Tetra-arm Polymers. *Macromol. Rapid Commun.* **31,** 1954–1959 (2010).

26. Shibayama, M. Small-angle neutron scattering on polymer gels: phase behavior, inhomogeneities and deformation mechanisms. *Polym. J.* **43,** 18–34 (2011).
27. Matsunaga, T. *et al.* SANS Studies on Tetra-PEG Gel under Uniaxial Deformation. *Macromolecules* **44,** 1203–1210 (2011).
28. Sakai, T. Gelation mechanism and mechanical properties of Tetra-PEG gel. *React. Funct. Polym.* **73,** 898–903 (2013).
29. Haraguchi, K. & Li, H.-J. Mechanical properties and structure of Polymer- Clay nanocomposite gels with high clay content. *Macromolecules* **39,** 1898–1905 (2006).
30. Haraguchi, K., Takehisa, T. & others. Nanocomposite hydrogels: a unique organic-inorganic network structure with extraordinary mechanical, optical, and swelling/de-swelling properties. *Adv. Mater.* **14,** 1120 (2002).
31. Haraguchi, K., Takehisa, T. & Fan, S. Effects of Clay Content on the Properties of Nanocomposite Hydrogels Composed of Poly(N-isopropylacrylamide) and Clay. *Macromolecules* **35,** 10162–10171 (2002).
32. Gong, J. P., Katsuyama, Y., Kurokawa, T. & Osada, Y. Double-Network Hydrogels with Extremely High Mechanical Strength. *Adv. Mater.* **15,** 1155–1158 (2003).
33. Mayumi, K., Marcellan, A., Ducouret, G., Creton, C. & Narita, T. Stress–Strain Relationship of Highly Stretchable Dual Cross-Link Gels: Separability of Strain and Time Effect. *ACS Macro Lett.* **2,** 1065–1068 (2013).
34. Haque, M. A., Kurokawa, T. & Gong, J. P. Super tough double network hydrogels and their application as biomaterials. *Polymer* **53,** 1805–1822 (2012).
35. Tominaga, T. *et al.* The molecular origin of enhanced toughness in double-network hydrogels: A neutron scattering study. *Polymer* **48,** 7449–7454 (2007).
36. Na, Y.-H. *et al.* Structural Characteristics of Double Network Gels with Extremely High Mechanical Strength. *Macromolecules* **37,** 5370–5374 (2004).
37. Ping Gong, J. Why are double network hydrogels so tough? *Soft Matter* **6,** 2583–2590 (2010).
38. Fletcher, D. A. & Mullins, R. D. Cell mechanics and the cytoskeleton. *Nature* **463,** 485–492 (2010).

39. Rochlin, M. W., Dailey, M. E. & Bridgman, P. C. Polymerizing Microtubules Activate Site-directed F-Actin Assembly in Nerve Growth Cones. *Mol. Biol. Cell* **10,** 2309–2327 (1999).

40. Pritchard, R. H., Shery Huang, Y. Y. & Terentjev, E. M. Mechanics of biological networks: from the cell cytoskeleton to connective tissue. *Soft Matter* **10,** 1864 (2014).

41. Huang, G. *et al.* Strain Hardening Behavior of Poly(vinyl alcohol)/Borate Hydrogels. *Macromolecules* **50,** 2124–2135 (2017).

42. Hyun, K., Kim, S. H., Ahn, K. H. & Lee, S. J. Large amplitude oscillatory shear as a way to classify the complex fluids. *J. Non-Newton. Fluid Mech.* **107,** 51–65 (2002).

43. Cziep, M. A., Abbasi, M., Heck, M., Arens, L. & Wilhelm, M. Effect of Molecular Weight, Polydispersity, and Monomer of Linear Homopolymer Melts on the Intrinsic Mechanical Nonlinearity ${}^{3}Q_{0}(\omega)$ in MAOS. *Macromolecules* **49,** 3566–3579 (2016).

44. Probing transmembrane mechanical coupling and cytomechanics using magnetic twisting cytometry - Biochemistry and Cell Biology. Available at: http://www.nrcresearchpress.com/doi/abs/10.1139/o95-041. (Accessed: 7th June 2017)

45. MacKintosh, F. C., Käs, J. & Janmey, P. A. Elasticity of semiflexible biopolymer networks. *Phys. Rev. Lett.* **75,** 4425 (1995).

46. Onck, P. R., Koeman, T., van Dillen, T. & van der Giessen, E. Alternative Explanation of Stiffening in Cross-Linked Semiflexible Networks. *Phys. Rev. Lett.* **95,** 178102 (2005).

47. Head, D. A., Levine, A. J. & MacKintosh, F. C. Deformation of Cross-Linked Semiflexible Polymer Networks. *Phys. Rev. Lett.* **91,** 108102 (2003).

48. Huisman, E., van Dillen, T., Onck, P. & Van der Giessen, E. Three-Dimensional Cross-Linked F-Actin Networks: Relation between Network Architecture and Mechanical Behavior. *Phys. Rev. Lett.* **99,** (2007).

49. Žagar, G., Onck, P. R. & Van der Giessen, E. Elasticity of Rigidly Cross-Linked Networks of Athermal Filaments. *Macromolecules* **44,** 7026–7033 (2011).

50. Okajima-Kaneko, M., Ono, M., Kabata, K. & Kaneko, T. Extraction of novel sulfated polysaccharides from Aphanothece sacrum (Sur.) Okada, and its spectroscopic characterization. *Pure Appl. Chem.* **79,** (2007).

51. Morita, T., Westh, P., Nishikawa, K. & Koga, Y. How Much Weaker Are the Effects of Cations than Those of Anions? The Effects of K^+ and Cs^+ on the Molecular Organization of Liquid H_2O. *J. Phys. Chem. B* **118,** 8744–8749 (2014).
52. de Xammar Oro, J. R. Role of co-solute in biomolecular stability: Glucose, urea and the water structure. *J. Biol. Phys.* **27,** 73–79 (2001).
53. Zangi, R. Can Salting-In/Salting-Out Ions be Classified as Chaotropes/Kosmotropes? *J. Phys. Chem. B* **114,** 643–650 (2010).
54. Tobias, D. J. & Hemminger, J. C. Getting Specific About Specific Ion Effects. *Science* **319,** 1197–1198 (2008).
55. Mitchell, J. R. The rheology of gels. *J. Texture Stud.* **11,** 315–337 (1980).
56. Wyss, H. *et al.* Strain-Rate Frequency Superposition: A Rheological Probe of Structural Relaxation in Soft Materials. *Phys. Rev. Lett.* **98,** (2007).
57. Mason, T. G. & Weitz, D. A. Optical measurements of frequency-dependent linear viscoelastic moduli of complex fluids. *Phys. Rev. Lett.* **74,** 1250 (1995).
58. Mason, T. G., Ganesan, K., van Zanten, J. H., Wirtz, D. & Kuo, S. C. Particle Tracking Microrheology of Complex Fluids. *Phys. Rev. Lett.* **79,** 3282–3285 (1997).
59. Levine, A. J. & Lubensky, T. C. One- and Two-Particle Microrheology. *Phys. Rev. Lett.* **85,** 1774–1777 (2000).
60. Schnurr, B., Gittes, F., MacKintosh, F. C. & Schmidt, C. F. Determining Microscopic Viscoelasticity in Flexible and Semiflexible Polymer Networks from Thermal Fluctuations. *Macromolecules* **30,** 7781–7792 (1997).
61. Indei, T., Schieber, J. D., Córdoba, A. & Pilyugina, E. Treating inertia in passive microbead rheology. *Phys. Rev. E* **85,** (2012).
62. Monti, F. Microrhéologie de suspensions colloïdales non ergodiques: relaxation locale, dynamiques lentes et vieillissement. (Université Pierre et Marie Curie, 2010).
63. Gunes, D. Etude de la floculation colloïdale par diffusion multiple de la lumière et spectroscopie ultrasonore. (Université Louis Pasteur de Strasbourg).

64. Gittes, F. & MacKintosh, F. C. Dynamic shear modulus of a semiflexible polymer network. *Phys. Rev. E* **58,** R1241 (1998).

65. Willenbacher, N. *et al.* Broad Bandwidth Optical and Mechanical Rheometry of Wormlike Micelle Solutions. *Phys. Rev. Lett.* **99,** (2007).

66. Oelschlaeger, C., Cota Pinto Coelho, M. & Willenbacher, N. Chain Flexibility and Dynamics of Polysaccharide Hyaluronan in Entangled Solutions: A High Frequency Rheology and Diffusing Wave Spectroscopy Study. *Biomacromolecules* **14,** 3689–3696 (2013).

67. Brown, W. *Light Scattering: Principles and Development.* (Clarendon Press, 1996).

68. Bednar, J. *et al.* Determination of DNA Persistence Length by Cryo-electron Microscopy. Separation of the Static and Dynamic Contributions to the Apparent Persistence Length of DNA. *J. Mol. Biol.* **254,** 579–594 (1995).

69. Berret, J.-F. Rheology of Wormlike Micelles: Equilibrium Properties and Shear Banding Transitions. in *Molecular Gels* 667–720 (Springer, Dordrecht, 2006). doi:10.1007/1-4020-3689-2_20

70. Odijk, T. Polyelectrolytes near the rod limit. *J. Polym. Sci. Polym. Phys. Ed.* **15,** 477–483 (1977).

71. Isambert, H. & Maggs, A. C. Dynamics and Rheology of Actin Solutions. *Macromolecules* **29,** 1036–1040 (1996).

72. Shikinaka & Kaneko. Solution structure of cyanobacterial polysaccharide, sacran. *Polymer* **99,** 767

73. Buhler, E. & Boué, F. Chain Persistence Length and Structure in Hyaluronan Solutions: Ionic Strength Dependence for a Model Semirigid Polyelectrolyte. *Macromolecules* **37,** 1600–1610 (2004).

74. Rubinstein, M. & Colby, R. H. *Polymer Physics.* (Oxford University Press, 2003).

75. Okajima, M. K. *et al.* Double-metal complexation of heterogels containing cyanobacterial polysaccharides. *J. Appl. Polym. Sci.* **128,** 676–683 (2013).

76. Hinner, B., Tempel, M., Sackmann, E., Kroy, K. & Frey, E. Entanglement, elasticity, and viscous relaxation of actin solutions. *Phys. Rev. Lett.* **81,** 2614 (1998).

77. Goldenberg, C. & Goldhirsch, I. Friction enhances elasticity in granular solids. *Nature* **435,** 188–191 (2005).

78. Collins, K. Ions from the Hofmeister series and osmolytes: effects on proteins in solution and in the crystallization process. *Methods* **34,** 300–311 (2004).

79. Grover, P. K. & Ryall, R. L. Critical Appraisal of Salting-Out and Its Implications for Chemical and Biological Sciences. *Chem. Rev.* **105,** 1–10 (2005).

80. Chrastil, J. Gelation of calcium alginate. Influence of rice starch or rice flour on the gelation kinetics and on the final gel structure. *J. Agric. Food Chem.* **39,** 874–876 (1991).

81. *Chemical Design of Responsive Microgels*. **234,** (Springer Berlin Heidelberg, 2011).

82. Shimojo, A. A. M., Pires, A. M. B., Lichy, R. & Santana, M. H. A. The Performance of Crosslinking with Divinyl Sulfone as Controlled by the Interplay Between the Chemical Modification and Conformation of Hyaluronic Acid. *J. Braz. Chem. Soc.* (2015). doi:10.5935/0103-5053.20150003

Résumé substantiel en français

1. Introduction

Les filaments de protéines jouent un rôle important dans la mécanique et la mobilité cellulaire dans le vivant. On sait que ces filaments présentent généralement un strain-hardening sous de larges déformations. Le strain-hardening induit par la rigidité peut être prometteur dans le cadre du renforcement mécanique des hydrogels, mais il reste difficile de synthétiser un système modèle. La relation entre ces propriétés viscoélastiques et l'architecture du réseau d'un gel composé de chaînes rigides n'a pas encore été étudiée expérimentalement.

Dans ce travail, en tant que polymère modèle capable de former un réseau rigide, nous avons utilisé un nouveau polysaccharide cyanobactériel, le "sacran". Ce polysaccharide géant chargé négativement montre une masse molaire supérieure à 16 millions de g/mol et une longueur de contour > 10 µm observable sur la Figure 119. Il est extrait de la matrice extracellulaire d'une algue japonaise. Ce polysaccharide géant est capable de former des phases nématiques liquides cristallines (au-dessus de 0,5 wt%) sous cisaillement, ce qui indique la présence de domaines rigides en forme de tige[2]. La longueur de persistance intrinsèque est estimée à 60 nm, donc, à une échelle micrométrique, le sacran se comporte comme une chaîne flexible du fait de sa grande longueur de contour. Cependant, une fois que les chaînes de sacran sont réticulées et qu'un gel est formé, la taille du maillage peut être comparable à la longueur de la persistance, donc à cette échelle de longueur (plusieurs dizaines de nm), la chaîne sacran est considéré comme rigide.

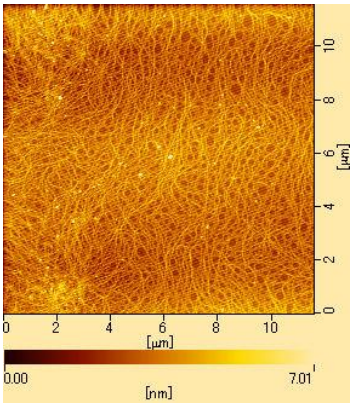

Figure 119 Image AFM de chaines de sacran séchées à partir d'une solution concentrée à 0.5 wt%.

La réaction de l'association chaîne-chaîne peut induire non seulement une gélification, mais aussi des précipités, et en particulier la formation de faisceaux de chaînes rigides qui peut conduire à de grandes structures peut se produire. Par conséquent, il est important de contrôler la balance entre gélification/précipitation en modulant les interactions à l'échelle moléculaire. Sacran est un polyélectrolyte contenant 22 mol% de fonctions carboxyles et 11 mol% de fonctions sulfates. Des hydrogels dits physiques peuvent ainsi être formés par l'ajout de cations divalents ou trivalents spécifiques. Dans ce projet, afin de caractériser les propriétés rhéologiques des gels physiques de sacran, des cations divalents choisis dans la

famille des métaux alcalino-terreux, $CaCl_2$, $SrCl_2$ et $BaCl_2$ ont été utilisés comme agents de réticulation physiques.

Le sacran étant un polysaccharide, les chaines le composant supportent nombre de fonctions alcools (250 mol%). Ces fonctions alcools mise en condition basique se chargent négativement et deviennent capable de réagir par une addition dite d'Oxa-Michael avec des molécules de divinyl sulfone (DVS) formant ainsi des ponts covalents entre chaines de sacran. Les gels ainsi formés sont nommés gels chimiques du fait des liens covalents qui les composent. Ces liaisons covalentes sont ici mises en opposition avec les liaisons transitoires formées par les interactions ioniques desquelles découle la formation de gels physiques de sacran.

Afin de déterminer deux longueurs caractéristiques de ces gels, la taille du maillage et la longueur de persistance, une étude rhéologique dans le domaine linéaire a été menée sur ces gels de sacran utilisant la rhéologie conventionnelle par cisaillement et la microrhéologie par diffusing-wave spectroscopy (DWS). De la rhéologie conventionnelle sont obtenus les paramètres rhéologiques à basse fréquence permettant de déterminer la taille de maillage à partir du plateau élastique du gel. De la microrhéologie, on accède aux propriétés rhéologiques à haute fréquence (de 1 à 10^5 rad/s), domaine où la dynamique de la chaîne unique domine et la longueur de la persistance peut être mesurée. L'observation du strain-hardening se faisant à haute déformation, une étude du régime non-linéaire des gels de sacran est menée par rhéologie conventionnelle dans l'optique d'observer et modéliser cette propriété mécanique.

2. Solution de sacran

Dans un premier temps, une étude rhéologique est menée sur des solutions aqueuses de sacran à différentes concentrations qui sera par la suite considérée comme référence pour nos caractérisations d'hydrogels de sacran. La rhéologie par DWS et la rhéologie par DLS dites microrhéologies sont utilisées dans l'optique d'observer la dépendance entre la concentration en chaines de polymère et l'évolution de la longueur de persistance de ces chaines. Ces deux techniques de microrhéologie sont assez similaires et se différencient principalement par leur hypothèse de base. Des particules sondes micrométriques et diffusantes de polystyrène sont introduites dans l'échantillon testé considéré comme non diffusant et leur déplacement quadratique moyen est lié aux propriétés rhéologiques du milieu environnant par l'équation généralisée de Stoke-Einstein. Ces particules mono-disperses sont considérées comme ne réagissant pas avec leur environnement et leur diamètre de ces particules est choisi comme très supérieur aux longueurs caractéristiques de l'échantillon. La DLS se base sur une diffusion simple d'un photon durant la traversée de l'échantillon testé alors que la DWS est basé sur une diffusion multiple. Aussi les solutions peu concentrées seront étudiées par DLS et les plus concentré le seront par DWS.

La microrhéologie par DWS permet l'obtention de réponses rhéologiques à hautes fréquences entre 1 et 10^5 rad/s. Dans ce domaine de fréquences, la dynamique de la chaîne unique domine la rhéologie et la longueur de persistance peut être mesurée à l'intersection entre les modes dynamiques de Zimm-Rouse et de flexion.

Le mode de Zimm-Rouse décrit la diffusion d'une chaîne simple comme le mouvement brownien des billes reliées par des ressorts harmoniques. Zimm inclut dans cette description les interactions hydrodynamiques dues au solvant entre les différentes parties de la chaîne. Le mode de Zimm-Rouse est classiquement décrit par une loi de puissance en $G^* \sim \omega^{5/9}$.

Le mode de flexion décrit la flexion d'un segment de chaine rigide. Ce mode est caractérisé par une loi de puissance en $G^* \sim \omega^{3/4}$. Ces deux modes sont appliqués à l'évolution du module complexe de nos solutions de sacran (G^*) en fonction de la fréquence corrigée par le modules complexe du solvant (G_S^*) et sont représentés sur la Figure 120, qui illustre les résultats obtenus pour une solution de sacran concentré à 0.25 wt%.

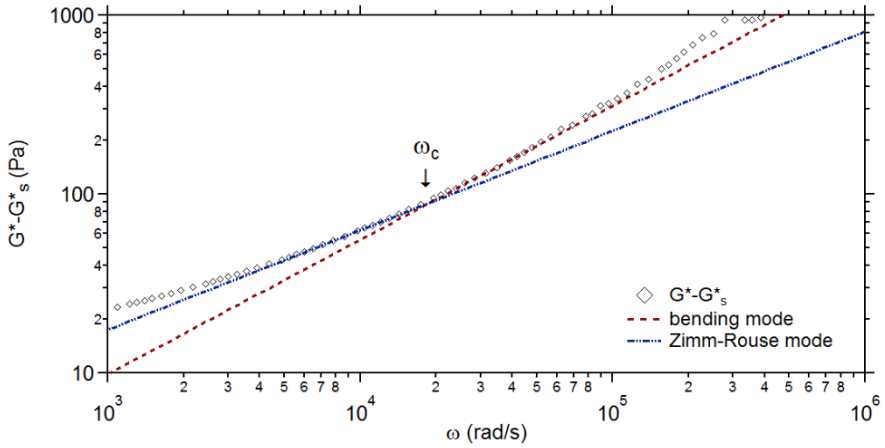

Figure 120 Module complexe ($G^* - G^*_s$) en fonction de la fréquence pour une solution de sacran de 0.25 wt%. La dynamique à haute fréquence est ajustée par le mode Zimm-Rouse ($n = 5/9$) et le mode pliage ($n = 3/4$). La fréquence critique, ω_c (définie précédemment), est déterminée comme la jonction du mode Zimm-Rouse et le mode de flexion des chaînes rigides.

Des solutions de sacran concentrées de 0.02 à 0.5 wt% sont testées par microrhéologie DLS et/ou DWS. Une bonne superposition entre la DLS et la DWS est observée à des C_{sacran} < 0.2 wt%.

L'évolution de modules $G^*(\omega) - G^*_s(\omega)$ en fonction de la fréquence obéit aux modes de Zimm-Rouse et de flexion. De l'intersection de ces deux modes dynamiques, une fréquence critique est déterminée et liée à la longueur de persistance (l_p) du système sondé par :

$$\omega_c = \frac{k_B T}{8\,\eta_s\,{l_p}^3}.$$

où η_S est la viscosité du solvant.

L'évolution de l_p ainsi calculé est reportée en fonction de la concentration en chaines de sacran dans les solutions testées. Cette évolution est tracée sur la Figure 121. On observe très clairement que la longueur de persistance des chaines de sacran décroit lors de l'accroissement de leur concentration en solution.

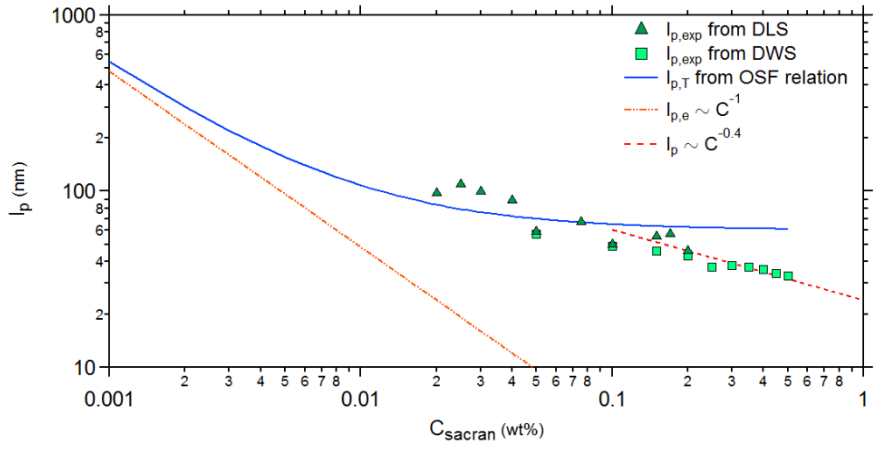

Figure 121 Longueur de persistance des chaînes de sacran obtenus expérimentalement par DLS ou DWS ($l_{p,exp}$) en fonction de la concentration de polysaccharides dans le milieu.

En effet, la longueur de persistance des polyélectrolytes dépend fortement de leur concentration. La théorie sur la longueur de persistance des polyélectrolytes développée par Odijk-Skolnick-Fixman (OSF) supposent que les interactions électrostatiques contribuent à la rigidité de flexion de la chaîne indépendamment des autres interactions. La longueur de persistance effective obtenue expérimentalement l_p est donc écrite comme[66]:

$$l_p = l_{p,e} + l_{p,o} ,$$

où $l_{p,e}$ est la longueur de persistance électrostatique, et $l_{p,o}$ est la longueur de persistance intrinsèque reflétant la rigidité de la chaine non-chargée.

La longueur de persistance électrostatique est calculée par :

$$l_{p,e} = \frac{(l_B/b)^2}{4\, l_B} \kappa^{-2} ,$$

avec

$$\kappa^{-1} = \frac{1}{\sqrt{4\pi\, l_B\, C_f}} ,$$

où l_B est la longueur de Bjerrum (0.71 nm dans l'eau), b est la distance entre les charges portées par l'électrolyte, κ^{-1} est la longueur de Debye-Hückel and C_f est la concentration ionique de la solution. La distance entre les charges portées par les chaines de sacran est un paramètre inconnu. Considérant 33 mol% d'unités monosaccharides composant le sacran sont négativement chargées, la distance moyenne entre ces charges est ainsi calculée comme 1.5 nm (considérant la taille d'un monosaccharide égale à 0.5 nm).

Cette variation théorique de $l_{p,T}$ est comparée à la variation de l_p expérimentale sur la Figure 121. On observe qu'à partir de C_{sacran} > 0.5 wt%, la variation de $l_{p,exp}$ dévie de la théorie d'OSF et commence à suivre une loi de puissance avec en exposant -0.4. Aussi lorsque la concentration en polymère augmente, au-dessus d'une certaine concentration, la distance entre deux points d'enchevêtrement, l_e, devient plus courte que la longueur de la persistance. Dans cette situation, la longueur de persistance ne peut pas être mesurée rhéologiquement, mais la longueur entre enchevêtrements l'est à la place. Isamber et Maggs[71] démontrent que l_e varie ainsi comme $l_e \sim C^{-0.4}$.

Ainsi, passé 0.1 wt%, les solutions de sacran sont enchevetrés en deçà de leur longueur de persistence. Ainsi la réticulation de gels de sacran concentré au-delà de 0.1 wt% formerait des réseaux rigides de chaines de sacran.

3. Gels physiques de sacran – régime linéaire et signatures de réseaux rigides

Des hydrogels de sacran dits physiques sont réticulés par liaisons ioniques formées de l'ajout de cations divalent choisis ici dans la famille des métaux alkalino-terreux (Ca^{2+}, Sr^{2+} et Ba^{2+}). Les gels ainsi formés sont composés de liaisons dites transitoires (réversibles) et de réseaux de chaines rigides comme l'a montré l'évolution de l_p en fonction de la concentration en chaines en solution (Figure 121). C'est cette particularité liée à la rigidité des réseaux de chaines de sacran qui fait l'objet de cette étude. Un réseau rigide est défini lorsque la taille de sa maille et inférieure à la longueur de persistance du polymère qui le compose.

La rhéologie multi-échelle de gels de sacran réticulés par différentes concentrations de Ba^{2+} est étudiée. Ces gels de sacran réticulés ont été étudiés comme base de réflexion quant à une utilisation du sacran comme agent de décontamination. Le Ba^{2+} étant l'ion le plus proche du Ra en terme structural et son étude restant plus simple à mener d'un point de vu législation, il est ici utilisé. Ainsi comme décrit en introduction de ce résumé, le couplage de la microrhéologie par DWS et de la macrorhéologie permet de mener une étude sur une très large gamme de fréquence suivant ainsi la dynamique du réseau de chaines et celle d'une chaine individuelle composant ce réseau. Les graphs de la Figure 122 représentent les modules viscoélastiques obtenus par macrorhéologie et microrhéologie DWS en fonction de la fréquence pour des gels de sacran concentré à 0.25 wt% et réticulés par différentes concentrations de Ba^{2+}. Une bonne superposition de ces modules mesurés par macrorhéologie et microrhéologie DWS est obtenue sans ajustement, validant ainsi l'utilisation de la microrhéologie DWS pour ces systèmes.

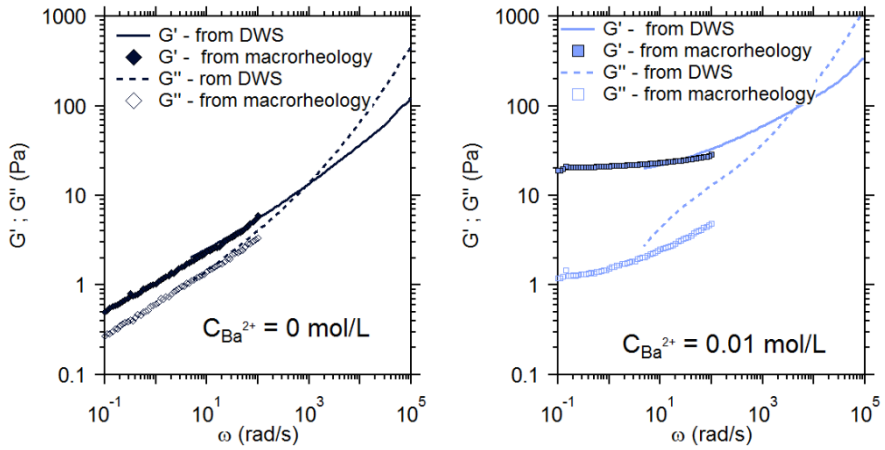

Figure 122 Modules viscoélastiques (G' ; G'') en fonction de la fréquence pour des gels de sacran à 0.25 wt% avec ou sans réticulation par le Ba^{2+}. Points: macrorhéologie. Lignes : DWS.

De cette étude rhéologique multi-échelle, sont calculées les tailles de maille (ξ) par macrorhéologie et les longueurs de persistance de ces gels de sacran par microrhéologie DWS. Les résultats obtenus sont représenté sur la Figure 123. On observe que la taille de maille décroit de 180 à 60 nm lors de l'augmentation de la $C_{Ba^{2+}}$ passant de 10^{-3} à $5\ 10^{-3}$ mol/L. Au-delà de $C_{Ba^{2+}} = 5\ 10^{-3}$ mol/L, la taille de maille reste

constante et autour de 60 nm, la longueur de persistance intrinsèque déterminée sur la Figure 121. Ainsi les gels de sacran à C_{sacran} = 0.25 wt% sont composés d'un réseau rigide lorsqu'ils sont réticulés par une $C_{Ba^{2+}} \geq 5\ 10^{-3}$ mol/L.

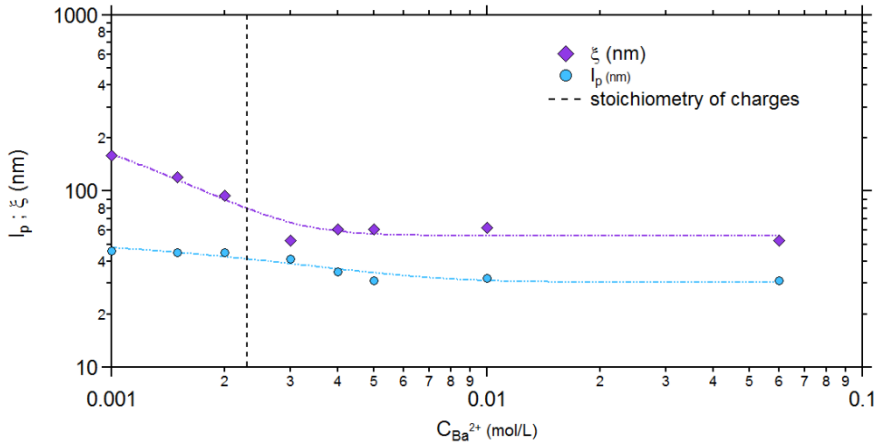

Figure 123 Tailles de maille (losanges violets) et longueurs de persistance (cercles bleus) en fonction de la concentration de Ba^{2+} pour des gels de sacran à 0.25 wt%. ξ est calculé à partie du G_e à 1 rad/s.

Dans l'idée de comparer l'action des cations réticulants les chaines de sacran, les modules élastiques au plateau G_e déterminés par macrorhéologie sont reportés en fonction de la concentration en Ca^{2+}, Sr^{2+} ou Ba^{2+} utilisés comme réticulants ioniques des chaines de sacran à C_{sacran} = 0.25 wt%. Les gels réticulés par le Sr^{2+} et le Ba^{2+} montrent une augmentation de leur élasticité (décrite ici par G_e) lorsque la C_{ion} augmente de 10^{-3} à $5\ 10^{-3}$ mol/L. Passé cette concentration critique, l'élasticité des gels de sacran n'évolue plus et se stabilise autour de 20 Pa. Les gels de sacran réticulés par le Ca^{2+} forment des gels plus mous et l'évolution de $G_e(C_{ion})$ est plus chaotique. La particularité du Ca^{2+} réticulant des chaines de sacran est discuté plus tard. Le $G_{e,max}$ observé ici et égale à 20 Pa, corresponds à une taille de maille (ξ) autour de 60 nm. Rappelons que la distance moyenne entre les charges négatives portées par les chaines de sacran (b) est estimée à 1.5 nm en considérant 33 mol% d'unités monosaccharides composant le sacran comme négativement chargées. Ainsi b est la taille de maille minimale ne considérant pas la rigidité des chaines de sacran. b est ainsi 40 fois inférieure à ξ_{exp}, ainsi la rigidité des chaines de sacran joue un rôle limitant quant au ratio de réticulation maximal des chaines sacran.

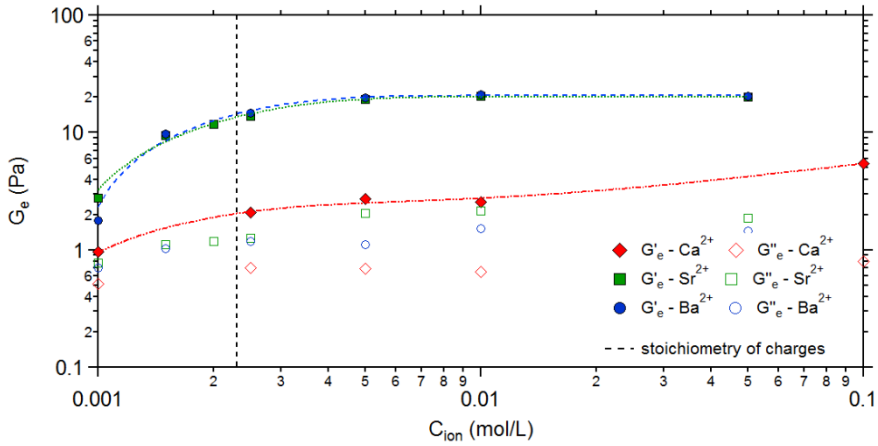

Figure 124 Modules élastiques au plateau (G_e) en fonction de la concentration en ions réticulants pour des gels de sacran à 0.25 wt% réticulés par du Ba^{2+} (cercles bleus), du Sr^{2+} (carrés verts) ou du Ca^{2+} (losanges rouges).

Enfin, la signature de la rigidité des gels de sacran est aussi observée en suivant l'évolution du G_e en fonction de la concentration en chaines dans le réseau. La proportionnalité entre le G_e, la concentration de chaines polymères d'un système enchevêtré et l'exposant de Flory est décrit par Rubinstein & Colby comme:

$$G_e \sim C_s^{\frac{3\nu}{3\nu-1}}.$$

En y insérant un exposant de Flory égal à 1, cette relation décrit ainsi un réseau dont les segments de chaine sont rigides entre les enchevêtrements et devient $G_e \sim C_s^{1.5}$. Une déviation due à la rigidité des chaines a été observée pour des solutions d'actine donnant ainsi une loi de puissance en $G_e \sim C_s^{1.4}$.[71]

Conservant leur taux de réticulation constant, des gels de sacran réticulés par du Ca^{2+}, Sr^{2+} et Ba^{2+} ont été testés rhéologiquement et leurs G_e ont été tracés en fonction de leur différentes concentrations en chaines. La loi de puissance $G_e \sim C_s^{1.5}$ est identifiée quel que soit l'ion réticulant utilisé. Ainsi, le Ca^{2+}, le Sr^{2+} et le Ba^{2+} conduisent à la formation de réseaux rigides de chaines de sacran.

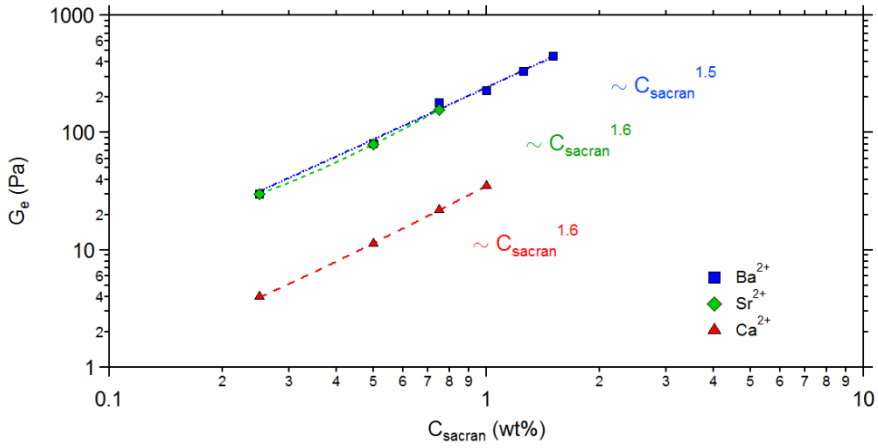

Figure 125 Module élastique au plateau (G_e) en fonction de la concentration en chaines de sacran réticulées par du Ba^{2+} (carrés bleus), du Sr^{2+} (losanges verts) ou du Ca^{2+} (triangles rouges) à un taux de réticulation fixe à C_{sacran} / $C_{crosslinkers}$ égal à 0.25 / 0.01.

La différence de gélification du sacran par le Ca^{2+} a été étudiée en effectuant des tests de cinétique de gélification sur de long temps de gélification. Une évolution chaotique et peu reproductible des modules viscoélastiques est observée sur plus de 20 h, cette évolution est répétée trois fois à partir d'échantillons frais et est chaque fois observée. En comparaison, les gels de sacran réticulés par du Sr^{2+} et du Ba^{2+} produisent des gels après 1h30 de gélification. Ces évolutions chaotiques de modules viscoélastiques observées pour la réticulation du sacran par le Ca^{2+} est attribué à la formation de structures de type paquets hétérogènes et ainsi peu reproductible.

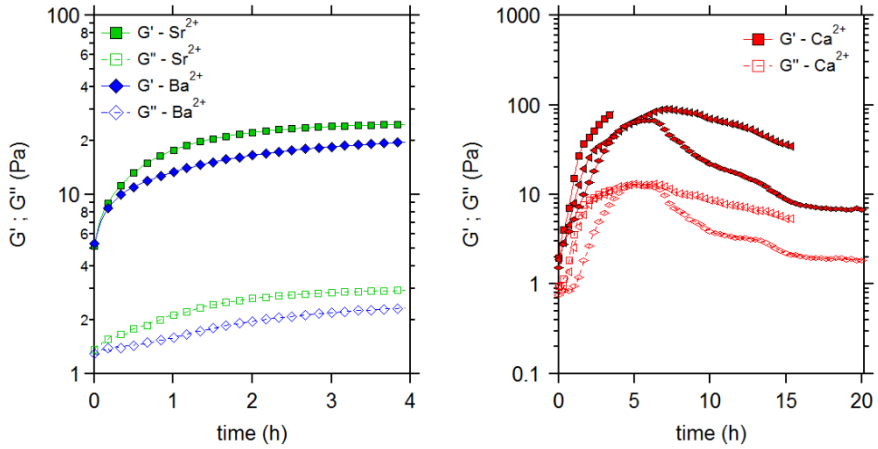

Figure 126 (gauche) Modules viscoélastiques (G' ; G'') en fonction du temps pour un gel de sacran à 0.25 wt% réticulé par 0.05 mol/L de Ba^{2+} (losanges bleus) et de Sr^{2+} (carrés verts) ; (droite) Modules viscoélastiques (G' ; G") en fonction du temps pour un gel de sacran 0.25 wt% réticulé par 0.05 mol/L de Ca^{2+}. Trois balayages aux mêmes conditions sont ici montrés.

4. Gels physiques de sacran – régime non-linéaire, rigidité de réseau et hétérogénéités

Les gels physiques de sacran sont étudiés dans leurs régimes non-linéaires dans l'optique d'observer le comportement de ces réseaux rigides soumis à de larges amplitudes de déformation.

Des gels de sacran plus concentrés ont été utilisés dans cette partie dans l'optique d'obtenir des matériaux plus élastiques et simple à manipuler. Sur le Figure 72, on observe qu'à une concentration en sacran de 0.5 wt%, la gélification par le Ca^{2+} est plus stable qu'à 0.25 wt% tout en restant moins efficiente élastiquement parlant que celles par le Ba^{2+} et le Sr^{2+}. Les modules viscoélastiques de gel de sacran à 0.5 wt% réticulés par 0.1 mol/L de Ca^{2+}, Sr^{2+} et Ba^{2+} sont tracés en fonction de l'amplitude de déformation sur la Figure 127. On observe ici des corrélations entre la nature de l'ion réticulant, l'élasticité du gel formé (G_e), sa capacité à durcir sous déformation (Q) et sa fragilité (γ_{max}).

Ainsi, les relations suivantes sont établies :

$G_e(Ba^{2+}) > G_e(Sr^{2+}) > G_e(Ca^{2+})$,

$Q(Ba^{2+}) < Q(Sr^{2+}) < Q(Ca^{2+})$,

$\gamma_{max}(Ba^{2+}) < \gamma_{max}(Sr^{2+}) < \gamma_{max}(Ca^{2+})$.

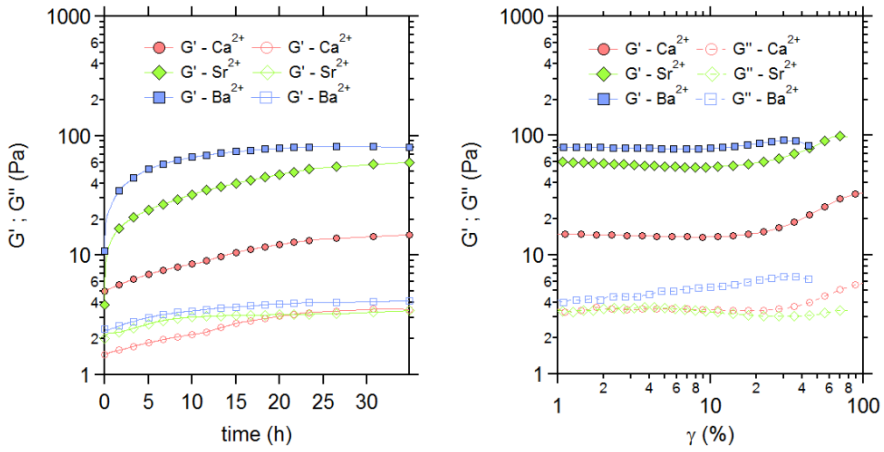

Figure 127 (gauche) Modules viscoélastiques (G' ; G") en fonction du temps ; (droite) Modules viscoélastiques (G' ; G") en fonction de l'amplitude de déformation pour des gels de sacran à 0.5 wt% réticulés par 0.1 mol/L de Ba^{2+} (carrés bleus), de Sr^{2+} (losanges verts) et de Ca^{2+} (cercles rouges).

A la fin des mesures rhéologiques, les échantillons de gels sont observés à l'œil nu et des structures blanches sont présentes dans ces gels (Figure 128), structures qui ne sont pas présentes dans les échantillons au repos.

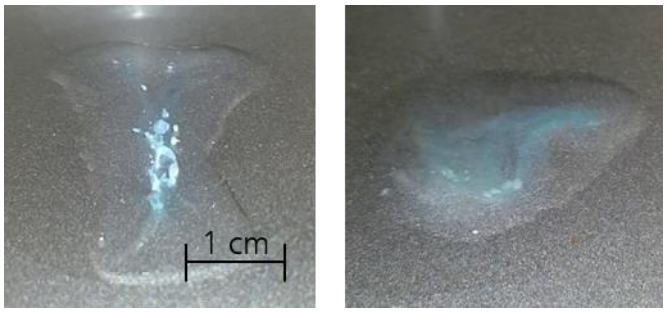

Figure 128 Images de gels de sacran à 0.5 wt% après stimulation à 100 % d'amplitude de déformation (gauche) réticulé par 0.1 mol/L de Ca^{2+} ; (droite) 0.1 mol/L de Ba^{2+}.

Dans l'optique de comprendre la provenance de ces strain-hardening, un test par paliers d'amplitude de déformation est réalisé sur un gel de sacran à 0.5 wt% réticulé par du Ca^{2+}. Sur la Figure 129, on observe l'évolution de G_e et Q en fonction de l'amplitude de déformation appliquée au gel de sacran. Le G_e décroit à chaque palier d'amplitude de déformation de 170 à 50 Pa et Q s'accroit de 0 à 5.5. Ainsi les propriétés viscoélastiques non-linéaires des gels physiques de sacran sont très dépendantes de l'amplitude de déformation qui leur est appliquée.

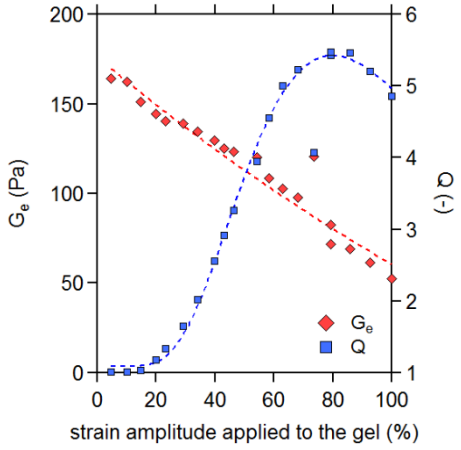

Figure 129 Modules élastiques à 1 % de déformation et 6.28 rad/s (G_e) et amplitudes de strain –hardening (Q) en fonction de l'amplitude de déformation maximale appliquée à un gel de sacran à 0.5 wt% et réticulé par 0.1 mol/L de Ca^{2+}.

Des gels de sacran mis en présence de sels NaCl ont été étudiés dans l'optique de distinguer l'effet de la réticulation ionique et celui des sels sur les chaines de sacran. On n'observe la formation de gels de sacran peu élastiques (~ 20 Pa) comparables à ceux formés par l'action du Ca^{2+}. Sur la Figure 130, les modules viscoélastiques de ces gels sont tracés en fonction de l'amplitude de déformation en présence de différentes concentrations de NaCl. Les amplitudes de strain-hardening (Q) observées pour ces gels de sacran en présence de NaCl peuvent aller jusqu'à 10.

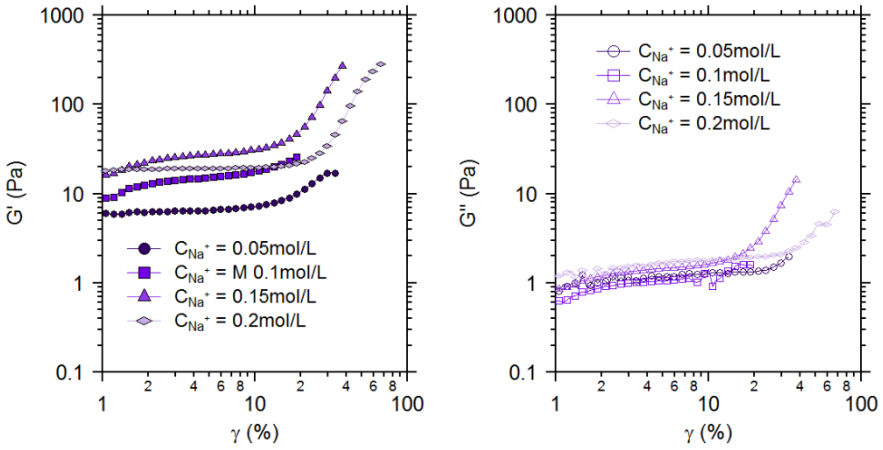

Figure 130 Modules viscoélastiques (*G'* ; *G''*) en fonction de l'amplitude de déformation imposée à des gels de sacran à 0.5 wt% en présence de différentes concentration de sel NaCl.

Enfin la relaxation à basses fréquences des gels physiques de sacran a pu être observée par l'utilisation de la Strain Rate Frequency Superposition (SRFS) à plusieurs températures permettant ainsi l'utilisation de la loi d'Arrhénius dans l'optique de mesurer les énergies d'activation des réticulations ioniques des chaines de sacran. Ces relaxations à basses fréquences ne sont pas observables par rhéologie conventionnelle du fait de la taille des chaines de sacran décalant ces relaxations à des fréquences trop basses pour être mesurées. Les énergies d'activation mesurées pour la réticulation des chaines de sacran par 0.01 et 0.1 mol/L de Ca^{2+}, Sr^{2+} et Ba^{2+} sont compilées dans la Table 13. On observe que les énergies d'activation sont faibles, témoignant ainsi de réactions faciles à amorcer et peu dépendantes de la température.

Crosslinking ion	C_{ion} (mol/L)	E_a (kJ.mol^{-1})
Ca^{2+}	0.01	21
	0.1	26
Sr^{2+}	0.01	12
	0.1	11
Ca^{2+}	0.01	8
	0.1	6

Table 3 Energies d'activation des réticulations du sacran en fonction de la nature de l'ion réticulant et de sa concentration.

5. Gels chimiques de sacran

Des gels de sacran réticulés chimiquement (par des liaisons covalentes) sont étudiés ici dans l'optique d'observer plus nettement des strain-hardening classiquement produit par des réseaux de biopolymères réticulés par des liaisons covalentes. Ces gels sont formés de la réaction des alcoolates, formés par la basification des fonctions alcools supportées par les chaines de sacran, sur des molécules de vinyl sulfone (DVS) bi-fonctionnelles.

Dans un premier temps, une étude de microrhéologie permet de vérifier la possible modification de l'architecture des chaines de sacran soumises à des conditions basiques nécessaires pour enclencher la réticulation chimique. Sur la Figure 131, aucune différence n'est observée entre les longueurs de persistance mesurées pour ces gels chimiques et celles mesurées pour des solutions aqueuses de sacran à pH neutre. Ainsi, l'ajout de base ne modifie pas ou peu l'architecture des chaines de sacran.

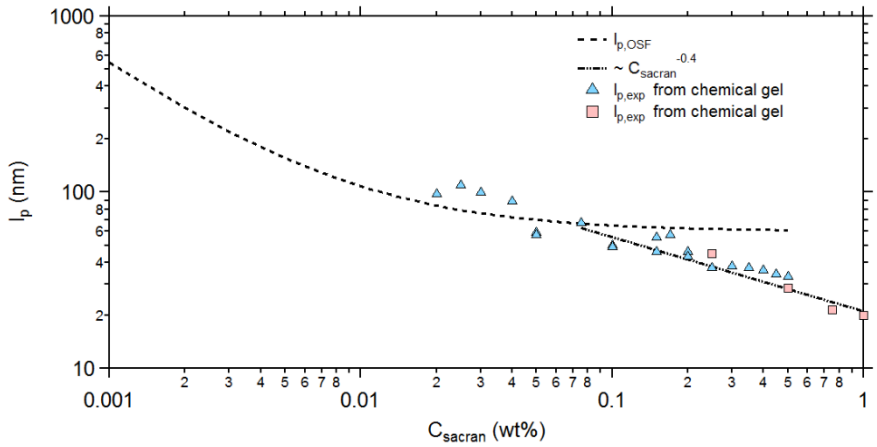

Figure 131 Longueurs persistance en fonction de la concentration en sacran pour des (a) gels chimiques de sacran (carrés rouges) ; (b) solutions de sacran (triangles bleus) mesurées par microrhéologie DWS avec l'apparition de la prédiction d'OSF et de la divergence en -0.4 attendu pour des $l_p < l_e$.

Les modules élastiques au plateau de gels chimiques de sacran à 0.5 wt% sont reportés sur la Figure 132 en fonction de leur concentration en C_{DVS} (C_{NaOH} fixée à 0.2 mol/L) et C_{NaOH} (C_{DVS} fixée à 0.15 mol/L) contrôlant toutes deux le taux de réticulation du réseau de chaines de sacran. Ainsi plus la C_{DVS} et la C_{NaOH} augmente, plus l'élasticité du gel formé augmente, atteignant un maximum de 7.8 kPa pour cette concentration en chaines de sacran.

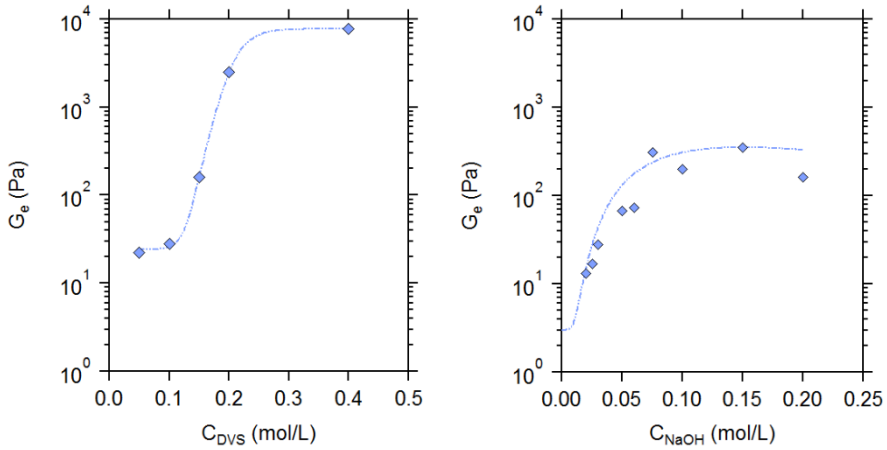

Figure 132 Modules élastiques au plateau (G_e) en fonction de (a) la C_{DVS} pour des gels de sacran à 0.5 wt% en présence de C_{NaOH} = 0.2 mol/L et (b) la C_{NaOH} pour des gels de sacran à 0.5 wt% en présence de C_{DVS} = 0.15 mol/L.

Les régimes non-linéaires de ces gels sont mesurés par le suivi de leurs modules viscoélastiques en fonction de l'amplitude de déformation imposée. La Figure 133 montre ces évolutions normalisées par le G_e des gels testés. On observe ainsi que plus le réseau de sacran est réticulé, plus il devient cassant et moins l'amplitude de son strain-hardening devient importante.

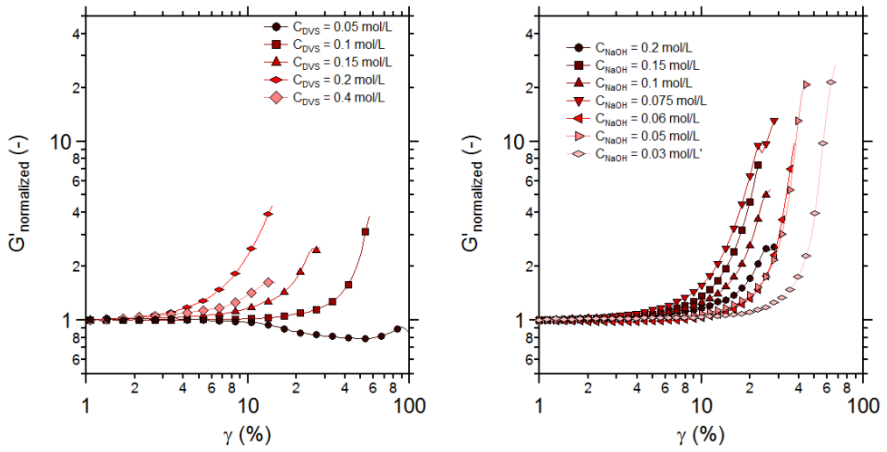

Figure 133 Modules élastiques normalisés par le G_e à 1 % ($G'_{normalized}$) en fonction de l'amplitude de déformation imposée à des gels chimiques de sacran à 0.5 wt% (a) à différentes C_{DVS} en présence de C_{NaOH} = 0.2 mol/L ; (b) à une C_{DVS} = 0.15 mol/L et en présence de différentes C_{NaOH}.

Les amplitudes de strain-hardening (Q) et maximum d'amplitude de déformation supporté par le gel (γ_{max}) sont tracés sur la Figure 134 en fonction de l'élasticité linéaire des gels chimiques de sacran. Ainsi, comme décrit plus haut, Q et γ_{max} décroissent quand G_e augmente.

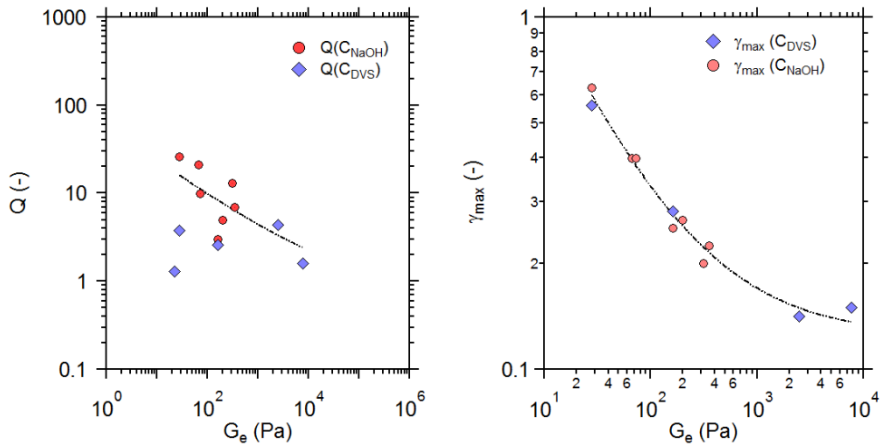

Figure 134 Amplitudes de strain-hardening (Q) et amplitudes de déformation engendrant la fracture (γ_{max}) en fonction du module élastique au plateau (G_e) des gels chimiques de sacran.

L'utilisation d'un model développé par McKintosh et al. simulant des déformations non-linéaires de réseaux polymères est utilisé pour interpréter les résultats expérimentaux. De ce model sont obtenus trois variables : le ratio d'élongation des chaines entre points de réticulation (β), la constante de fléchissement des chaines (κ) et le ratio entre la longueur de Kuhn (b_K) et la longueur de liaison dans le système (b). L'évolution de ces paramètres est tracée en fonction de l'élasticité du réseau sur les Figure 135 et Figure 136. κ et b_K/b sont constant pour l'ensemble des gels de sacran quelle que soit leur élasticité et respectivement égal à 140 et 300. Ces paramètres ne dépendent donc pas du taux de réticulation des réseaux testés, mais semblent liés à la nature du polymère. β évolue fortement avec l'élasticité du réseau passant de 0.77 à 1 lorsque G_e augmente de 30 à 200 Pa. β stabilise autour de 1 pour des valeurs de G_e supérieures, décrivant ainsi les chaines de polymère entre réticulations comme totalement tendues.

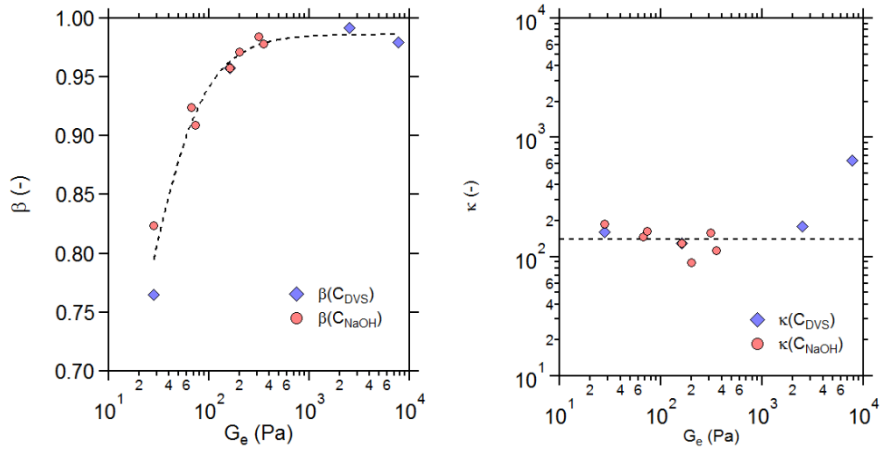

Figure 135 Ratios d'élongation des chaines de sacran entre points de réticulation (β) et constantes de flexion des chaines de sacran (κ) obtenus depuis le modèle de McKintosh et al. en fonction du module élastique au plateau (G_e) des gels chimiques de sacran.

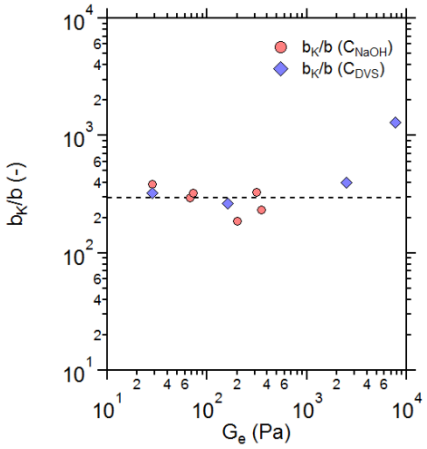

Figure 136 Ratios de la longueur de Kuhn sur la longueur de liaison (b_K/b) obtenus depuis le modèle de McKintosh et al. en fonction du module élastique au plateau (G_e) des gels chimiques de sacran.

L'étude des gels chimique de sacran se conclue donc par l'observation de large strain-hardening d'amplitude pouvant dépasser 25. Ces strain-hardening ont pu être modélisés permettant ainsi l'obtention des paramètres structurels décrivant le mécanisme architectural impliqué dans le phénomène de strain-hardening observé pour les gels de sacran.

Conclusion

Ces études ont montré la possibilité de réticuler physiquement et chimiquement des gels de sacran.

La rigidité de ces gels de sacran a pu être déterminée par microrhéologie passive DWS. Cette technique microrhéologique non-conventionnelle a permis la mesure de la longueur de persistance de ces gels.

Les gels physiques de sacran ont montré de multiples signatures de leur rigidité dans le régime linéaire. Les gels de sacran réticulés par le Ca^{2+} ou en présence de Na^{+} ont montré des propriétés de strain-hardening surprenantes. Ces propriétés ont pu être liées à la formation de structures en paquets, observées à l'œil nu à la suite de l'application de large amplitude de déformation à ces gels de sacran. Ces structures sont favorisées par un effet d'écrantage des charges portées par les chaines et l'effet kosmotropique de ces ions. Enfin les énergies d'activation des réticulations du sacran par le Ca^{2+}, sr^{2+} et Ba^{2+} ont été mesurées utilisant la SRFS à différentes températures et la loi d'Arrhénius. Les énergies d'activation sont assez faibles témoignant de réticulation facile à amorcer et peu dépendante de la température. L'énergie d'activation de la gélification calcium sacran (21 kJ/mol) est assez proche de celle de la gélification calcium alginate trouvée dans la littérature (20 kJ/mol).

Les gels chimiques de sacran ont montré des élasticités contrôlées par la quantité de DVS et le pH du milieu réactionnel. Ces gels ont produit de large strain-hardening dans le domaine non-linéaire. Ces strain-hardening ont pu être modélisés utilisant un model permettant l'obtention de paramètres structurant les réseaux de polymère. Ainsi la rhéologie non-linéaire des gels chimiques de sacran ont pu être décrit par la flexion des chaines caractérisée par $\kappa = 140$. La diminution des amplitudes de strain-hardening observée lors de l'augmentation de l'élasticité du gel testé a ainsi été décrite par l'élongation des chaines de sacran entre les points de réticulation du réseau.

Ainsi les propriétés mécaniques spécifiques attendues pour les gels de sacran ont été expérimentalement observés et ont pu être décrites par un modèle théorique faisant leur lien avec la structure des réseaux de sacran.

Résumé

Nous étudions la relation structure/propriétés d'hydrogels rigides composés d'un nouveau polysaccharide géant, le sacran. Ce nouveau polysaccharide possède une longueur de contour supérieure à 10 μm et une longueur de persistance intrinsèque d'à peu près 60 nm. Ainsi la réticulation de ces chaines polysaccharides est capable de former des réseaux dits rigides, dans lesquels la taille de maille est contrôlée par des segments de chaines rigides. A partir du sacran, des hydrogels physiques (liaisons transitoires) et chimiques (liaisons covalentes) ont été fabriqué dans l'optique d'observer des différences comportementales entre ces réseaux. La formation de réseaux rigides de sacran à être démontrée par l'utilisation de la microrhéologie non-conventionnelle par DWS permettant le suivi de la dynamique d'une chaine polymère individuelle composant le réseau. Différentes signatures rhéologiques propres à ces réseaux rigides ont été mises en évidence et des propriétés de strain-hardening ont été observées dans le régime non-linéaire des gels chimiques de sacran, et plus étonnamment des gels physiques également. Les strain-hardening observés pour les gels chimiques de sacran, grands devant ceux reportés dans la littérature, ont pu être modélisés permettant l'obtention des paramètres structurant ces réseaux et conduisant à leur durcissement.

Mots clefs : biopolymères, hydrogels, rhéologie, réseaux rigides, renforcement mécanique, diffusion de la lumière

Abstract

We study the relationship structure/properties of rigid hydrogels composed of a new giant polysaccharide, sacran. This novel polysaccharide has a contour length larger than 10 μm and an intrinsic length of persistence of approximately 60 nm. By crosslinking the chains of this polysaccharide we expect prepare rigid networks, in which the mesh size is controlled by rigid chain segments. Physical (transient bonds) and chemical hydrogels of sacran have been prepared and their rheological properties have been studied. The formation of rigid networks of sacran has been demonstrated by using the non-conventional microrheology by DWS allowing to characterize the dynamics at single chain scale of the network. Different specific rheological signatures of these rigid networks have been highlighted and strain-hardening properties have been observed in the non-linear regime for the chemical gels, as well as for the physical gels. The strain-hardening observed for the chemical gels, which are large compared to those of other biopolymers reported in the literature, were modeled to obtain the structural parameters of these networks which lead to their hardening.

Keywords: biopolymers, hydrogels, rheology, rigid networks, mechanical reinforcement, light scattering